

SOME ASPECTS OF DYNAMICAL METEOROLOGY

27 FEBRUARY - 8 MARCH 0900-1000

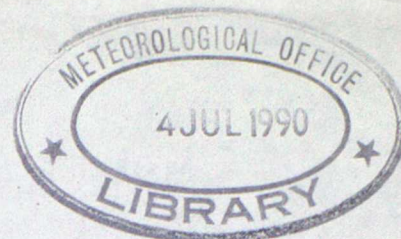
In the atmosphere there is a great variety of phenomena covering a large range of scales. As well as being interesting in their own right, many of these phenomena are important because it is necessary to forecast their behaviour. This series of lectures will consider the following eight.

- Monday 27 Hurricanes (R W Riddaway)
- Tuesday 28 Polar Lows (R W Riddaway)
- Wednesday 29 Orographic Lows (R W Riddaway)
- Thursday 1 Tornadoes (R W Riddaway)
- Friday 2 No lecture
- Monday 5 Sea Breezes (R W Riddaway)
- Tuesday 6 Blocks (R W Riddaway)
- Wednesday 7 East African Jet (R W Riddaway)
- Thursday 8 Monsoons (R W Riddaway)

For each of these the structure and possible origins will be described. An indication will be given of how simple models have led to an insight into the basic physics of the processes involved. Finally there will be a description of how more sophisticated models have been used to simulate the detailed structure of the disturbances.

Dr R W Riddaway
ECMWF
Reading

HURRICANES



1. Introduction

Hurricanes are tropical cyclones with sustained one-minute winds of more than 64 kts. They form over the tropical oceans and are accompanied by violent rotating winds and torrential rain. The typical horizontal extent of a hurricane (as measured by the radius of sub-normal pressure anomaly) is about 1000 km, although individual storms may vary within a factor of 2 of this. The average radial extent of hurricane force winds is about 100 km, but gale force winds may extend up to 500 km from the centre. The life span of a hurricane is of the order of 1 week; however if the storm remains over the warm tropical oceans it may survive for more than a month. Movement of the storms out of the warm moist tropics into the more hostile environment of the middle latitudes is the main reason why storms decay.

2. The structure of hurricanes

The storms form from large scale disturbances that already exist over the tropical oceans. Often the lower portion of these disturbances have a cold core, but then they develop warm cores - this change first becomes evident at upper levels and is related to the release of latent heat in rain areas. The warm core spreads downwards and the total conversion to a warm core may take several days. Once the warm core becomes established the chances of intensification increase.

As intensification occurs the characteristic ring of cumulus convection around the vortex (the eye wall) forms and the strong winds form a tight band around the vortex centre. The intensification can be very rapid with maximum winds increasing from 15 ms^{-1} to 50 ms^{-1} within 12-24 hours.

Now consider the structure of a mature hurricane.

(i) The eye and its wall

The eye is a calm cloudless region at the centre of the storm. It has a diameter of between 5 and 50 km and only takes up about 5% of the storm's volume. Within the eye there is subsidence and this gives rise to high temperatures and low pressures. Surrounding this region of light and variable winds is the eye wall - here the winds are a maximum and there is vigorous convection.

(ii) Temperature

Outside the eye wall there are only small variations in temperature. The highest temperatures are found in the eye and the strongest gradients occur through the eye wall. In terms of anomalies (deviations from mean tropical conditions) the largest values occur in the upper troposphere and the anomalies decrease downwards and outwards.

(iii) Pressure

Typical central surface pressures are about 950 mb. In the low and middle troposphere pressure decreases rapidly as the eye is approached and again the strongest gradients are in the eye wall; only slight variations of pressure with azimuth are found. At upper levels the horizontal pressure

gradient decreases rapidly due to the large positive temperature anomaly

$$\frac{\partial}{\partial z} \left(\frac{\partial p}{\partial r} \right) = \frac{g p}{R T^2} \frac{\partial T}{\partial r} < 0$$

(iv) Wind

Winds spiral inwards in a cyclonic fashion at low levels and there is anti-cyclonic outward flow at upper levels; in mid-troposphere there is little inflow or outflow. The strongest tangential winds are found near the region of maximum pressure gradient (i.e. near the eye wall). In the lower troposphere the winds do not vary much with height, but at upper levels the winds decrease rapidly with height due to the strong positive temperature anomaly. If there is gradient wind balance

$$\frac{\partial v}{\partial z} \left(f + \frac{v}{r} \right) \approx \frac{1}{\rho} \frac{\partial}{\partial z} \left(\frac{\partial p}{\partial r} \right) = \frac{g}{T} \frac{\partial T}{\partial r} < 0$$

and so $\frac{\partial v}{\partial z} < 0$

At low levels the flow is usually quite symmetric, but at upper levels the flow becomes asymmetric and the outflow occurs in one or two anticyclonic jets.

(v) Vertical velocity

Between the eye and about 500 km there is ascent with the largest values occurring in the eye wall. Beyond this there is moderate subsidence in the middle and lower troposphere.

(vi) Cloud and precipitation

Cloud occurs mainly in the region of mean upward motion and the dominant cloud form is Cb. The convection is most intense in the eye wall and beyond this most of the active convection is confined to intense cyclonically curving squall lines known as spiral or feeder bands. Outside these bands there are clear areas (moat region) with little or no intense convection. In the outflow region the Cb generate a dense cirrus canopy.

3. Eye formation

One of the most obvious features of a mature hurricane is the eye. Kuo (1959) put forward a saimple explanation of why the eye exists.

Consider an adiabatic frictionless vortex. Along a streamline the total energy, absolute angular momentum and potential temperature are conserved. If ψ is the stream-function then

$$c_p T + gz + \frac{(u^2 + v^2 + w^2)}{2} = E(\psi)$$

$$vr + \frac{f r^2}{2} = M(\psi)$$

$$T \left(\frac{p_0}{p} \right)^{\kappa} = \Theta(\psi)$$

Since the absolute angular momentum is conserved the tangential velocity v increases as the radius decreases. But, since the energy is also conserved v cannot go on increasing without limit. Therefore the current cannot penetrate beyond some small radius and so the current must turn upwards - this is the eye wall.

If the inward flowing current starts from rest at a distance r_0 from the centre, then it can be shown that a good estimate of the radius beyond which the current cannot go (r_m say) can be found as a function of r_0 and the ratio of the pressure at the centre to that at r_0 (P_c/P_0 say). Values of r_m along with the maximum wind v_m are given below

P_c/P_0	v_m (ms ⁻¹)	r_m (km)		
		10°N	15°N	20°N
0.95	93.7	33.4	50.2	66.8
0.97	71.0	44.0	66.2	88.0
0.98	58.0	53.8	81.0	107.6

These values are really too high compared with those observed, but when friction is taken into account the values of r_m are quite realistic.

If this theory is correct the air inside the central core does not participate in the circulation and the air would be calm. However observation reveal subsidence in the eye - why is this?

4. The energetics

Kinetic energy must be produced to maintain the extreme winds against the dissipation of KE by surface friction and mixing. This is done by converting APE to KE by accelerating the air towards low pressure in the inflow layer. The store of APE is maintained by diabatic heating.

If the KE equation is integrated over the storm volume (V) and it is assumed that there is no flux of KE through the side boundaries, then

$$\frac{\partial K}{\partial t} = \int_V \left(-\frac{v}{r} \frac{\partial p}{\partial \lambda} - u \frac{\partial p}{\partial r} \right) dV + \int_V c \frac{v}{r} \cdot F dV$$

where λ is the azimuth. The first term represents the conversion of APE to KE and the second is the frictional dissipation. Consider the first part of the conversion term. In the middle and lower troposphere the isobars are nearly circular, and higher up the pressure gradient weak; therefore this part of the term makes little contribution to the production of KE. Now consider the second part. In the inflow layer - u and $\frac{\partial p}{\partial r}$ are positively correlated, but in the outflow layer the pressure gradient's weak. Therefore the main source of KE is in the boundary layer. Since dissipation occurs both inside and outside the boundary layer, the boundary layer must be a net source of KE. Hence a paradox - the surface friction is responsible for a net gain of KE and without friction a hurricane could not exist.

Consideration of the production of APE shows that most of the generation is due to the release of latent heat, but infra-red cooling in the surrounding air also contributes.

5. Conditional instability of the second kind (CISK)

Disturbances can become hurricanes very rapidly and this suggests the release of some kind of instability - such an instability was suggested by Charney and Eliassen (1964) and Ooyama (1964) and has become known as CISK.

Budget studies have shown that the rainfall rates in mature storms are almost balanced by the water vapour convergence in the lowest layers of the atmosphere. This suggests that the large scale vortex and the cloud system act in such a way that the clouds supply the heat required to drive the vortex; whilst the vortex, by providing low-level water vapour convergence, organises and maintains the cloud system.

Suppose we have a weak tropical vortex. Frictionally induced flow will develop at low levels and where there is convergence moisture will be carried upwards in cumulus clouds. The latent heat released will warm the inner portion of the vortex and lower the pressure. The inward pressure gradient is then increased - this in turn increases the inflow and the convection. This process does not go on indefinitely because the temperature increases are concentrated at upper levels and so the convective instability is reduced.

Now consider the problem of how to parameterise cumulus convection in a numerical model. When the equations of motion are averaged over a grid square we get eddy correlation terms that represent subgridscale motions such as convection. The problem is then to replace these terms with virtual sources and sinks of heat moisture and momentum. There are essentially two problems when convection is considered

- (i) What is the vertically integrated heating in an atmospheric column?
- (ii) What is the vertical distribution of the heating?

In most convection schemes it is assumed that the vertically integrated condensation rate is given by the frictional convergence of water vapour (i.e. no water is stored or transported away). The convection scheme of Kuo (1965) then assumes that the heating at any level is proportional to the difference between the temperature of a parcel undergoing saturated adiabatic ascent and the environment. Physically the idea is that all the water vapour that converges in the boundary layer is used to make clouds. The clouds then impart their properties to the environment by instantaneous horizontal mixing. The physics behind these ideas is questionable (they neglect environmental subsidence) but Kuo's scheme has been used extensively in hurricane modelling as well as in NWP models.

6. Circularly symmetric hurricane models

Rosenthal (1971) did some experiments with a 7 level model that had a 10 km horizontal mesh; the domain was 440 km. The initial conditions represented a weak warm core vortex in gradient wind balance. The sea surface temperature was 2°C higher than the initial sea level air temperature. The model developed a storm with many realistic features (see Fig 1) and so a series of sensitivity experiments were carried out (see Fig 2)

- (i) Strength of initial vortex - when the initial vortex was intensified the storm reached its mature stage more rapidly because the frictional convergence was increased and this in turn increased the convection.

(ii) Water vapour content - entrainment of dry air by cumulus convection suppresses the vertical development. Experiments carried out with moist air (RH = 90%) in the middle and upper troposphere instead of dry air caused the hurricane to reach maturity 48 hours earlier.

(iii) Drag coefficient (C) - when the surface drag was increased the inflow, and hence the primary source of energy, was increased; however increased drag also leads to an increase in dissipation. During the early stages of the storm the growth rate increased with C, but the peak intensity was inversely related to C.

(iv) Air-sea interaction - observations indicate that hurricanes only form over sea with temperatures greater than 26°C; this suggests that evaporation and the transfer of sensible heat must be vital. The explanation appears to be that outside the main core there is subsidence of mid-tropospheric dry air into the boundary layer. If there is not enough evaporation to raise the humidity of this air before it reaches the inner convective regions then the convective activity will be weakened. This argument suggests that evaporation should be more important than the sensible heat flux and this was confirmed by Rosenthal's experiments.

(v) Non-developing experiments - overall he found that rapid storm formation only occurred with a combination of high humidity, high sea temperatures and small static stabilities. Small changes in any of these were sufficient to delay or entirely inhibit cyclone developments.

Recently some interesting experiments have been carried out into the necessity of having a cumulus parameterisation scheme. Yamasaki (1977) used a non-hydrostatic model with a minimum grid-length of 400 m. He did not use a convection scheme and found that the organisation of the model could be predicted by the model itself - that is CISK can occur by the models internal structure. Rosenthal (1978) has carried out an even more interesting experiment with a 20 km grid model that did not have a convection scheme. In the initial stages of the simulations there were small-scale large amplitude features (as in earlier experiments in the 1960's), but eventually non-linear effects managed to control their growth. The final result was a realistic disturbance.

7. Asymmetric hurricane models

In these models the initial conditions are similar to those used in the symmetric models, but now asymmetries are allowed to develop. In some of the first experiments Anthes (1972) used a model with only 3 levels, but the results are not unlike those from more sophisticated models used later. During the integrations two main asymmetries developed (see Fig 3).

(i) In the outflow region asymmetric unsteady flow developed and most of the flow took place in two anticyclonic jets (as in many real storms). Anthes suggested that the asymmetries are a result of the inertial instability with the KE of the eddies derived from the KE of the azimuthal flow. However Jones (1977) has argued that although inertial instability was present the main effects are due to the release of barotropic instability.

(ii) The vertically integrated convective heat release show spiral rainbands of the type found in real disturbances. These bands rotate cyclonically about

the storm centre and propagate outwards. Anthes thought that these bands were gravity waves and this was supported by Jones (1977) who thought they were caused by barotropic instability near the eye wall.

Recently Willoughby (1978) has examined the behaviour of outward propagating waves excited near the storm centre. He found that such waves did produce realistic spirals. However for some eye diameters the period of the spirals was much too small (tens of minutes rather than hours). This led Willoughby to consider inward propagating inertia-buoyancy waves excited on the storm periphery. The small initial waves then amplify into spiral bands as they propagate inwards. Willoughby claims that this mechanism can explain many of the deserved features of real spiral bands.

So far we have only considered models of stationary hurricanes. To overcome this restriction Jones (1977) devised a 3 level triple nested model with the two finest nests moving with the storm centre. The results were encouraging and this led to the development of a 12 level version (Jones (1980)). Following Rosenthal's suggestion a cumulus parameterisation scheme was not included. This model has been used to study the formation of spiral bands (see Fig 4). He found that he could reproduce spiral bands that propagated outwards at between 10 to 15 ms^{-1} . Such bands are found in nature, but the most commonly observed bands are much slower and these were not reproduced.

Some of the outstanding problems are

- (i) how and why do easterly waves develop into tropical storms
- (ii) what causes the spiral bands
- (iii) how does the vortex interact with the basic current
- (iv) how to initialise models with real data so they can be used to make forecasts
- (v) how to modify hurricanes to make them less destructive

8. References

In this lecture use has been made of the review article and book.

Anthes, R.A., 1974, Rev. of Geoph. and Space Physics, 12, 495-522

Rosenthal, S.L., 1974, *Weather and Climate Modification*, Ed. W.N. Hess, 522 - 551

Other references are

Anthes, R.A., 1972, M.W.R., 100, 461-476

Charney, J.G., and Eliassen, A., 1964, 21, 68-75

Jones, R.W., 1977, J.Atms.Sc., 34, 1528-1553

Jones, R.W., 1980, J.Atms.Sc., 37, 930-938

- Kuo, H.L., 1959, The atmosphere and the sea in motion, 413-424
- Kuo, H.L., 1965, J.Ats.Sc., 22, 40-63
- Ooyama, K., 1964, Geofis. Int., 4, 187-198
- Rosenthal, S.L., 1971, M.W.R., 99, 767-777
- Rosenthal, S.L., 1978, J.Ats.Sc., 35, 258-271
- Willoughby, H.E., 1978, J.Ats.Sc., 35, 838-848
- Yamasaki, M., 1977, J.Met.Soc. Japan, Ser. 2, Vol. 55, 11-31

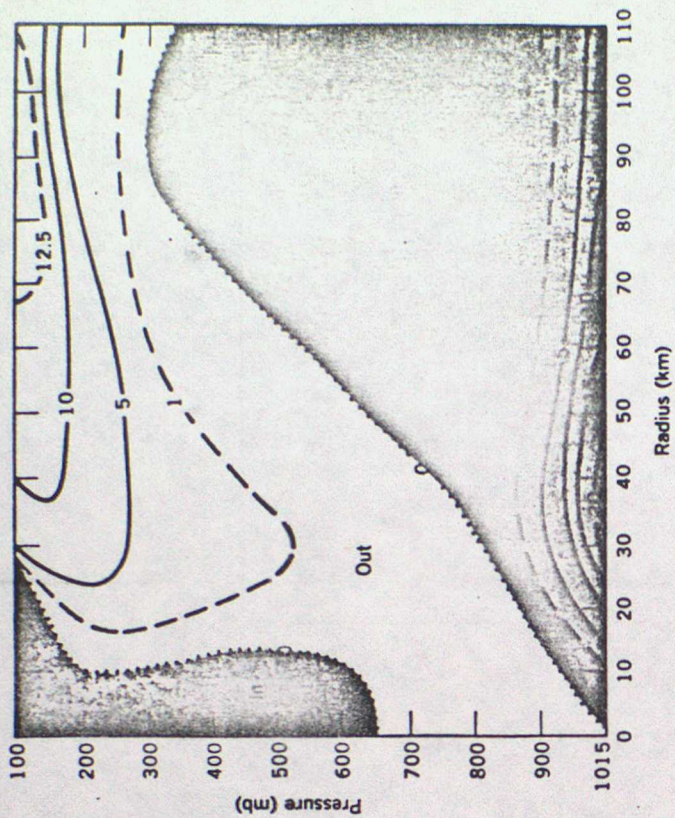


Figure 1a Cross-section of temperature anomalies at 312 hr of experiment S-35. Isotherms are labeled in degrees K.

Figure 1b Cross-section of radial velocity at 312 hr of experiment S-35. Hatched areas depict inflow.

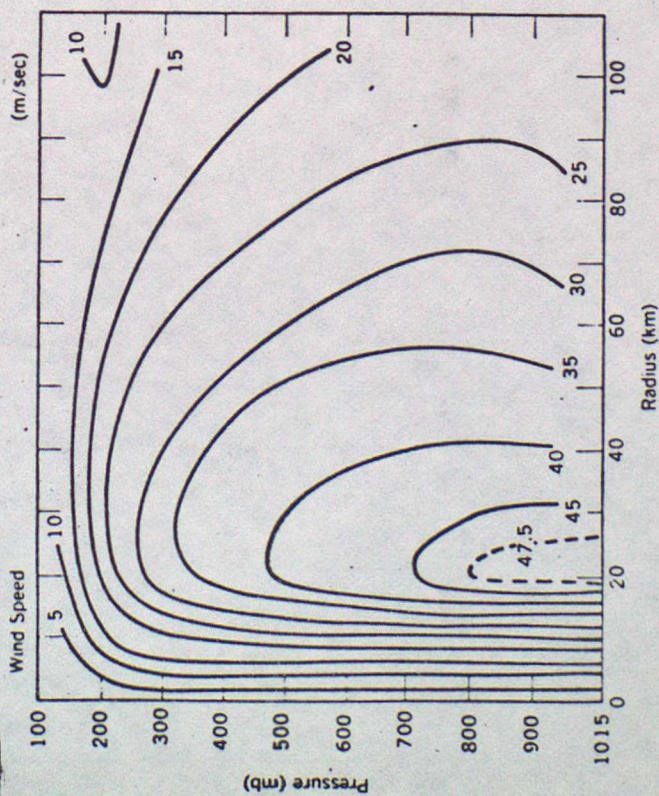


Figure 1c Cross-section of wind speed at 312 hr of experiment S-35. Isotherms are labeled in m/sec.

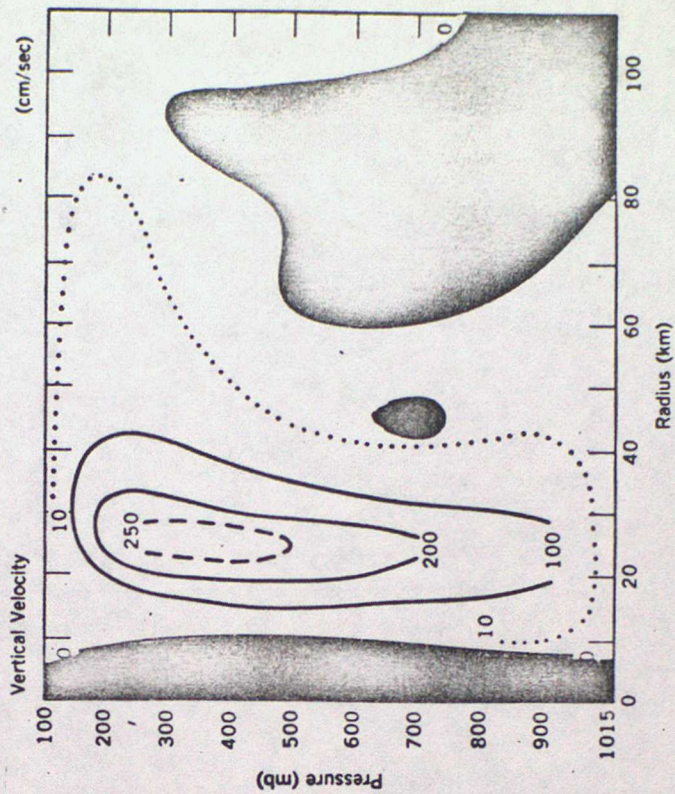


Figure 1d Cross-section of vertical velocity at 312 hr of experiment S-35. Isotherms are labeled in cm/sec. Hatched areas indicate negative values (subsidence).

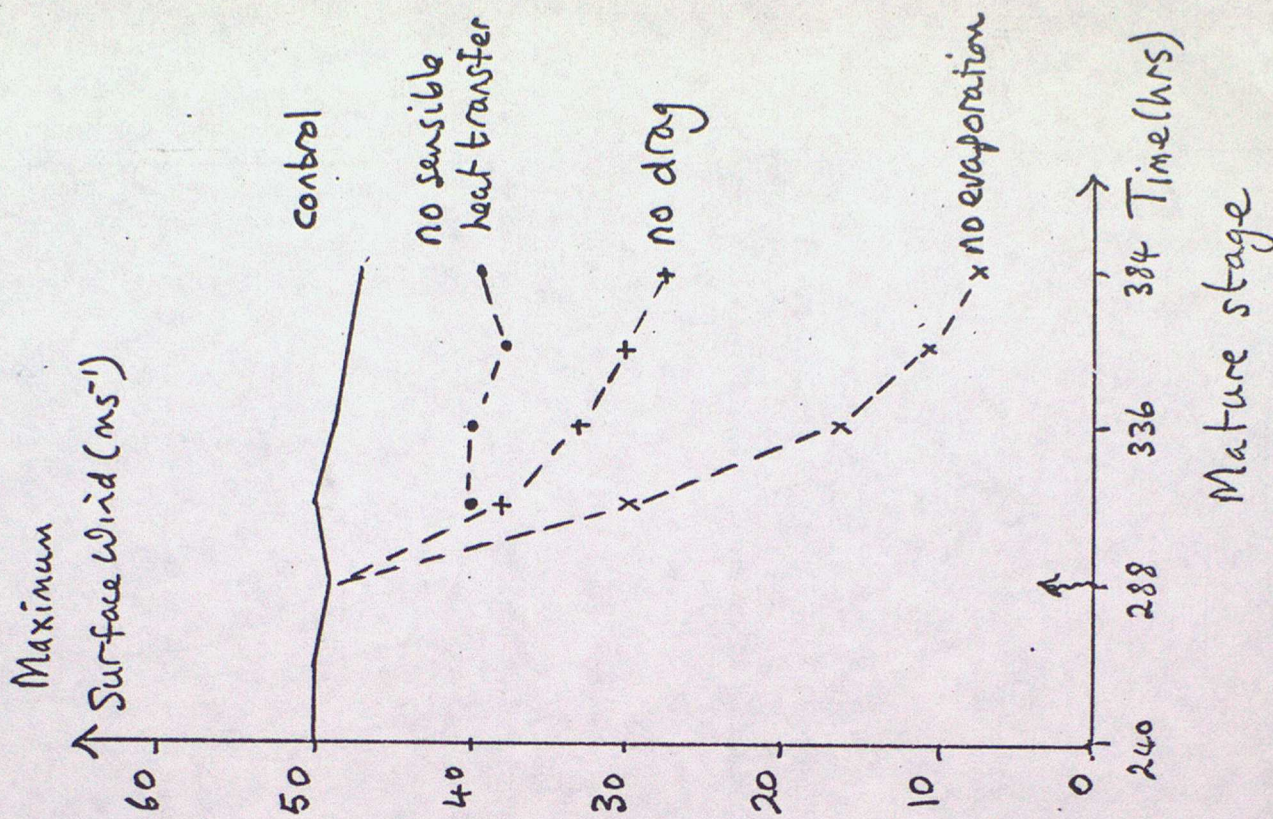
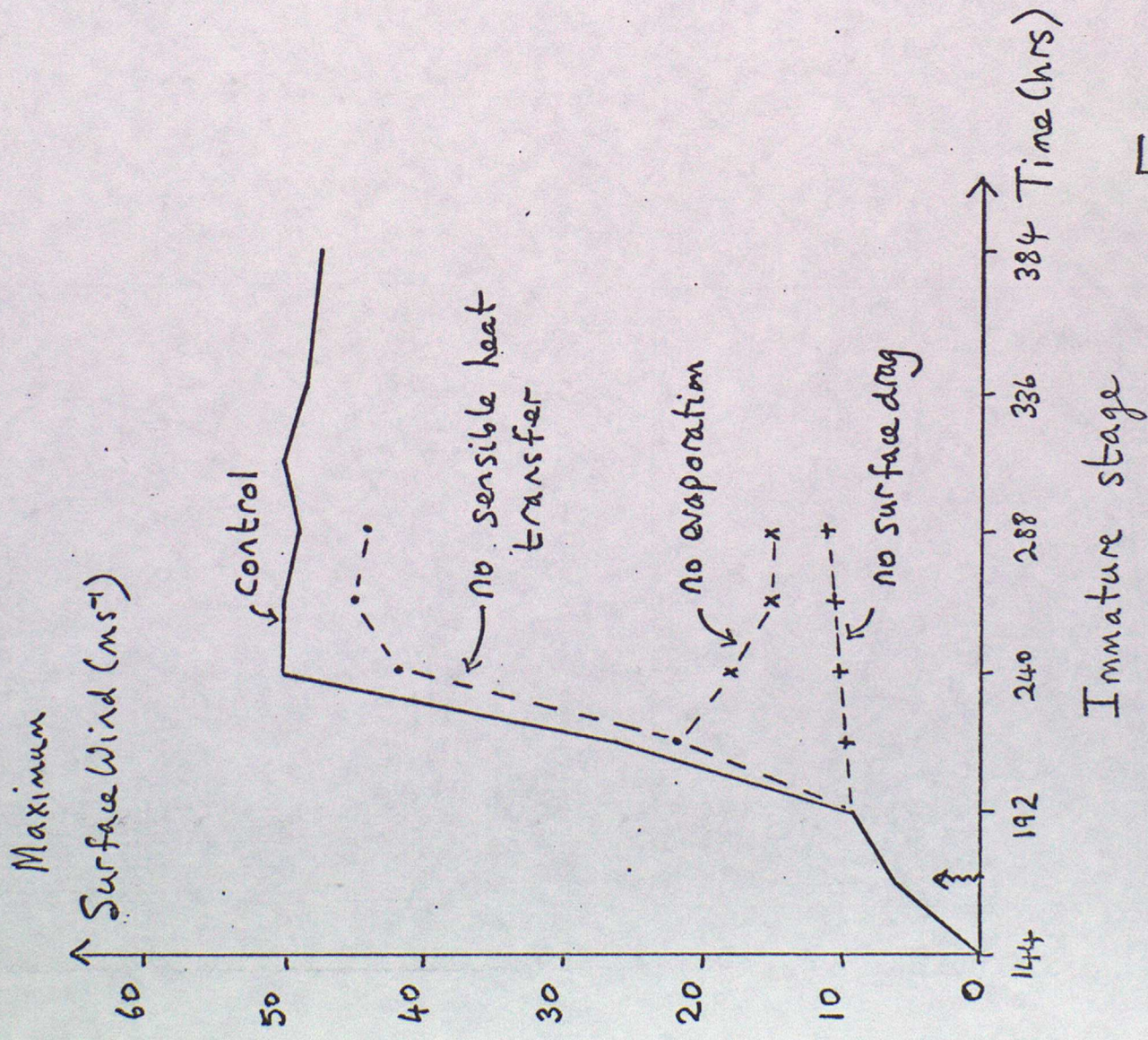


Figure 2

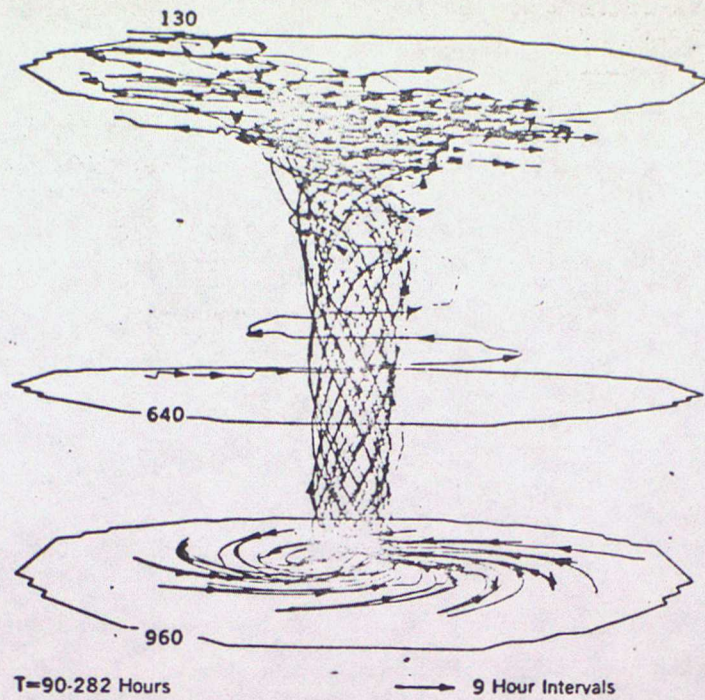


Figure 3c. Particle trajectories calculated over a 9-day period in an experiment. The three levels are labeled in millibars (approximate). All particles start in boundary layer except one, which is started in the middle troposphere.

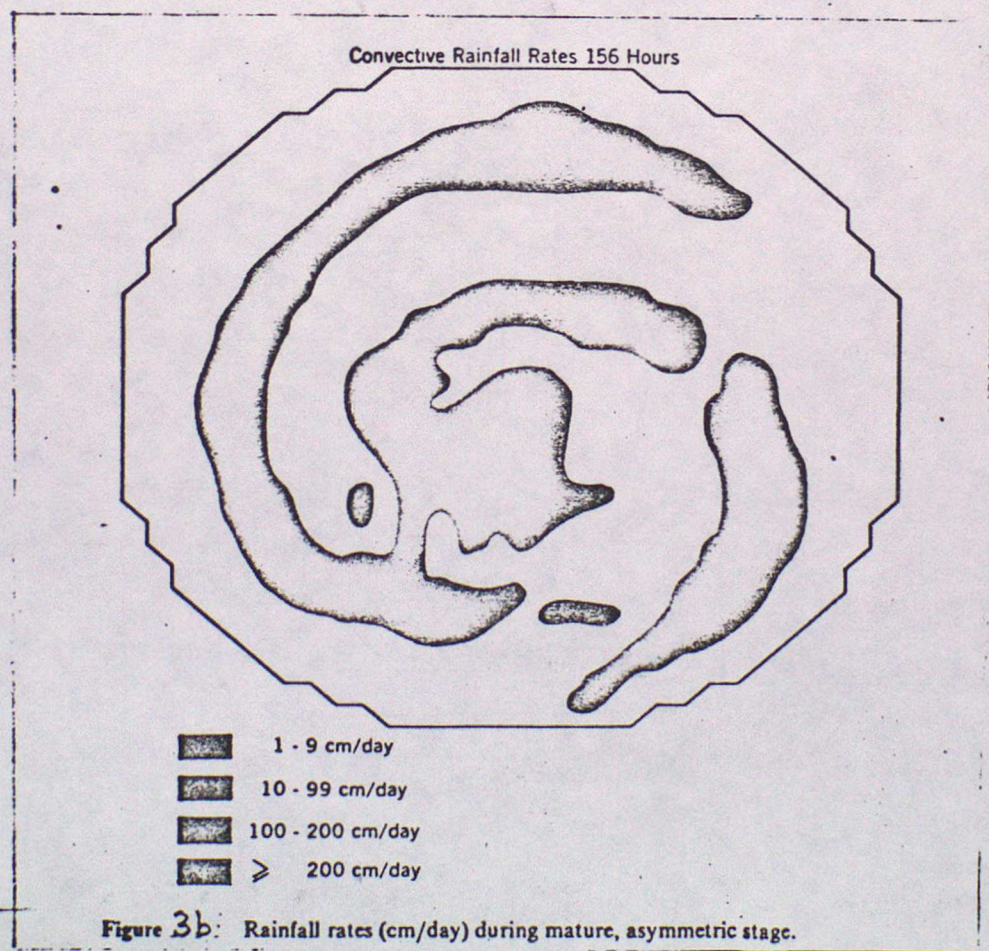
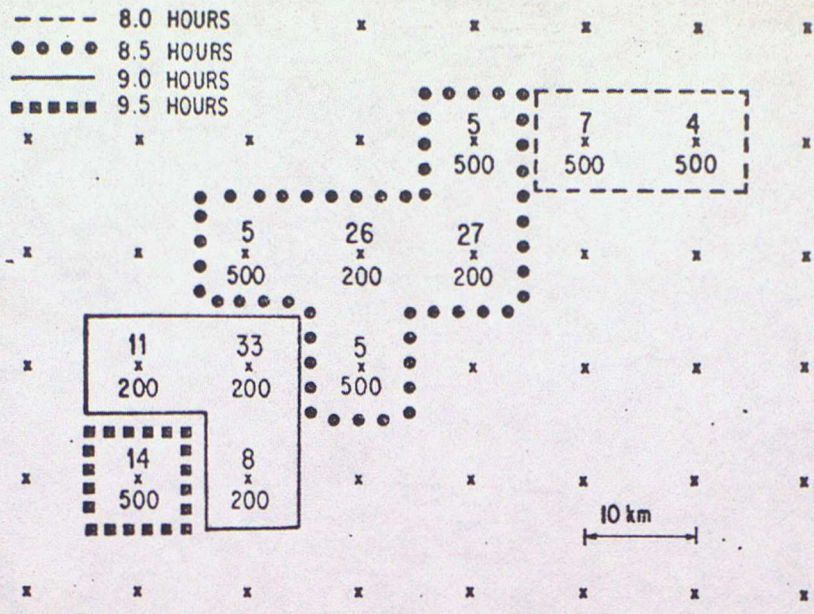
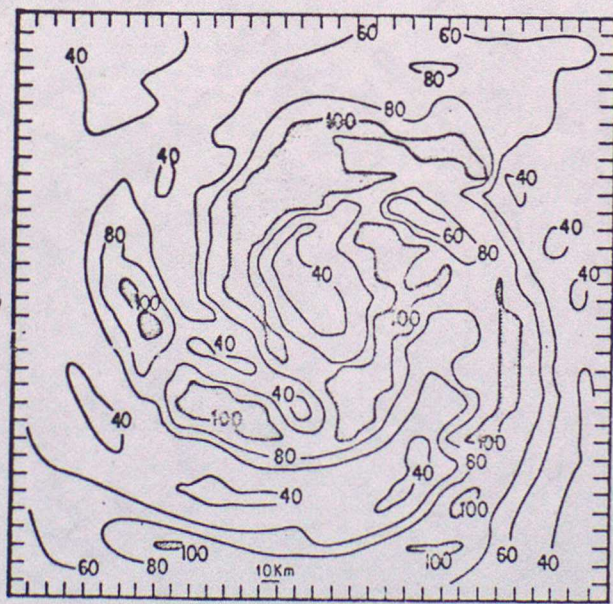


Figure 3b: Rainfall rates (cm/day) during mature, asymmetric stage.



(a) Schematic diagram of the time history of a cluster of convective cells. Areas denote upward motion greater than 2.5 m s^{-1} at 500 mb. Maximum updraft speed is given for each point in the cluster at the level given. Vortex center is located 25 km east of 85 km south of lower right corner grid point.



(b) Relative humidity (percent) at 550 mb at 24 h. Shaded areas denote saturation and presence of cloud.

Figure 4

POLAR LOWS



1. Introduction

The Meteorological Glossary defines a polar low as "A secondary depression of non-frontal character which forms, more especially in winter, within an apparently homogeneous polar air mass; near the British Isles the development is usually within a N'ly or NW'ly airstream. The chief characteristics of this type of depression, which seldom becomes intense, are a movement in accordance with the general current in which the depression forms and the development of a belt of precipitation near the depression centre and along a trough line which often forms on the side farther from the parent depression where also the pressure gradient (and surface winds) is increased".

Despite this definition there appears to be no agreement about exactly what constitutes a polar low. Mansfield (1974) defined polar lows as shallow disturbances growing entirely within a polar air mass - this then excluded

- (i) small surface lows associated with upper air troughs
- (ii) small and initially shallow depressions that form on the boundary of the polar air SE of Greenland, but which are soon seen to be as extensive in depth and horizontal extent as normal mid-latitude cyclones.

However Reed (1979) does not restrict himself in this way and the examples he considered are characterised by a mid-tropospheric vorticity maximum that is seen as a comma-shaped cloud pattern on a satellite picture; hence Reed does not exclude deep systems. Here we will be mainly concerned with polar lows that have only a limited vertical extent.

Polar lows (however defined) do not occur very frequently. Harrold and Browning (1969) suggest that in the vicinity of the British Isles they occur once or twice every year. This estimate was supported by Mansfield who found that between 1960 and 1969 there were 43 outbreaks of cold air (defined in his context by air flowing off the ice sheet for 48 hours or more) which covered a total of 114 days. During these outbreaks he identified 36 disturbances which occurred in 25 of the outbreaks and of these only 13 reached the British Isles.

Although polar lows do not cross the British Isles very often, when they do they can create chaos because they sometimes produce large amounts of snow.

Because of the lack of observations in the vicinity of polar lows there has always been some doubt about how they form. Originally it was thought that they formed as a result of thermal instability as cold air moved over the warm sea. However no detailed study was made until Harrold and Browning used radar to examine a series of polar lows; they found that the lows were associated with low level baroclinicity. This prompted Mansfield (1974) and then Duncan (1977) to do some theoretical investigations to see if a simple model of baroclinic instability could account for the observed growth rate, wavelength and phase speed of the lows. Their results confirmed the idea that polar lows are shallow baroclinic disturbances. However Rasmussen (1979) argued that this is not so, and that the polar lows are an example of a mid-latitude CISK phenomena. Finally Reed (1979) supported the view that polar lows are caused by baroclinic instability, though he did think that other processes could have a significant secondary effect. However he did not accept that polar lows are necessarily shallow.

2. Structure

Harrold and Browning examined the structure of a polar low that crossed the country on the 7 December 1967. In their analyses they used information from radio-sonde ascents (winds, temperature and humidity) and from Doppler radar (horizontal and vertical velocities).

In order to examine the structure of the flows within the disturbance they used the technique of isentropic analysis. First the motion of the system is subtracted from the observed winds to give the relative winds; this wind is then computed for a variety of values of θ_w . Next all the relative winds for a particular θ_w surface are plotted on a chart along with the topography of the surface. If it is then assumed that

- (i) θ_w is conserved by a parcel of air
- (ii) the structure of the disturbance does not change during the time taken for a parcel of air to pass through the system

then streamlines derived from the relative winds are also trajectories.

Fig 1 shows a composite diagram based on both radar and θ_w analyses. Clearly the cloud and rain are associated with an ascending tongue of relatively warm air. This slant-wise convection implies baroclinicity which was indeed found in the observations. The organisation of the flows is similar to that found in large-scale baroclinic disturbances. The velocity of the system was consistent with it being steered with the winds at about 850 mb which suggests that the polar low was associated with low level baroclinicity.

The origin of the polar low was also examined. They found that it formed in an area of slack winds between Iceland and Greenland, and only moved into a N'ly airstream later. Soundings in the vicinity showed that convection was either impossible or confined to low levels; there were no surface reports of deep convection. This suggests that the lows did not form as a result of enhanced small-scale convection. However there was appreciable low level baroclinicity prior to the development of the low.

3. Theoretical studies of baroclinic instability

3.1 The Eady model

In this model it is assumed that

- (i) the flow is quasi-geostrophic
- (ii) the basic flow has a uniform vertical shear

$$\bar{u} = \Lambda z + \bar{u}_0 \quad \text{with} \quad \Lambda = \frac{\partial \bar{u}}{\partial z} = -g \frac{\partial \bar{\theta}}{\partial y}$$

- (iii) both the density and Brunt-Vaisala frequency are constant

$$N^2 = \frac{g}{\bar{\theta}} \frac{\partial \bar{\theta}}{\partial z} \quad \text{is constant}$$

(iv) the flow is on a f plane ($f=f_0, \beta=0$)

(v) the flow is adiabatic and frictionless

(vi) the flow is bounded above and below by rigid walls at $z=0$ and $z=H$

It is convenient to write the equations in terms of the stream function ψ ; the vorticity and thermodynamic equations then become

$$\begin{aligned} \frac{\partial \xi}{\partial t} + v_g \cdot \nabla \xi - \frac{f_0}{\rho_0} \frac{\partial}{\partial z} (\rho_0 w) &= 0 & \xi &= \nabla^2 \psi \\ f_0 \left(\frac{\partial}{\partial t} \frac{\partial \psi}{\partial z} + v_g \cdot \nabla \frac{\partial \psi}{\partial z} \right) + N^2 w &= 0 & v_g &= \underline{k} \times \nabla \psi \end{aligned}$$

Eliminating w between these equations gives the potential vorticity equation

$$\frac{\partial q}{\partial t} + v_g \cdot \nabla q = 0 \quad \text{with} \quad q = f_0 + \nabla^2 \psi + \frac{f_0^2}{\rho_0} \frac{\partial}{\partial z} \left(\frac{\rho_0}{N^2} \frac{\partial \psi}{\partial z} \right)$$

This equation is now linearised about a basic state

$$v_g = \bar{v} + v' \quad \text{and} \quad \psi = \bar{\psi} + \psi' \quad \text{with} \quad \bar{v} = (\bar{u}, 0)$$

The resulting equation is

$$\left(\frac{\partial}{\partial t} + \bar{u} \frac{\partial}{\partial x} \right) \left\{ \nabla^2 \psi' + \frac{f_0^2}{\rho_0} \frac{\partial}{\partial z} \left(\frac{\rho_0}{N^2} \frac{\partial \psi'}{\partial z} \right) \right\} + \bar{q}_y \frac{\partial \psi'}{\partial x} = 0$$

with $\bar{q}_y = -\frac{\partial^2 \bar{u}}{\partial y^2} - \frac{f_0^2}{\rho_0} \frac{\partial}{\partial z} \left(\frac{\rho_0}{N^2} \frac{\partial \bar{u}}{\partial z} \right) = 0$ in our case

Assume that the perturbation has the form

$$\psi' = R \left\{ \phi(z) e^{ik(x-ct)} \right\}$$

Since c may be complex ($c = c_r + ic_i$) and we get

$$\psi' = e^{kc_i t} R \left\{ \phi(z) e^{ik(x-c_r t)} \right\}$$

Clearly $k c_i$ is the growth rate and c_r the phase speed. The stability is determined by the sign of c_i , if $c_i > 0$ we have instability. Substituting for ψ' in the perturbation equation gives

$$\frac{f_0^2}{N^2} \frac{d^2 \phi}{dz^2} - k^2 \phi = 0$$

The boundary conditions are

$$w = 0 \text{ at } z = 0 \text{ and } z = H$$

In terms of ϕ this becomes

$$\begin{aligned} (u_0 - c) \frac{d\phi}{dz} - \Omega \phi &= 0 & z=0 \\ (u_0 + \Omega H - c) \frac{d\phi}{dz} - \Omega \phi &= 0 & z=H \end{aligned}$$

The solution of the perturbation equation is

$$\phi(z) = A \cosh(\alpha z) + B \sinh(\alpha z) \quad \text{where } \alpha = \frac{N^2 k^2}{f_0^2}$$

Using the boundary conditions gives us A and B; we also get

$$c = \bar{u}_0 + \frac{\Omega H}{2} \pm \frac{\Omega}{2} \sqrt{1 + \frac{X^2}{4} - X \coth X} \quad X = \alpha H$$

The flow can only be unstable if there is a complex root; this occurs if $X = \alpha H < 2.4$. When this condition is satisfied there will be one growing and one decaying mode each moving with the speed of the mid-level. It can also be shown that

- (i) the maximum growth rate is $0.31 \frac{f_0 \Omega}{N}$
- (ii) the dominant wavelength is $3.9 \frac{HN}{f_0}$

3.2 A comparison between theory and observations

Mansfield examined the observations for the 8 December case and derived the following quantities as being typical for the area where the polar low first developed

$$\begin{aligned} H &= 1.6 \text{ km} & N^2 &= 1.6 \times 10^{-4} \text{ s}^{-2} & f &= 1.3 \times 10^{-4} \text{ s}^{-1} \\ \frac{\partial \bar{\theta}}{\partial y} &= 1.4 \times 10^{-2} \text{ }^\circ\text{C/km} & \text{giving } \Omega &= 6 \text{ m s}^{-1} / 1.6 \text{ km} \end{aligned}$$

Using these he derived the characteristics of the Eady wave (see Fig 2) and compared them with values estimated from the observations

	Th.	Obs
max growth rate (hours)	23	24
dominant wavelength (km)	620	650
phase speed (ms^{-1})	6	6

Clearly the Eady analysis gave surprisingly good results considering the simple nature of the model.

Mansfield thought that frictional effects could be important so he added a friction layer. This was done by assuming that the effects of friction could be adequately described by introducing a frictionally induced vertical velocity at the lower boundary (Charney and Eliassen (1949) again). The results are shown in Fig 3. The friction makes the waves grow less rapidly (especially the shortest waves) and the maximum growth rate is shifted towards longer wave lengths. This analysis suggests that in strong winds the development of polar lows is retarded. Mansfield also found that growth was retarded when the air was travelling parallel to the sea isotherms. Hence the most favourable conditions for the growth of polar lows is when there is a shallow baroclinic zone coinciding with light surface winds blowing parallel to sea isotherms. However it should be noted that Mansfield did not consider the effects of the release of latent heat which could have important effects on the theoretical growth rates.

Duncan (1977) tried to overcome some of the rather gross assumptions made in the Eady model by using a model devised by Brown (1969). In this model

- (i) vertical variations of static stability are allowed
- (ii) the wind is allowed to vary both horizontally and vertically
- (iii) the upper lid is at 300 mb.

Three different cases were investigated and it was found that in each one the amplitude of the disturbance diminished rapidly with height and the growth by baroclinic processes was mainly at low levels (there was no significant growth by barotropic processes). Comparisons were made between the observed and predicted characteristics.

	Wavelength (km)		Phase speed (ms^{-1})	
	obs	model	obs	model
5 April 1968	1200	1300	17.3	21.0
7 Dec 1967	1200	475	15.3	9.8
2 Jan 1965	800	650	17.0	12.2
Error	± 150		± 2.0	

Duncan argued that the poor result for 7 December could be explained by the neglect of the horizontal variation of static stability.

Perhaps the most important aspect of Duncan's work is that it emphasised the importance of low level static stability.

4. Rasmussen's CISK theory

In tropical regions the lower troposphere is usually conditionally unstable and it is in such an environment that hurricanes grow. The CISK theory suggests that the growth comes about by the co-operation between Cb convection and the large scale circulation. In mid-latitudes the atmosphere is usually conditionally stable, but when cold air flows southwards over a progressively warmer sea there is low level conditional instability. Rasmussen (1979) argued that in such conditions there may be mid-latitude CISK development leading to the formation of a polar low. He constructed a simple model to see if this type of mechanism could produce disturbances with the correct characteristics.

Rasmussen used a barotropic, quasi-geostrophic 3-level model that was linearised about a constant N'y flow; the growth rates and structure of the unstable modes could then be examined. The effect of convection was included by assuming that all the water vapour transferred through the top of the boundary layer condensed immediately and that the heat was distributed throughout the atmosphere according to some specified heating function.

Fig 4 shows the derived growth rates based on ascents at Long Kesh for the December 1967 polar low outbreak. Clearly the growth rates are sensitive to the way in which the heating is divided between the two layers - unfortunately there is no way of knowing how the heating should be divided. However the dominant wavelength does lie in the range of 300 to 400 km. The structure of the fastest growing wave is shown in Fig 5. Note that over the surface low there is an upper high with an amplitude of about twice that of the low. Rasmussen could find no evidence of this high, but he did put forward an argument for why that should be. He also examined the origin of the polar low and found that it first formed as a lee vortex to the south of Iceland. Once convection started in this vortex it would develop due to the CISK mechanism and as it moved southwards the instability, convection and growth rate would increase.

Overall the evidence for polar lows being a CISK phenomena is rather meagre. However once the polar low has formed due to baroclinic instability it could be that the convection in the disturbance becomes organised and has some effect on the subsequent growth.

5. References

- Duncan, C.N., 1977, Q.J.R.M.S., 103, 255-268
Harrold, T.W. and Browning, K.A., 1969, Q.J.R.M.S., 95, 710-723
Mansfield, D.A., 1974, Q.J.R.M.S., 100, 541-554
Rasmussen, E., 1979, Q.J.R.M.S., 105, 531-549
Reed, J.R., 1979, M.W.R., 107, 38-52

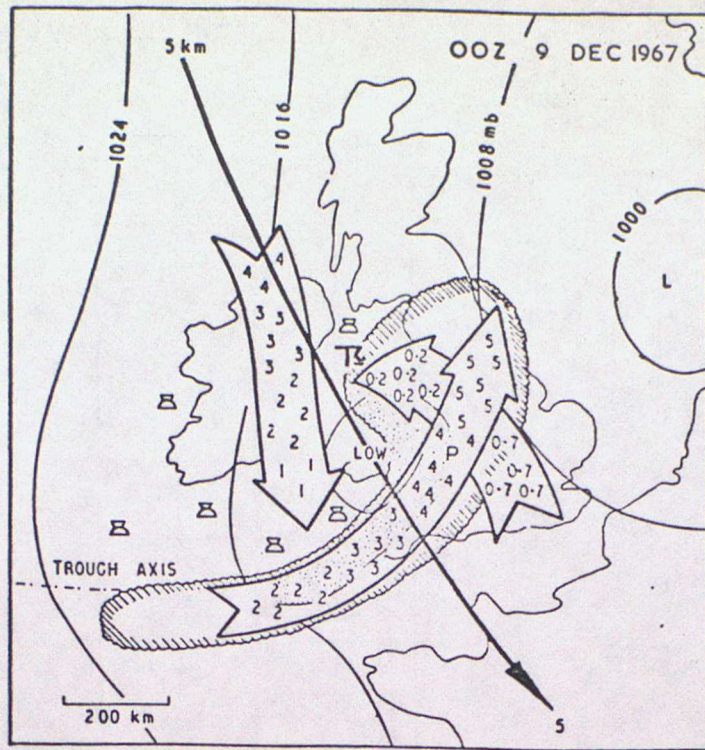


Figure 1 Composite diagram showing flow relative to the polar low, based on Doppler radar and θ_w analyses. Numerals within the flow denote heights in km.

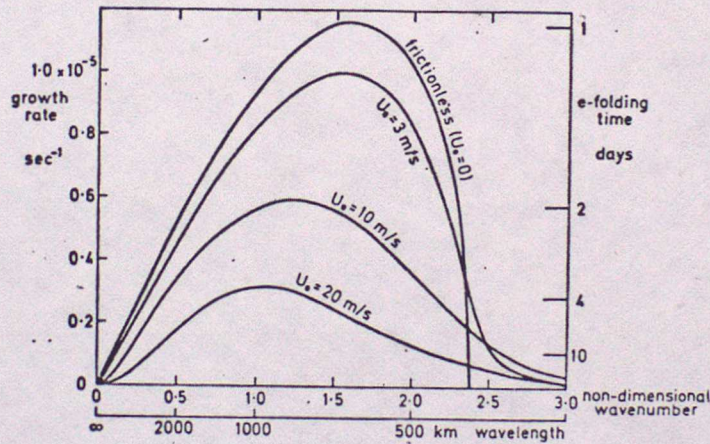


Figure 2 The effect of the inclusion of friction in Eady's model. The growth rate is shown as a function of wavelength for various surface wind speeds (U_0). Other parameters of the mean flow are as listed in section 2.

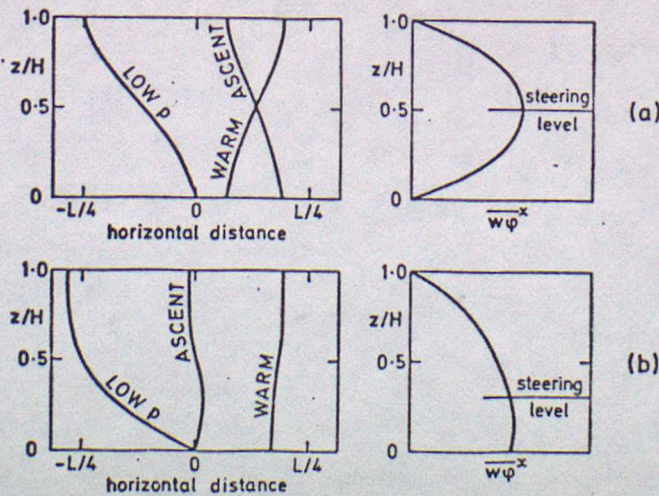


Figure 3 The structure of the growing wave according to the Eady theory, showing the vertical variation of the phases of the pressure, entropy and vertical velocity fields, and the horizontally averaged vertical entropy transport as a function of height: (a) no friction (surface wind speed zero); (b) friction included (surface wind 10 m s^{-1}). Other parameters of the mean flow are as listed in section 2.

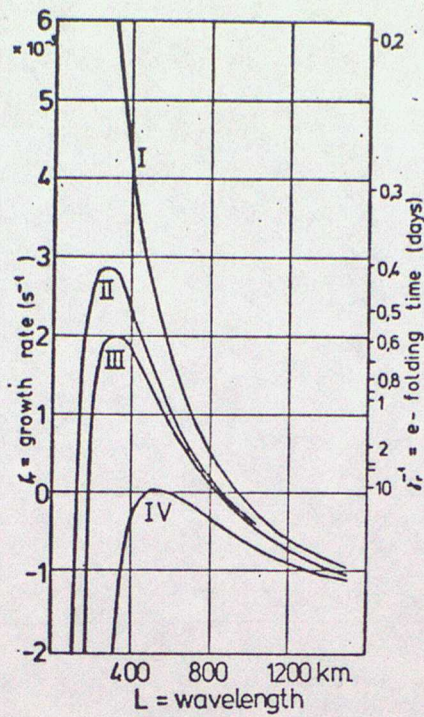


Figure 4 As Fig. 5, but for 'Iceland conditions'. Curves I to IV correspond to $\bar{r} = 0.7, 0.78, 0.8$ and 0.9 , respectively.

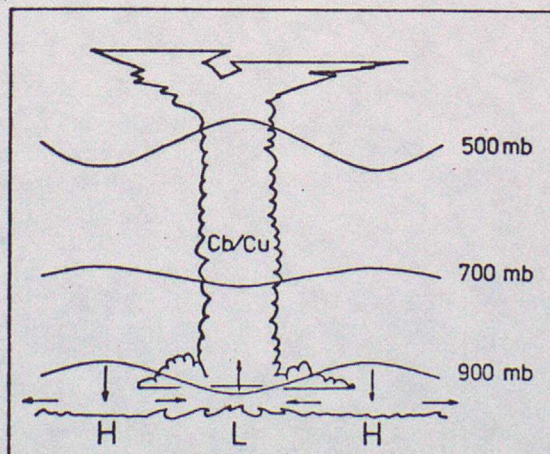


Figure 5 Schematic vertical cross-section through a polar low along the x axis. The arrows indicate horizontal and vertical flow in the Ekman layer.



OROGRAPHIC LOWS

1. Introduction

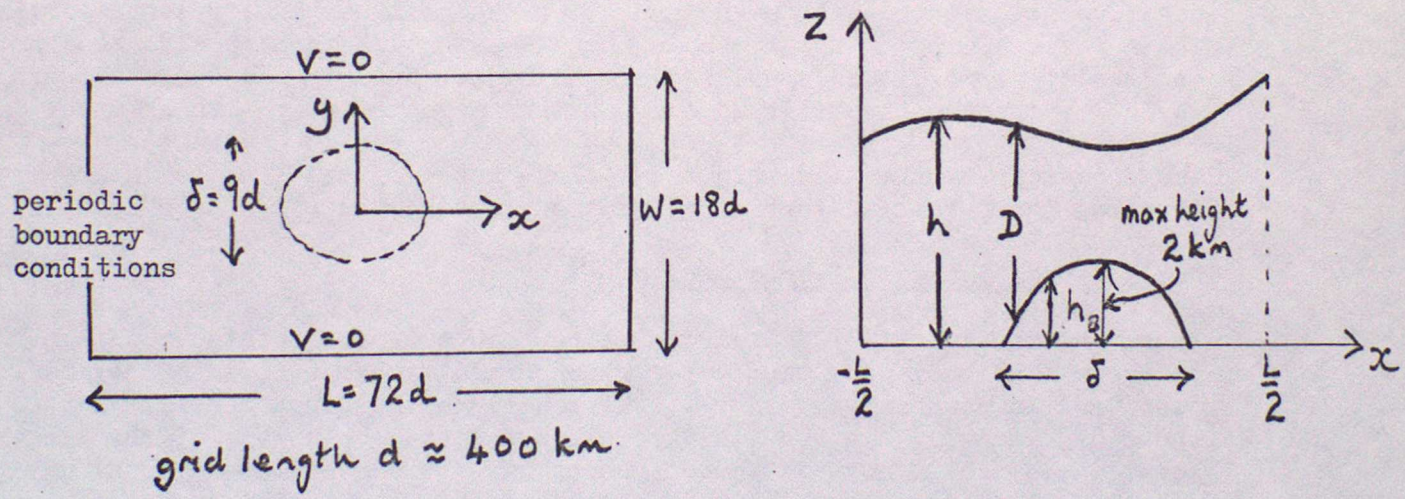
The earth's topography influences the atmosphere on a variety of scales. On the largest scale the extensive mountain complexes, such as the Rockies and Himalayas, force quasi-stationary planetary waves whereas on the small scale hills, valleys and even small undulations in topography cause variations in the boundary layer flow. In between these two extremes there are synoptic scale effects that must be taken into account when trying to predict the weather. For example several investigations have shown that a favoured place for cyclogenesis is in the lee of mountain ranges (e.g. the Rockies) or of isolated massifs (e.g. Greenland and the Alps). Here we will be mainly concerned with the lows that form in the lee of the Alps.

Before discussing these orographic lows further it is important to make a clear distinction between cyclogenesis and the formation of shallow semi-permanent lows that form part of a high-low couplet when there is steady flow over an obstacle. Here we will regard cyclogenesis as referring to baroclinic development leading to a deep cyclone whereas the other kind of low can form in a barotropic flow.

2. Barotropic flow over topography

2.1 The numerical approach

Kasahara (1966) considered the flow of an incompressible, hydrostatic inviscid atmosphere over an isolated hill - such a flow is described by the shallow water equations



Initially uniform zonal flow was assumed

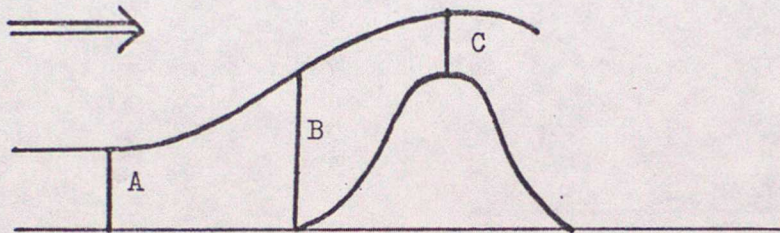
$$u = \bar{u} \quad v = 0 \quad \frac{\partial h}{\partial x} = 0 \quad \frac{\partial h}{\partial y} = -\frac{f\bar{u}}{g}$$

These conditions are solutions of the shallow water equations when there is no topography. Therefore when the topography is introduced the wind and mass fields are not in balance.

Fig 1a shows the results after 2 and 8 days when a constant f is used. Initially a ridge forms over the obstacle with a trough in the lee. Thereafter the ridge remains fixed to the obstacle but the trough is advected downstream. However when f is allowed to vary by using a β -plane approximation a series of waves form as shown in Fig 1b.

The behaviour of the flow can be readily interpreted by considering the potential vorticity equation

$$\frac{d}{dt} \left(\frac{\beta + f}{D} \right) = 0 \quad \text{where} \quad D = h - h_b$$



When f has a constant value f_0 , $(\beta + f_0)/D$ is conserved by a column of air. Suppose that at A there is zero relative vorticity. As the column of air approaches B stretching occurs and so $(\beta + f_0)$ must increase - ζ then becomes positive and the flow acquires cyclonic curvature. The air then ascends the hill and the column shrinks. This causes ζ to decrease and eventually become negative so that the flow over the top of the hill has anticyclonic curvature. The air descending on the lee side then goes through the opposite sequence and the final result is a ridge over the hill. However this does not explain why a lee trough first formed and was then advected away - think about it!

The behaviour of the flow when the β -plane was used can also be interpreted by using the potential vorticity equation (see Holton (1972) for details).

2.2 Some analytical solutions

Buzzi and Tibaldi (1977) also considered flow over an isolated mountain. In their case they were particularly concerned with the Alps so they felt justified in using a constant β . The equations they used were similar to those of Kasahara, but they only considered steady solutions of the linearised equations. The effect of the topography was introduced in the usual way by relating the vertical velocity at the lower boundary to the horizontal wind and the slope of the topography. Surface friction was introduced by using the Charney and Eliassen (1949) expression for the vertical velocity induced at the top of the boundary layer by frictional convergence. Therefore at the lower boundary

$$w_0 = u \frac{\partial h_b}{\partial x} + K \beta$$

where K is related to the eddy viscosity, ν in the boundary layer.

Introducing the horizontal wind scale (\bar{u}), the dynamical vertical scale (H_0) and the horizontal and vertical scales of the obstacle (a and H) it is possible to derive the non-dimensional perturbation equations. When doing this it is found that the flow is described by three non-dimensional numbers - the Rossby number $R_0 = \frac{\bar{u}}{fa}$, the Ekman number $E = \frac{\nu}{fH_0^2}$ and the vertical aspect ratio

$\gamma = \frac{H}{H_0}$. All the perturbation quantities are now expanded in powers of R_0 ($R_0 < 1$)

For example

$$u = \frac{\gamma}{R_0} \sum_{i=0}^{\infty} R_0^i u^{(i)} = \frac{\gamma}{R_0} \left\{ u^{(0)} + R_0 u^{(1)} + R_0^2 u^{(2)} + \dots \right\}$$

These expressions are now substituted into the perturbation equations and it is required that there is separate balance for each order of R_0 . For example the non-dimensional perturbation equation for the x-momentum equation is

$$R_0 \frac{\partial u}{\partial x} - v + \frac{\partial p}{\partial x} = 0$$

and it is easy to show that

$$\frac{\partial u^{(i-1)}}{\partial x} - v^{(i)} + \frac{\partial p^{(i)}}{\partial x} = 0 \quad i=0, 1, \dots$$

where it is taken that when a term has a negative index it vanishes. Once the complete set of equations has been derived it is possible to compute the solution for a given hill and basic flow to any desired accuracy.

When $R_0 \ll 1$ and $E \rightarrow 0$ it is only necessary to use $i=0$ and $i=1$ - this is the quasi-geostrophic case and a solution is shown in Fig 2. As might be expected a ridge forms over the hill in accordance with the potential vorticity argument. When friction is introduced ($R_0 \ll 1$ and $E^2 = O[R_0^2]$) a marked asymmetry is introduced into the flow with the cyclonic vorticity created in the rear over-compensating for the anticyclonic vorticity created on the windward side (see Fig 3). The cyclonic vorticity is advected downwind, but a part of the trough remains attached to the lee of the hill.

Fig 4 shows an actual case when there was southerly flow over the Alps. Buzzi and Tibaldi argued that the existence of the lee trough suggests that friction is important and that the position of the high on the windward side of the Alps rather than over them is an indication that inertial effects are important ($R_0 < 1$, but not small).

3. Lee cyclogenesis

3.1 Observational studies

Buzzi and Tibaldi (1978) have studied in some detail the deep and rapid cyclogenesis that occurred in the lee of the Alps on 3 April 1973. This case is typical of lee cyclogenesis and the surface developments are shown in Fig 5.

On 2 April a deep low moved eastwards across Northern Europe. The associated surface cold front moved southeastwards and impinged on the Alps (as $t-t_0$ say). The low level cold advection is retarded in the mountain region until most of the cold air has started to flow round, rather than over, the mountain. This produces a pronounced deformation of the low level thermal field which gives rise to a small scale baroclinic vortex in the lee area (at $t=t_0+6$ hrs). The upper level vorticity advection associated with the movement of the planetary scale trough is only weakly slowed down and eventually it reaches the genesis region ($t=t_0+12$ hrs). From then on the cyclone develops and becomes more vertically coherent (it may extend throughout the troposphere); at the same time the horizontal scale of the vortex grows. The vortex then drifts away from the lee region and undergoes the "normal" development of mid-latitude disturbances.

In the upper air a cut-off low forms in the vicinity of the mountains and it appears that the main effect of the mountains is to cause the cut-off low to form in the lee of the Alps rather than downstream.

Now consider in more detail the initial formation of the lee low. Using the definition of geostrophic vorticity and the hydrostatic equation we get

$$\frac{\partial \zeta}{\partial \ln p} = -\frac{R}{f} \nabla^2 T \quad \text{hence} \quad \frac{\partial \zeta}{\partial z} \propto \nabla^2 T$$

In the lee of the Alps the thermal deformation causes $\nabla^2 T < 0$ and so ζ increases towards the surface producing a low level cyclonic circulation. This in turn advects warm air from the SW and this enhances the deformation of the thermal field. There is now cold air descending in the western lee area and ascent on the eastern edge of the obstacle - hence there is a baroclinic eddy with APE being converted to eddy kinetic energy.

3.2 Numerical modelling - idealised simulations

Egger (1972) made the first significant attempt at using a numerical model to simulate cyclogenesis in the lee of the Alps. He grew a baroclinic wave in a channel and allowed it to impinge on a mountain barrier that resembled the Alps. The blocking effect of the barrier was enhanced by having vertical walls with the wind speed normal to the barrier set to zero. Egger showed that it was possible to produce lee cyclogenesis and his diagnostics revealed the importance of the vertical variation of advection and the horizontal deformation of the thermal field. The importance of the arc-shaped barrier was investigated by replacing it by a straight one; it was found that the new barrier did not cause cyclogenesis.

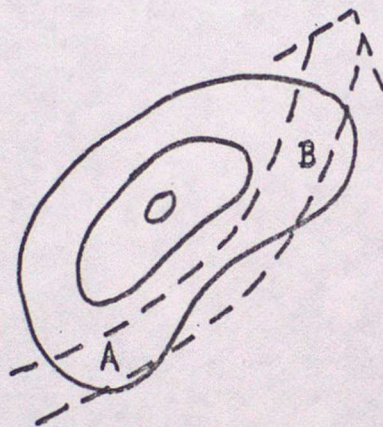
Buzzi et. al. (1979) carried out some similar experiments but they grew both the baroclinic wave and the mountain. Using a channel model they allowed a perturbation to develop on a baroclinically unstable current. After 96 hours it has a large amplitude and it was then that they grew an arc-shaped mountain in front of the advancing cold front. A control was also run in which the ground remained flat.

Fig 6 shows the experimental run. At $t_0 = 96$ hr the baroclinic wave had a realistic structure. During the next 24 hrs a high-low perturbation formed near the Alps and by $t_0 + 24$ hr the cold front reached the top of the Alps.

Cyclogenesis then started and by $t_0 + 36$ hr there was a closed circulation throughout the lower troposphere. Clearly the cold front has slowed down, but cold advection continues to the SW and NE of the mountains. Further deepening occurred during the next 12 hrs while the low remained stationary; the cold front continued to advance around the side of the Alps and frontogenesis occurred in the NE. By $t_0 + 60$ hr the lee cyclone drifted away from the lee region and began to fill. At 500 mb development continued and a closed circulation formed. This occurred about 24 hours after the surface low first formed whereas in reality it takes 6 to 12 hours. Straightening the mountain range only had the effect of slightly weakening the cyclogenesis.

A detailed study of the vertical velocity field revealed a two stage evolution of the initial disturbance.

- (i) The prefrontal SW'ly flow is forced to descend at A and rise at B



- (ii) The front moves over the mountain, but slower than in the secondary regions. This causes the thermal advection field to become correlated with the existing vertical velocity field; APE is then released.

3.3 Numerical modelling - real data simulations

Both Bleck (1977) and Tibaldi and Janjic (1977) have tried to model the 3 April cyclogenesis. They used completely different models, but both found that

- (i) the models predicted the cyclogenesis in the right place with about the correct intensity.
- (ii) both models failed to develop the 500 mb cut-off flow.

Messinger et. al. (1979) have used a more sophisticated model with a high resolution, time dependent boundary conditions and physical parameterisations. In the case they studied they found that the cut-off low did develop. However a cut-off low formed in almost the same place even when there were no mountains. The time dependent boundary conditions and parameterisations modified the cyclogenesis but were not essential for it.

4. Conclusions

Both the observational studies and numerical simulations emphasise the three stages of lee cyclogenesis

- (i) deformation of the thermal field due to orographic blocking causes a low level disturbance to form
- (ii) this disturbance triggers baroclinic instability that causes the disturbance to deepen rapidly
- (iii) developments aloft, which are initially independent of the low level changes, came into phase with the low level vortex and cause the disturbance to grow both vertically and horizontally.

This means that the scale of the changes in the flow brought about by the topography are on a larger scale than the topography itself.

5. References

In this lecture extensive use has been made of the following review articles.

Tibaldi, S., 1980, E.C.M.W.F. Seminar 1979, Vol. 2, 130-166

Other references are.

Bleck, R., 1977, M.W.R., 105, 428-445

Buzzi, A. and Tibaldi, S., 1977, Q.J.R.M.S., 103, 135-150

Buzzi, A. and Tibaldi, S., 1978, Q.J.R.M.S., 104, 241-287

Buzzi, A. et.al., 1979, E.C.M.W.F. Workshop on mountains and N.W.P., 166-208

Charney, J.E. and Eliassen, A., 1949, Tellus, 1, 38-54

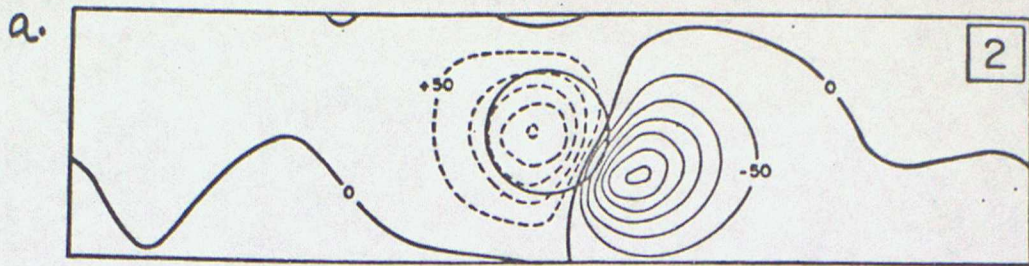
Egger, J., 1972, Beitr. Phys. Atmos., 45, 320-346

Holton, J.R., 1972, An introduction to dynamic met.

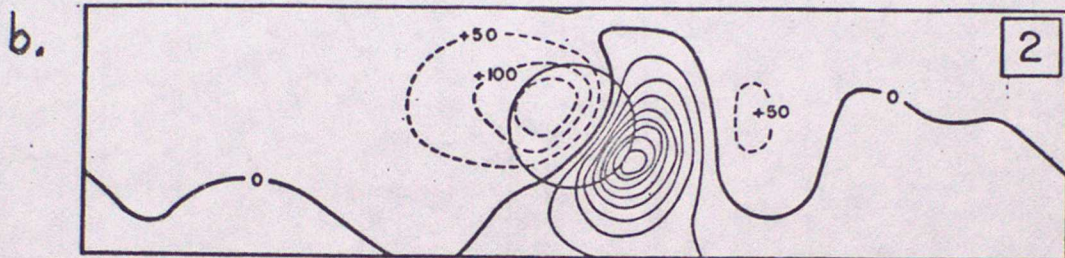
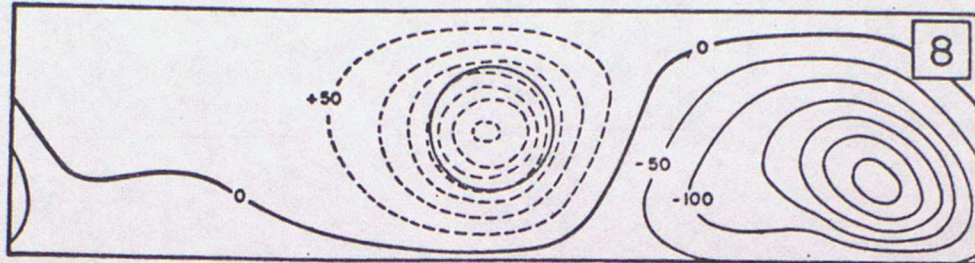
Kasahara, A., 1966, J.Atms.Sc., 23, 259-271

Messinger, F. et.al., 1979, Euromech Colloquium 2-5 April 1979

Tibaldi, S. and Janjic, 1977, GARP Mountain Subprogram, Venice



f constant



f variable

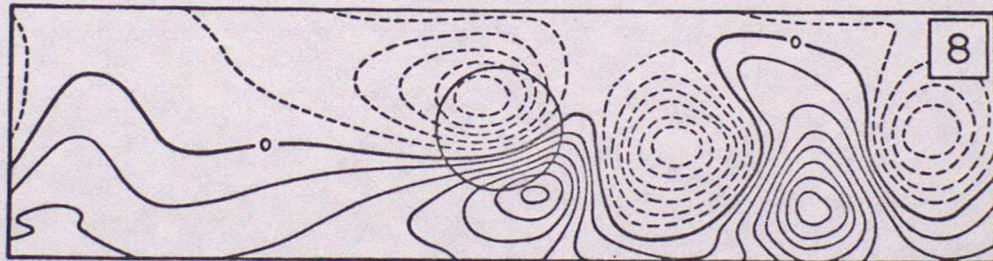


Figure 1

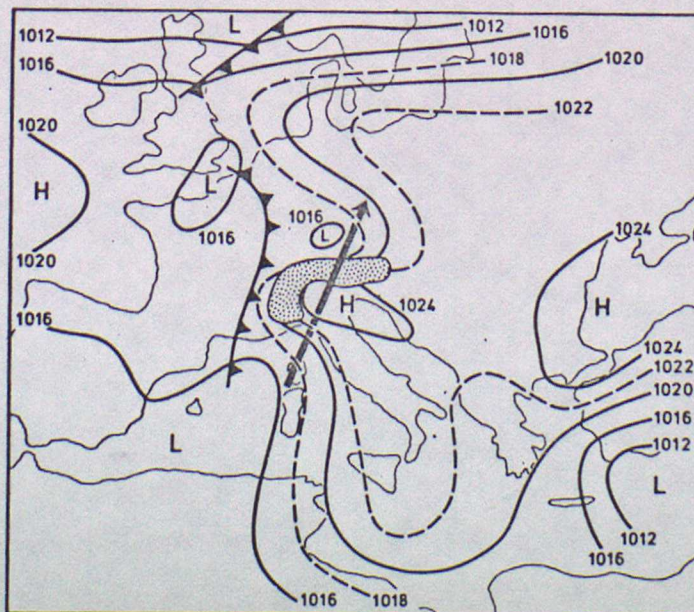


Figure 4. Surface analysis 16 September 1975, 1500 GMT. The thick black arrow indicates the direction of 700 mb flow over the Alps at the same time; and the dotted area presents a rough profile of the Alps.

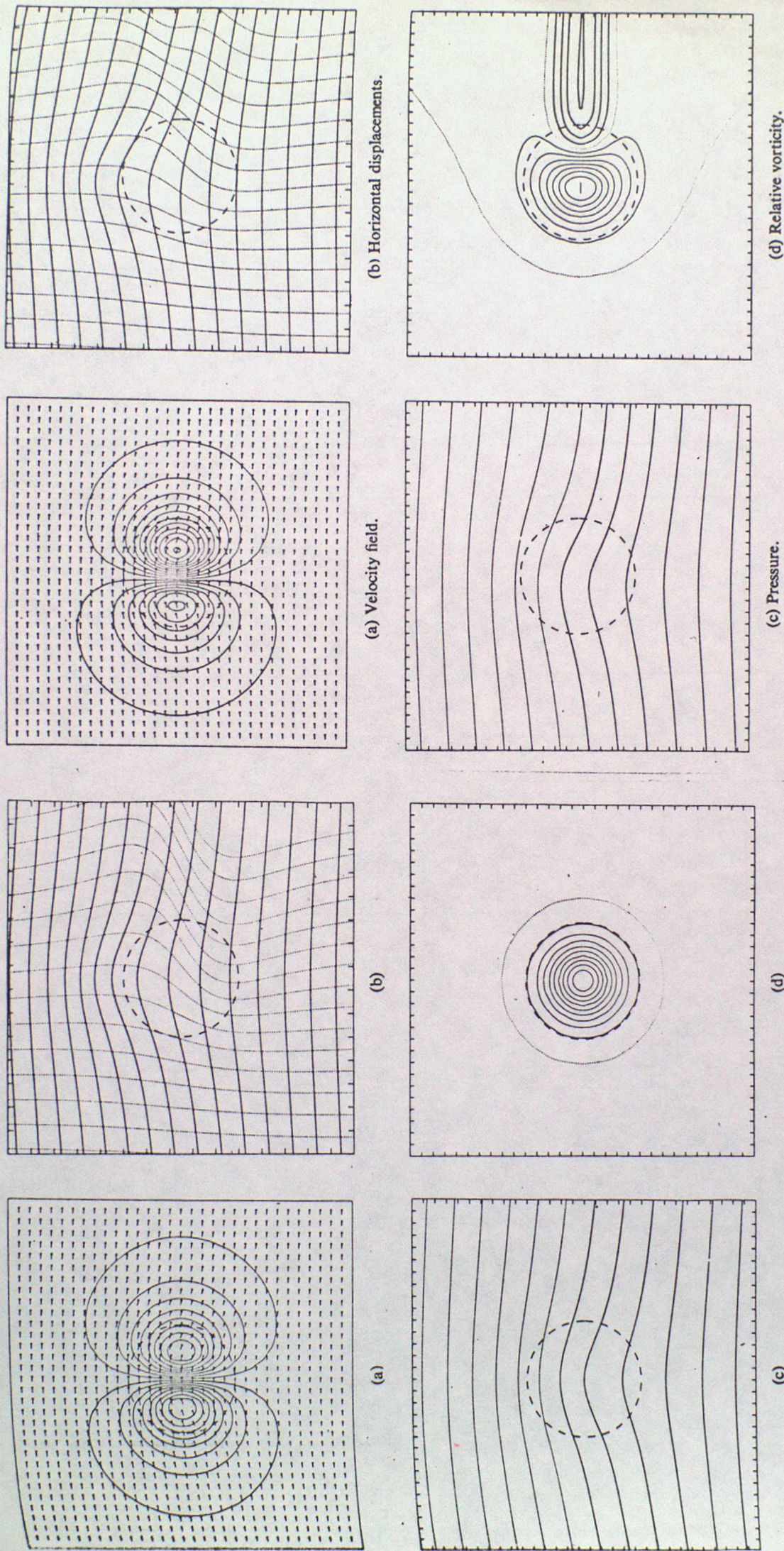


Figure 2. Quasi-geostrophic case. All quantities are non-dimensional. The dashed circle of radius unity represents the height contour of the obstacle at $\sqrt{1/4}$ of the top height. $Ro = 0.1$; $\gamma = 0.1$; $E = 0$.

(a) Arrows represent horizontal velocity, isolines vertical velocity; thick lines upwards, thin lines downwards. Isolines drawn at intervals of 0.1. Plane $z = 0$.

(b) Full lines are lines of lateral displacement, hence streamlines in the linear approximation; dotted lines are lines of longitudinal displacement, hence successive positions of a straight line of tracer released at $x = -\infty$. Plane $z = 0$.

(c) Isolines of pressure at intervals of 0.5 at $z = 0$. The dotted line marks the pressure value of the basic state at $y = 0$. Pressure decreases towards the top of the figure.

(d) Vertical component of relative vorticity: isolines drawn at intervals of 0.2. Plane $z = 0$. Thick lines cyclonic, thin lines anticyclonic, dotted line zero vorticity. In this particular example the positive vorticity region far from the mountain is weaker than 0.2 so no thick isolines appear.

Figure 3. Frictional case. $Ro = 0.4$; $\gamma = 0.4$; $E = 0.025$. Plane $z = 0$. For more specifications see Fig. 1.

(a) Velocity field.
 (b) Horizontal displacements.
 (c) Pressure.
 (d) Relative vorticity.

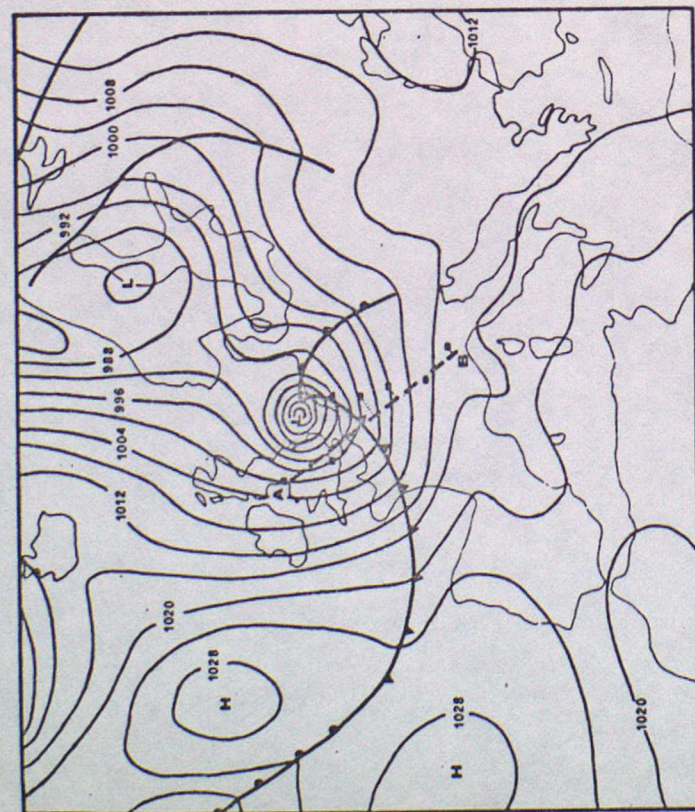


Fig. 5 (a). 2 April 1973, 12 GMT

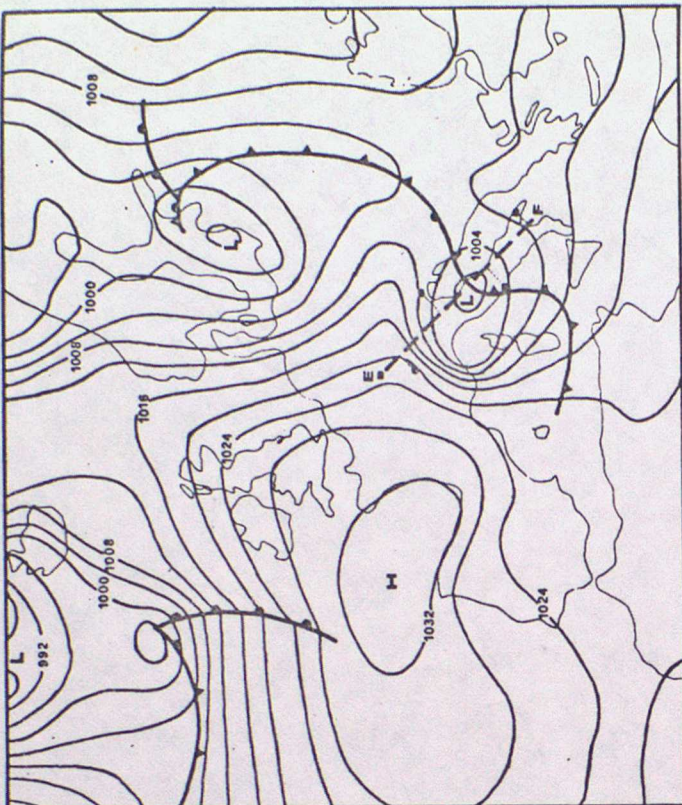


Fig. 5 (c). 3 April 1973, 12 GMT



Fig. 5 (b). 3 April 1973, 00 GMT

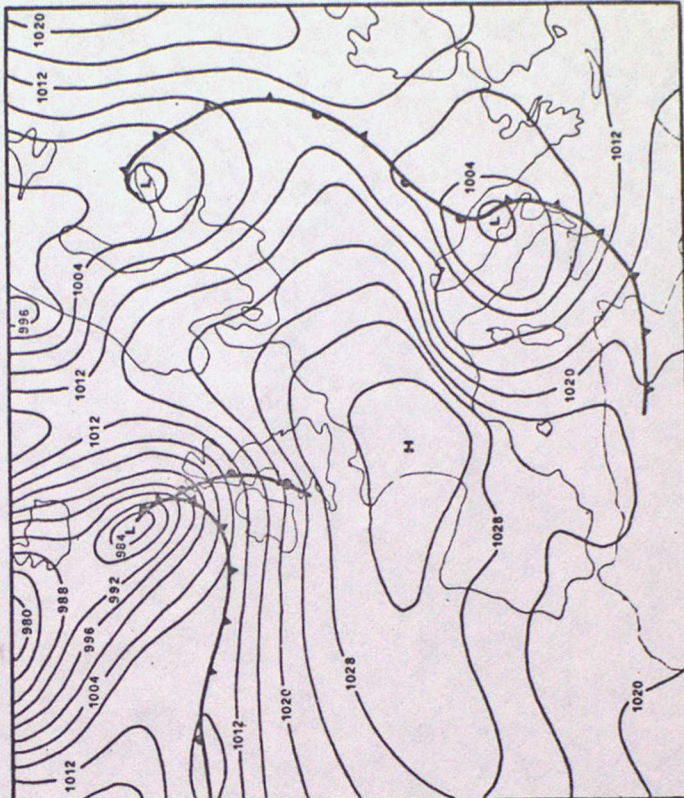
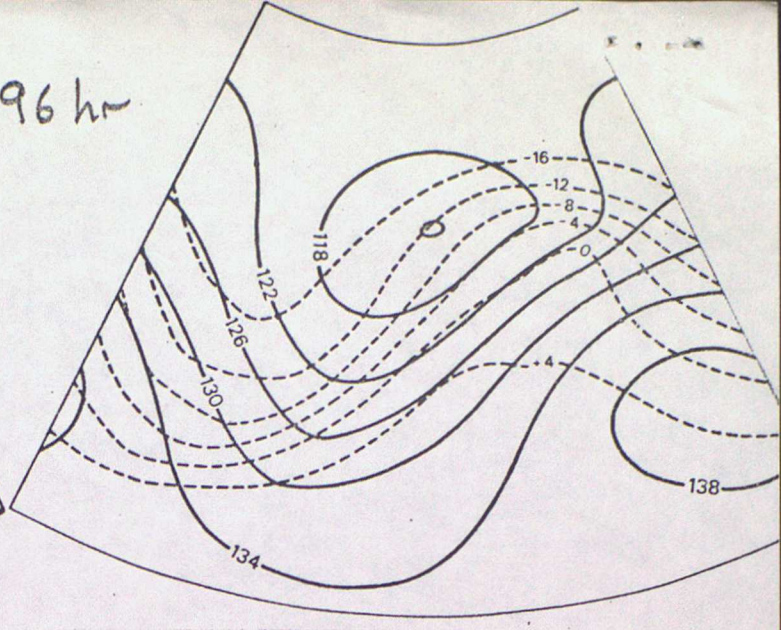
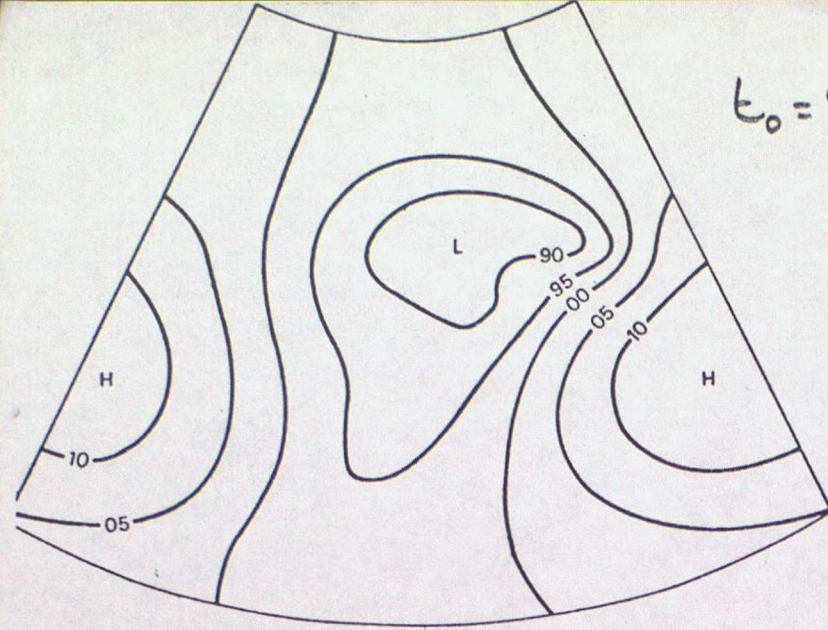


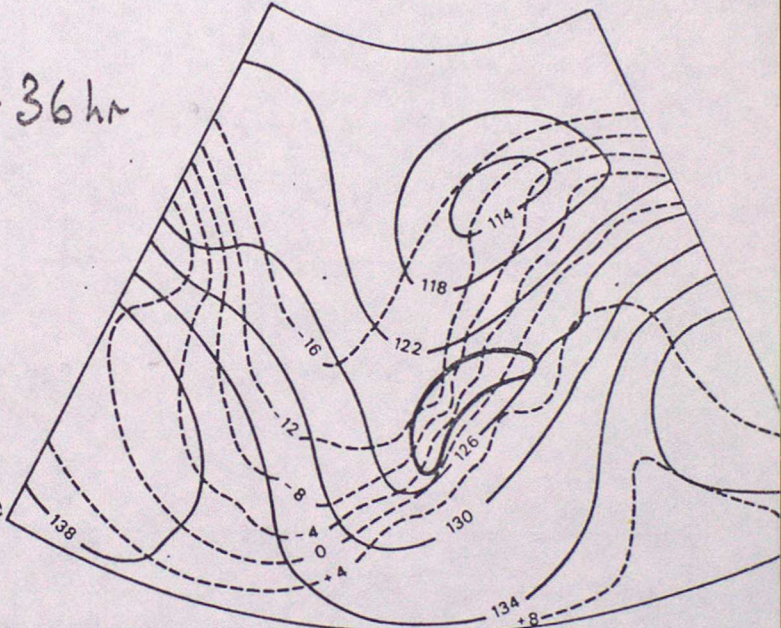
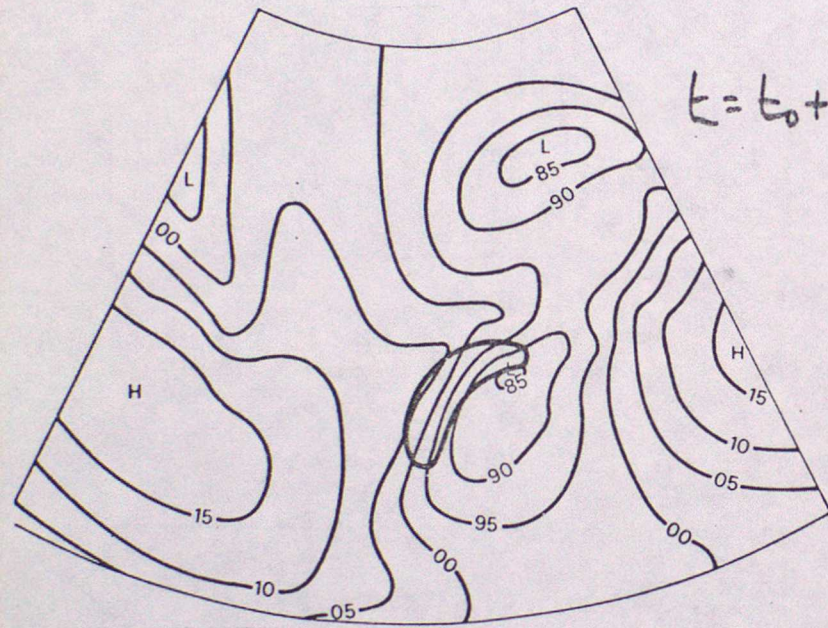
Fig. 5 (d). 4 April 1973, 00 GMT

Figure 5

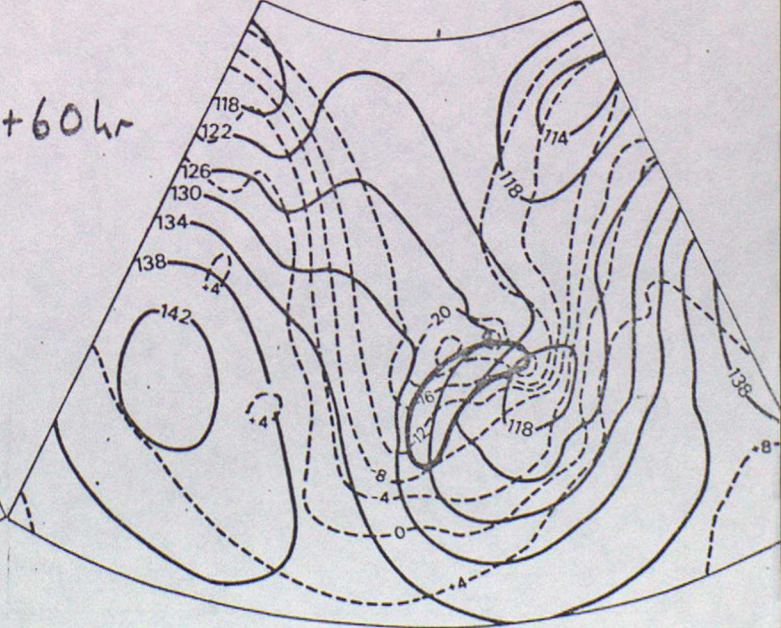
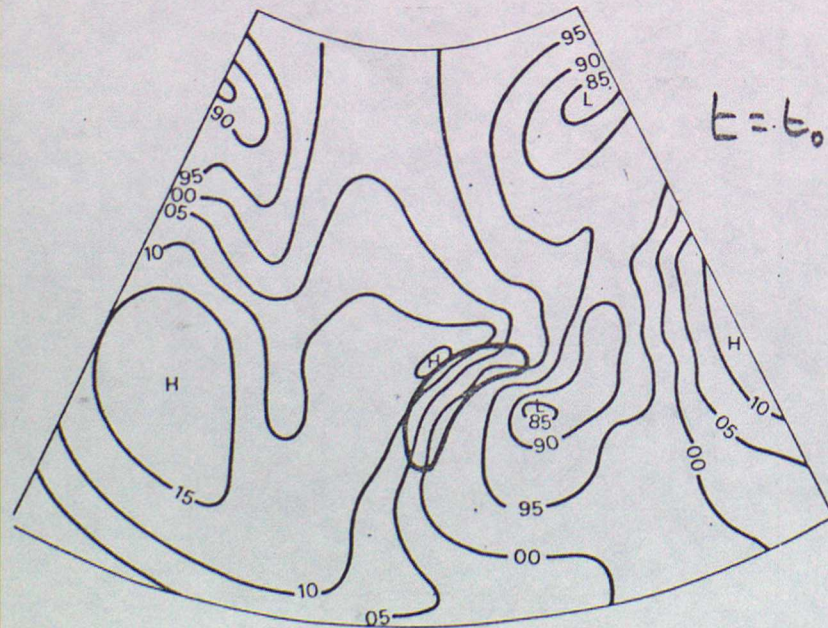
$t_0 = 96 \text{ hr}$



$t = t_0 + 36 \text{ hr}$



$t = t_0 + 60 \text{ hr}$



Surface Pressure

850 mb Geopotential and Temperature

Figure 6



TORNADOES

1. Introduction

Tornadoes are narrow vortices with violently rotating winds which extend from the parent cloud down to the ground. The very low pressure in the vortex leads to condensation of the subcloud moisture so that the vortex appears as a narrow cloud protruding from the base of the cloud and reaching down to the ground. Sometimes the tornado does not reach the ground so there is a suspended funnel cloud. Nearly all tornadoes rotate cyclonically although it is thought that anticyclonic ones may occur. Tornadoes are very destructive, but fortunately only occur in less than 1% of thunderstorms in the U.S.A. However this still represents about 700 reported tornadoes.

Most tornadoes are small and are on the ground for only a few minutes - they cause light damage along a path that's typically 60 m wide and 2 km long. These tornadoes form on the right rear flank of severe thunderstorms where new convective cells are continually developing (the pseudo-cold front caused by the rain-cooled downdraught).

The most severe tornadoes (consisting of about 5% of those reported) are responsible for most of the destruction. They may exist for several hours and create damage paths many hundreds of metres wide and several hundred kilometres long. The maximum winds are in the range 75 to 110 ms^{-1} and the pressure drop is in excess of 100 mb. These tornadoes develop under the updraught of massive rotating thunderstorms (often called tornado cyclones or mesocyclones). Unlike the more common Cb which have a multicell structure, these storms have a single intense updraught in the form of a supercell. Also in these storms dry air enters the system at mid-levels, is cooled by precipitation, and then flows cyclonically around the updraught as it descends. It is thought that the shearing region separating the updraught and downdraught may provide a suitable vertically orientated vorticity source for tornadogenesis.

For tornadogenesis we require a source of ambient rotation and a driving mechanism for concentrating it.

2. Observational studies

Burgess et. al. (1975) used Doppler radar, along with extensive photographic evidence, to investigate the 1973 Union City Tornado. The radar gave digital velocity measurements inside the parent thunderstorm and they related these to the observed position of the tornado. They found that the tornado position was marked by radial velocity maxima of opposite sign between two radar range gates of adjacent azimuth (the gates were about 1 km apart). This large shear has become known as the tornadic vortex signature (TVS) - see Figs 1 and 2.

The study of the TVS showed that it originated in storm mid-levels and descended progressively to lower levels reaching cloud base coincident with the appearance of the funnel cloud; after touchdown the tornado and TVS moved together. As the tornado shrank and decayed the TVS decreased at all heights, and after the tornado had dissipated the TVS was no longer detectable.

This evidence suggests that the tornado is initiated from above by convergence of existing cloud circulation - it is likely that the large accelerations associated with the cloud updraught are responsible for the convergence.

3. Laboratory models

There have been a number of experiments designed to generate concentrated vorticity in rotating tanks. In each case vortices are produced by using a driving force operating over a limited region of the axis to concentrate vorticity from the initial state of solid rotation. Turner and Lilly (1963) used a water tank and the vortices were driven by the drag exerted on the fluid by gas bubble released near the axis. They found that vortices were only produced within a certain range of rotation and bubble rates.

Care must be taken when trying to interpret these experiments in terms of atmospheric tornadogenesis. For example in the experiments there are lateral walls, forced axial updraught and no condensation. Also it was found that the Rossby number (defined in an appropriate way for vortices) was much too low in the experiments. Despite these problems Leslie (1971) constructed a numerical model in order to try to simulate and understand the laboratory models.

4. A model of tornadogenesis - Leslie (1971)

To simplify the problem Leslie got rid of the buoyancy variable by having a body force term in the vertical momentum equation. This was kept constant and was only non-zero in a narrow region around the axis of rotation. Initially the fluid is solid body rotation and then the body force is imposed at $t=0$; the equations are then integrated forward in time until a steady state is reached.

When there is no rotation the steady state streamlines show that the body force draws liquid from all parts of the bottom half of the tank (see Fig 3a). Now when the tank rotates the streamlines crowd together along the axis showing strong axial flow (see Fig 3b); note also the strong boundary layers at the top and bottom that control flow into and out of the vortex. The zonal velocity (Fig 3c) shows that over the tank there is cyclonic flow whose intensity increases towards the axis with a maximum of 20-30 times the rotation rate of the tank.

The evolution of the stream-function reveals that the vortex grows downward - the explanation is as follows. When the body force is turned on the fluid in the region of the body force converges. Angular momentum is conserved so the converging fluid increases its relative cyclonic vorticity. The fluid continues inwards until there is a local balance between the centrifugal force and the radial pressure gradient. At levels where balance is achieved further radial entrainment is inhibited. However entrainment is possible further down and so the vortex extends downwards until it reaches the lower boundary. Here cyclostrophic balance is no longer possible due to the friction and so an intense shallow inflow layer forms. The interaction with the boundary causes accelerated amplification because the bottom boundary layer can support a considerable pressure gradient - hence there is a reduction in pressure throughout the core and a strengthening of the vortex.

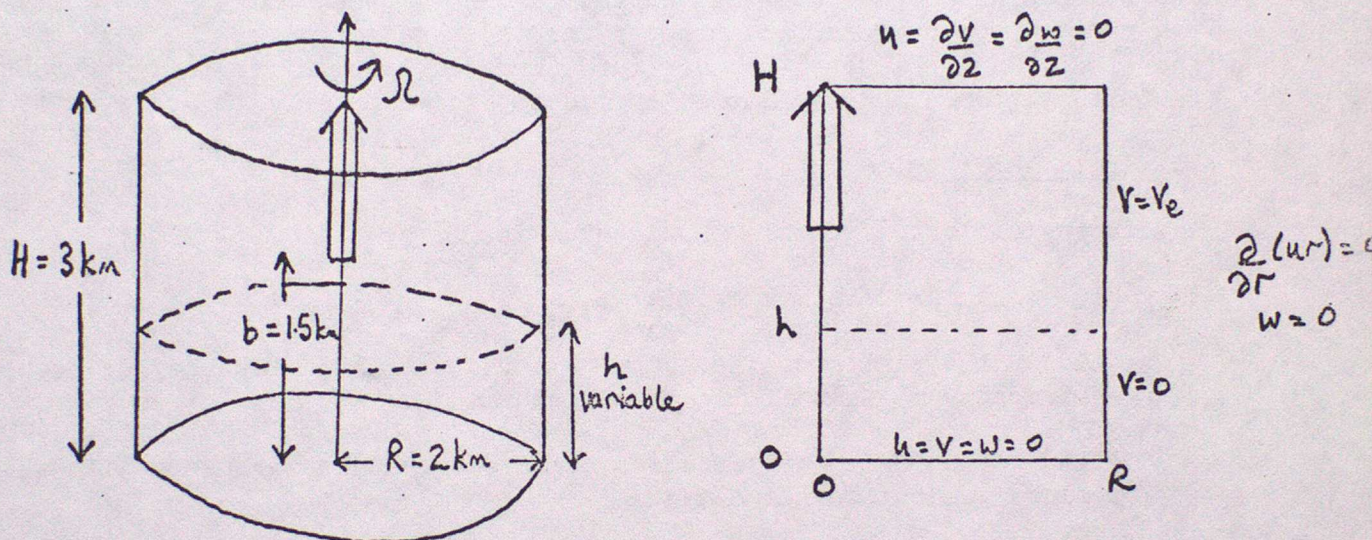
The formation of the vortex depended critically upon the strength of the body force. If it was too strong balance was never achieved whereas if it was too weak balance is obtained after only a small radial displacement and a concentrated vortex never forms.

These experiments provide some insight into why tornadoes grow downwards and why only a fraction of apparently suitable storms produce tornadoes.

5. Effect of low level rotation - Smith and Leslie (1978)

In the previous experiment there was always a sufficient supply of ambient low-level rotation so that whenever a vortex formed it always extended down to the lower boundary. However the most severe tornadoes form beneath a severe storm where the only source of ambient rotation is aloft in the storm itself. This led Smith and Leslie to examine the effect on tornadogenesis of the distribution of low level rotation. They used a similar model to that developed by Leslie, but altered the boundary conditions to that

- (i) air could enter or leave the cylindrical domain through the lateral or upper boundaries
- (ii) a swirling velocity could be imposed over a portion of the side boundaries



When $h = 1.5$ km was used (no ambient rotation below this height) the vortex developed downwards but as this happened the vortex was fed by air with less and less rotation until cyclostrophic balance could not be attained at any radius. The vortex cone then terminates aloft and there is a steady suspended vortex (see Fig 4a and 4b). When $h = 0.75$ km was used the vortex extended down to the ground (see Fig 4c and 4d) and compared with the $h = 1.5$ km case the vortex is narrower and more intense. Reduction to zero had little further effect other than to make the vortex stronger. These experiments provide an explanation of why not all pendant funnel clouds evolve to the tornado stage.

The results described here are encouraging, but problems remain. The body force used (chosen by trial and error) is much larger than might be anticipated in a thunderstorm; also the lateral extent of the model forcing is too small. Another problem is that the body force acts along the axis and this ensures axial upflow. In reality there is some evidence of axial downflow.

6. More realistic simulations - Smith and Leslie (1979)

So far all the models have used a body force to simulate the effects of the large updraughts. However it hasn't been possible to determine a realistic body force from buoyancy data so there is some doubt about whether the buoyancy field in a real storm could produce tornadoes in the way the models do.

To investigate this problem Smith and Leslie (1979) extended their earlier model so that the thermodynamic and moisture equations were included. Water vapour was allowed to condense to form cloud liquid water which carried aloft in the updraught (i.e. no precipitation). Initially the air is at rest and the potential temperature and humidity distribution were such that there was conditional instability. Then a potential temperature excess of 2°C was imposed over a cylindrical region in the centre of the domain and during the subsequent integration air passing through the porous side walls acquired a swirling velocity. In the early stages of the integration the temperature perturbation initiated motions that released the conditional instability and a cloud formed. As the cloud updraught became established it acquired rotation and vortex development ensued.

The vortex developed in a similar way to those in previous simulations with the vortex growing downwards and eventually reaching the ground. However now the vortex was also advected upwards so that the vortex extended over the full height of the computational area. This is consistent with the TVS which only varies slowly upwards and reaches heights of at least 10 km. As the imposed swirling velocity was increased the vortex became weaker and broader and the penetration of the pendent funnel cloud decreased. This happened because the increased swirling velocity increased the centrifugal force and so allowed cyclostrophic balance to be achieved at large radii.

7. Last thoughts

Any theory of tornadogenesis should explain

- (i) their downward growth
- (ii) the rarity of the event compared with the frequency of occurrence of what appear to be suitable thunderstorms
- (iii) the rarity of tornadoes compared with the frequency with which storms produce pendent funnel clouds.

The theories described here appear to explain all of these. However we have not considered how the meso-scale rotation is generated on the cloud scale.

8. References

- Burgess, D.W., et. al., 1975, Geoph.Res. Letters, 2, 183-184
- Leslie, L.M., 1971, J.Fluid Mech., 48, 1-21
- Smith, R.K. and Leslie, L.M., 1978, Q.J.R.M.S., 104, 189-198
- Smith, R.K. and Leslie, L.M., 1979, Q.J.R.M.S., 105, 107-128
- Turner, J.S. and Lilly, D.K., 1963, J.Atms.Sc., 20, 468-471

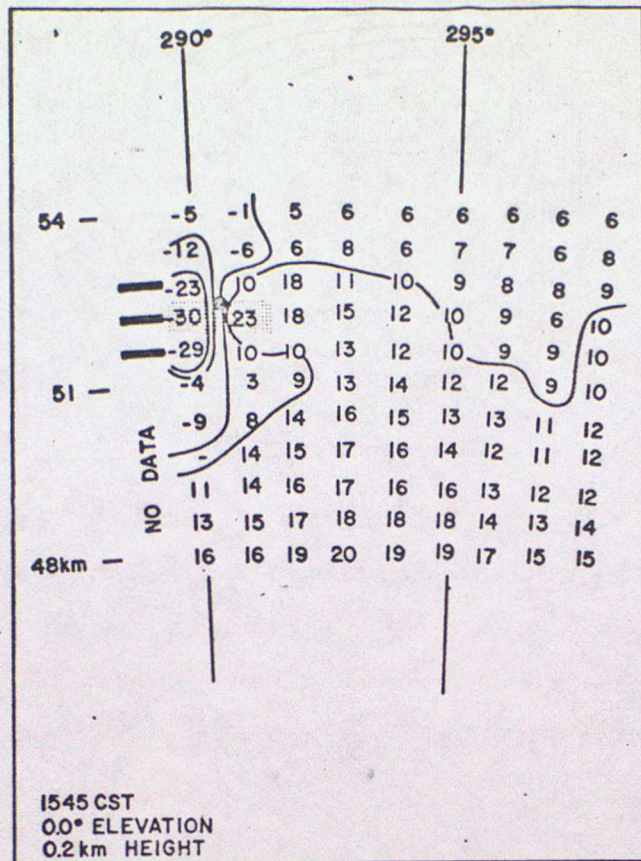


Figure 1. Gate-to-gate shear (GGS) signature (stippled) within a field of single-Doppler mean velocities (m s^{-1}). Velocities are relative to GGS motion. Short dash mark indicates no data and dark dot indicates tornado location. Dark rectangles show relative range gate size. Radar azimuths and ranges are included.

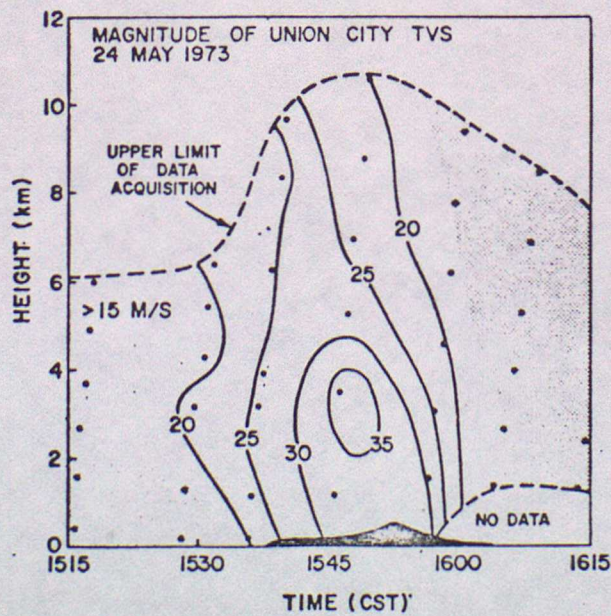


Figure 2. Time-height profile of the magnitude of the maximum Doppler velocity for each Union City TVS pair (adjusted for TVS motion). Dots indicate data points and dashed lines represent the limits of data collection. Velocity shear was less than the TVS threshold value in the lightly shaded regions. The black region at bottom centre is the diameter (using ordinate scale) of the tornado funnel near cloud base (after Brown *et al.* 1978).

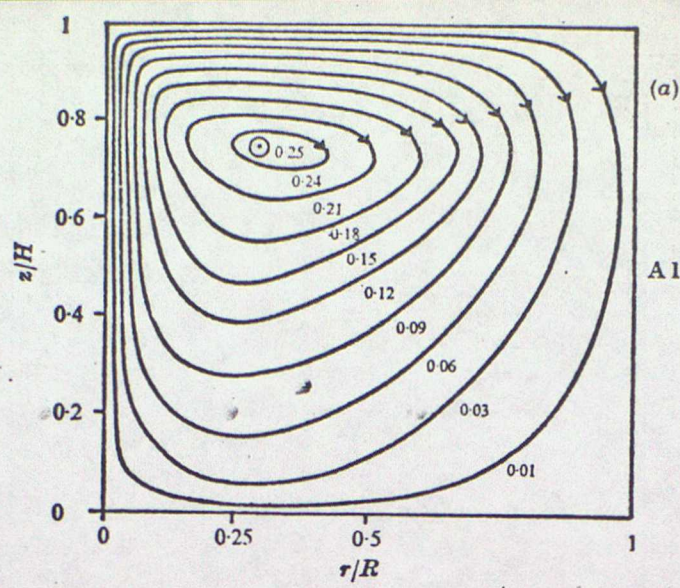


Fig 3a. Contours of the steady state streamlines (non-rotating tank)

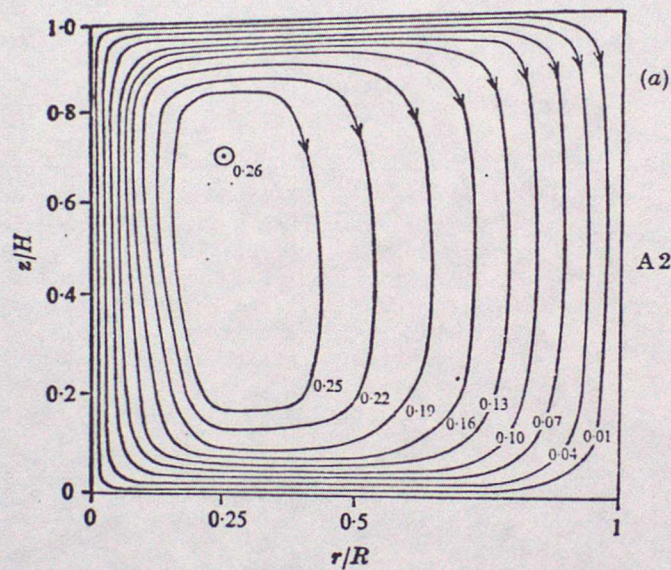


Fig 3b. Contours of the steady state streamlines (rotating tank)

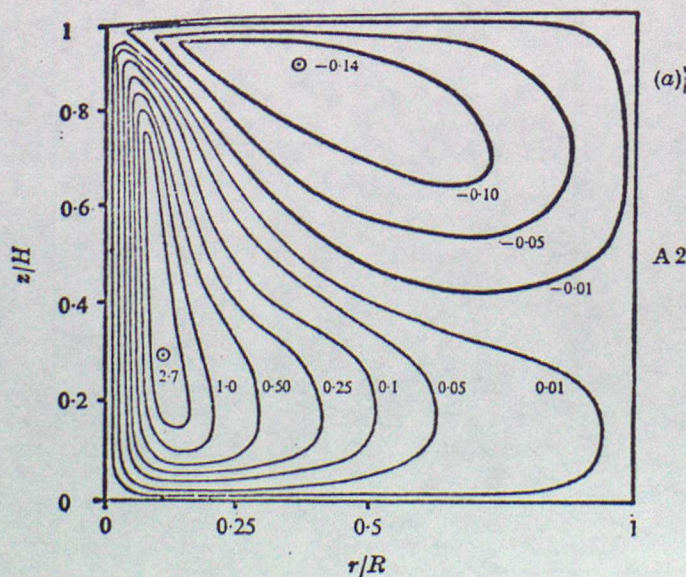
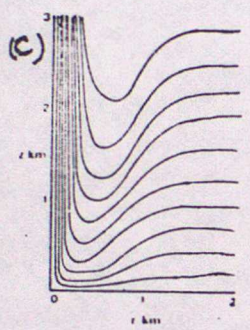
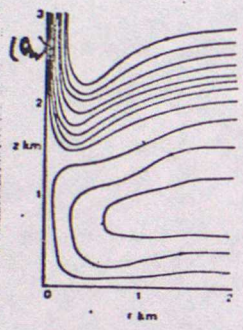


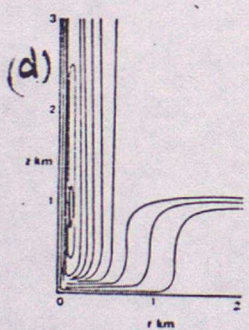
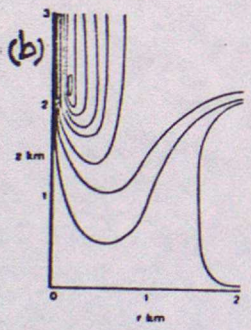
Fig 3c. Zonal velocity contours at steady state (rotating tank)

$h=1.5\text{ km}$

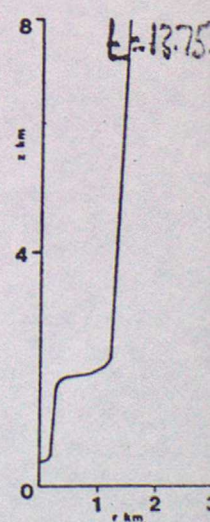
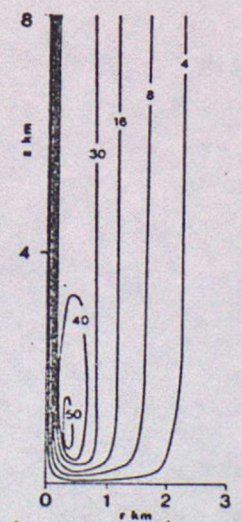
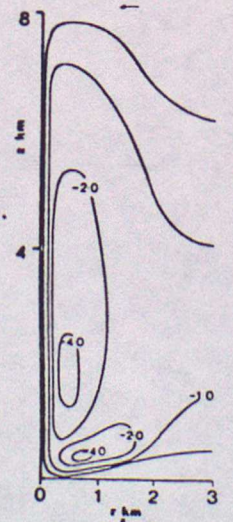
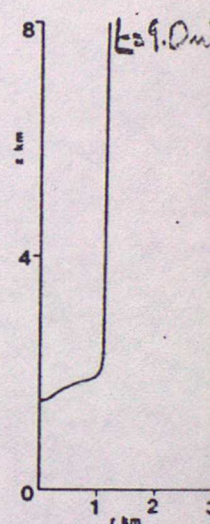
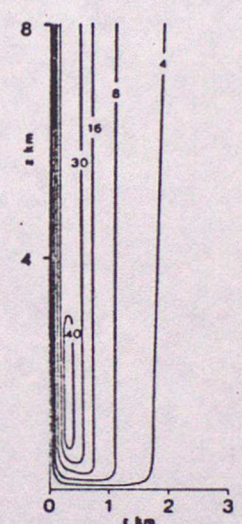
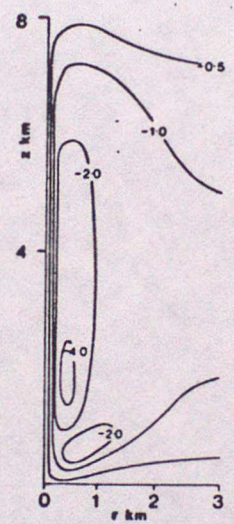
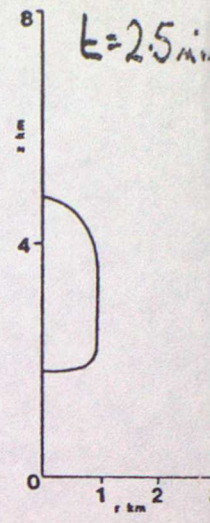
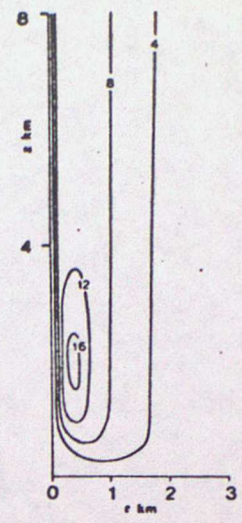
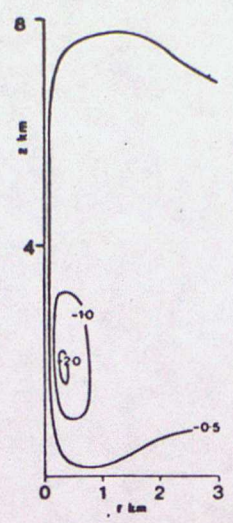
$h=0.75\text{ km}$



streamlines



swirling velocity
Figure 4

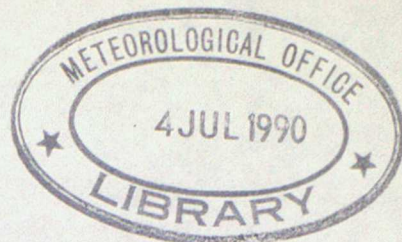


radial flow

tangential flow

cloud outline

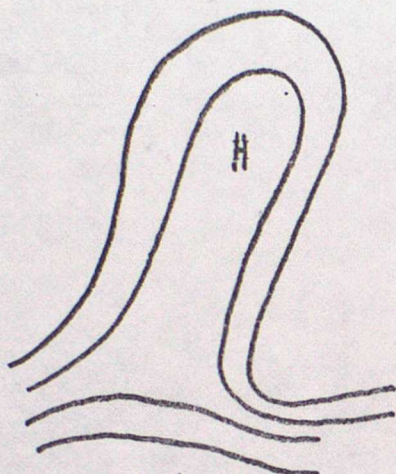
Figure 5



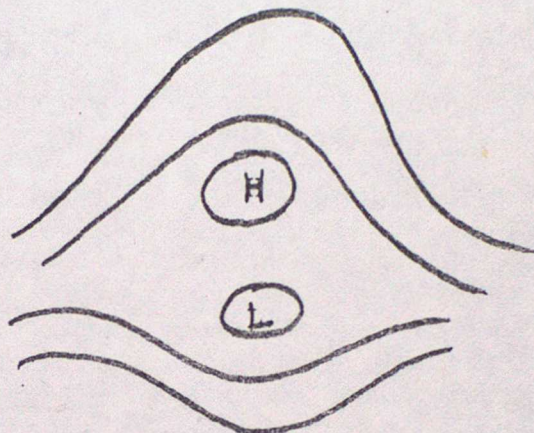
BLOCKING

1. Introduction

A block is a stationary high pressure cell that persists in a region where westerly winds are usually found. The anticyclonic circulation extends throughout the troposphere (indicating the barotropic nature of the flow) and the cell is warm in the troposphere and cold in the stratosphere. There are two main types of blocks



Meridional type



Diffluent type

The meridional type is essentially a single ridge of very large amplitude. This type tends not to persist although it may turn into the diffluent type which is the most common and the usual configuration for long lasting blocks.

The position of the atmosphere affected by a block varies a great deal. Short lived blocks (lasting about 1 week) appear localised whereas more persistent blocks, such as the one in 1963, affect the whole of the troposphere and stratosphere.

2. Some statistics

Rex (1950) investigated the statistical behaviour of blocks. In his work he used a strict definition of blocks that excluded large wave like perturbations in the zonal flow (nowadays the definition of blocking has been relaxed). Some of his results are as follows

(i) Fig 1 shows that there are two preferred geographical locations - one in the Pacific and one in the Atlantic. Later work has indicated that the position of the Atlantic blocks varies more than shown and that the range of Pacific blocks should be shifted about 20° westward. Nearly twice as many blocks occur in the Atlantic as in the Pacific.

(ii) Fig 2 shows the marked seasonal variation with a spring maximum and summer minimum; there are also substantial variations from year to year.

(iii) The time scale of the blocks ranges from several days to over a month; the most frequent duration is about 2 weeks.

(iv) The blocks have a characteristic variation in position. In the initial phases the blocks tend to retrogress, but in their final stages they move eastward.

Taljaard (1962) has examined blocks in the southern hemisphere and found that they are quite frequent in late winter and early spring especially in the region 135°E to 160°W . However they are less frequent than in the northern hemisphere and do not last as long.

3. The interference of planetary waves

Since blocking is a planetary scale phenomena it is reasonable to examine the relationship between the behaviour of planetary waves and the incidence of blocking. Therefore Austin (1980) examined the phases of the long waves at 500 mb for a "normal" January chart. The results are shown in Fig 3. There appear to be two main areas where the waves interfere constructively

(i) $0^{\circ}\text{--}40^{\circ}\text{E}$, $50^{\circ}\text{--}60^{\circ}\text{N}$ - waves 1 and 2

(ii) 140°W , 50°N - waves 2 and 3

These two regions correspond to where blocks usually occur and so, for example, it is possible that blocking occurs in the Atlantic sector when waves 1 and 2 have normal phases but unusually large amplitudes. Now if wave 1 is large (as it is usually in winter) it would interfere destructively with waves 2 and 3 in the Pacific and so in winter we would expect more blocks in the Atlantic than Pacific.

Using this evidence Austin set down the wave number signatures for blocking

	1	2	3
Atlantic	large	large	small
Pacific	small	large	large
Both	large	large	large

Austin illustrated here ideas with a case study. Fig 4 shows the amplitudes of waves 1 to 4 during January 1968 when there were two Pacific blocks. At the start of both periods of blocking wave numbers 2 and 3 were large and wave number 1 was small; also there was rapid growth of wave number 1 at the end of each block.

Austin examined the behaviour of wave number 1 in more detail. She found that during January there was a stationary wave number 1 and also a retrogressing wave of slightly larger amplitude; the block occurred when the travelling wave was 180° out of phase with the stationary wave. It was suggested that the travelling wave was associated with the stratospheric warming that lasted from 17 December to 14 January. The stratospheric easterlies that existing during the warming would trap wave number 1 in the troposphere. However after the breakdown of the warming the winds would become westerly and there would be upward propagation of wave number 1. This might then produce the desired retrogressive wave number 1.

Austin examined 6 cases of major stratospheric warmings and found that in 4 cases Pacific blocking occurred at the end of the warming. A link between blocks and warmings was also suggested by Labitzke (1965) who found that Atlantic blocks tended to form about 10 days after the commencement of minor stratospheric warmings.

4. Evidence from GCM's

Now consider the effect on blocking of changing the forcing that produces the planetary waves - this forcing is associated with orography and land-sea surface heating contrasts. Kikuchi (1971) examined the blocks that formed in a 150 day perpetual January integration of a quasi-geostrophic 2 layer model. He did 4 experiments with different combinations of forcing and found that

- (i) when both forcings were included he got the most realistic results
- (ii) the second best results were with topography alone
- (iii) when only differential heating was included he did not get the correct distribution of blocks with longitude
- (iv) when neither forcing was included some blocks still formed although they did not last long (on average about $1\frac{1}{2}$ days).

The last of these results contradicts the conclusions of Everson and Davies (1970) who found that blocking only occurred when zonal variations of surface heating were included. However this inconsistency may be due to Everson and Davies not regarding a block lasting only $1\frac{1}{2}$ days as a "true" block.

Mansfield (1981) has investigated the incidence of blocking in the 5-level model. He considered 77 forecasts each lasting 50 days. Because the model produces so few normal blocks, Mansfield relaxed the definition of blocks still further and considered only interruption of the 500 mb flow spanning at least 15° of latitude in mid-latitudes (note no splitting of the jet was required). He then examined the distribution of these blocks in both the model and real data.

The distribution of blocks month by month are shown in Fig 5a. The model distribution was similar to that observed although the model frequency was only about $\frac{1}{3}$ of what it should be. Differences between the actual distributions given by Rex and Mansfield are mainly due to the different definition of a block that were used. Fig 5b shows the geographical distributions of the blocks and again there is remarkable agreement between the model and actual blocks.

5. Interaction of a topographic wave with the zonal mean flow

Consider barotropic non-divergent flow on a channel β -plane; the governing equations for such a flow is

$$\frac{\partial \nabla^2 \psi}{\partial t} + J(\psi, \nabla^2 \psi + \frac{f_0 h_0}{H} + f) = -c \nabla^2 \psi + V$$

where ψ is the stream function, h_0 the topographic height, H the scale height and $f = f_0 + \beta y$. The two terms on the RHS represent linear damping and some kind of vorticity forcing. The use of variations of this equation has a long and honourable history. Charney and Eliassen (1949) used a steady linear version of the equation (with $\frac{\partial}{\partial t} = 0$, a constant zonal wind and a prescribed meridional variation in h_0) to study the response of the atmosphere to variations in the zonal topography. They found that they could reproduce the main features of the climatology of the 500 mb surface; in particular the ridges in the Atlantic and Pacific which coincide with the favoured regions for the development of blocks.

Charney and de Vore (1979) examined the steady state solutions of the non-linear problem using a severely truncated spectral model. With a judicious choice of topographic and vorticity forcing they found it was only necessary to use 3 sets of eigen functions

$$F_A = \sqrt{2} \cos \frac{y}{L} \quad F_K = 2 \cos \frac{n\pi x}{L} \sin \frac{y}{L} \quad F_L = 2 \sin \frac{n\pi x}{L} \sin \frac{y}{L}$$

They then used just one topographic mode F_K , and the vorticity forcing V ~~the zonal wave number~~ was defined in terms of F_A only. The solution ψ is then

$$\psi = \psi_A F_A + \psi_K F_K + \psi_L F_L$$

and by using these in the original equation they obtained equations for ψ_A , ψ_K and ψ_L . Setting the time derivations to zero gave the equilibrium equations, and from these they derived a cubic equation for ψ_A . When this gave just one equilibrium solution it was always stable, whereas when there were 3 of them it was found that for first mode perturbations ($n=1$) two were stable and one was unstable. However this was not necessarily so for the second mode where one of the stable modes became unstable for sufficiently large zonal forcing. Therefore there was a range of forcings for which two equilibria exist. Fig 6 shows the stream function for the two steady states when favourable forcing has been chosen. Note their similarity to a low index and high index cycle.

6. Interaction between topographically forced waves

Egger (1978) proposed that under favourable conditions the non-linear interaction of forced waves with slowly moving free waves could lead to the development of blocks. To test his ideas he used a barotropic non-divergent spectral model with topographic forcing. The forcing induces standing waves whereas the free waves will be Rossby-Haurwitz waves with a phase speed given by

$$c = \bar{u} - \frac{\beta}{k_{mn}^2}$$

where k_{mn} is the total wave number. Egger argued that blocking occurred when the speed of the westerly flow \bar{u} was such that $c \approx 0$ for some of the travelling waves; these waves were then stationary with respect to the surface forcing and resonance occurs.

It is instructive to follow Egger's argument. Let $\psi^* = \psi - \bar{\psi}$ be the eddy stream function. If there is no wave-mean flow interaction then the behaviour of the fluid is described by

$$\frac{\partial}{\partial t} \nabla^2 \psi^* + J^*(\psi, \nabla^2 \psi + f) + \frac{f_0 \bar{u}}{H} \frac{\partial h_0}{\partial x} = 0$$

where \bar{u} is the constant zonal wind.

We now represent ψ^* by a double Fourier series with mode (m,n) given by

$$\psi_{mn}^* = \psi_{mn}(c) \cos \frac{2\pi m x}{L} \sin \frac{\pi n y}{B} + \psi_{mn}(s) \sin \frac{2\pi m x}{L} \sin \frac{\pi n y}{B}$$

Here L and B are the length and breadth of the beta-plane with $\psi_{mn}(c)$ and $\psi_{mn}(s)$ the Fourier coefficients. The total wave number and amplitude are given by

$$k_{mn}^2 = 4\pi^2 \left(\frac{m^2}{L^2} + \frac{n^2}{4B^2} \right) = k_{mx}^2 + k_{ny}^2$$

$$|\psi_{mn}| = \sqrt{\psi_{mn}(s)^2 + \psi_{mn}(c)^2}$$

If T_{mn} represents the mountain forcing for mode (m,n) then the amplitude of the resulting standing wave can be estimated from the steady linear version of the prediction equation

$$|\psi_s| \approx \frac{|T_{mn}|}{|\bar{u}k_{mn}^2 - \beta|}$$

Now consider what happens if two forced standing waves (r,s) and (l,l) of about equal amplitude $|\psi_s|$ interact non-linearly. There will be a transfer of energy to modes $(r \pm l, s \pm l)$ and it can be shown that the mode (p,q) that grows most rapidly has a wave number k_{pq} such that

$$k_{rs}^2 < k_{pq}^2 < k_{ll}^2$$

This excited mode will be advected by the mean wind and influenced by β ; therefore it will be a free Rossby wave with phase speed c_{pq} given by

$$c_{pq} = \bar{u} - \frac{\beta}{k_{pq}^2}$$

For there to be a significant non-linear response for mode (p,q) it must be almost stationary with respect to the forcing so that c_{pq} must be small. This will happen if \bar{u} has an appropriate value. Then waves (r,s) , (l,l) and (p,q) will form a triad with almost stationary phases and large amplitudes.

The argument becomes a little clearer if we see how Egger set up his experiment. He prescribed forcings $T_{11}(c)$ and $T_{31}(s)$ which will give rise to corresponding standing waves $\psi_{11}(c)$ and $\psi_{31}(s)$. These waves interact non-linearly and excite modes $(4,2)$ and $(2,2)$ with most of the energy being transferred into $(2,2)$. Therefore we want $(2,2)$ to be the third member of the triad, and this must be stationary with respect to the forcing. Consequently \bar{u} is chosen so that c_{22} is zero (i.e.

$$\bar{u} = \beta/k_{22}^2).$$

Fig 7 shows some results of integrating the barotropic equations (without wave-mean flow interaction) in a channel. By day 25 a blocking high became established with a realistic horizontal extent and life-time (about 15 days). However it should be noted that the variability of the channel flow was low with the major features staying in the same place during the development of the block. It was found that blocks did not form when one or both of the forcing modes was absent. The inclusion of wave-mean flow interactions gave more realistic blocks, but there was little further improvement when a two-level baroclinic model was used.

Metz (1979) has integrated the non-linear equations on a sphere with realistic topography and a constant zonal wind. During the 100 day integration several blocks formed (especially in the Atlantic and Pacific); an example of such a block is shown in Fig 8.

7. Conclusions

Clearly there is still a great deal that is not known about blocks and there is no agreed theory of blocking. The primary importance of topographic forcing is accepted, but there are a variety of theories about exactly which type of interactions are responsible for the formation of blocks. There does appear to be a relationship between blocks and the breakdown of stratospheric warmings, but this requires much more investigation. Also it is necessary to understand how blocks are maintained once they have formed - in fact Austin has made an attempt at investigating this problem.

The way forward now is to do diagnostic studies of real blocks and of those which form in GCM's to try to understand the dynamics of these systems.

8. References

In this lecture use has been made of the following review articles.

Bengtsson, L., 1980, E.C.M.W.F. Seminar 1979, Vol. 2, 235-269

Egger, J., 1979, E.C.M.W.F. Workshop on Mountains and Numerical Weather Prediction, 98-108

Other references are

Austin, J.F., 1980, Q.J.R.M.S., 106, 327-351

Charney, J.G., and Eliassen, A., 1949, Tellus, 2, 38-54

Charney, J.G., and de Vore, J., 1979, J.Atms.Sc., 36, 1205-1216

Egger, J., 1978, J.Atms.Sc., 35, 1788-1801

Everson, P.J., and Davies, D.R., 1970, Q.J.R.M.S., 96, 404-412

Kikuchi, Y., 1971, J.Met.Soc. Japan, 49, 137-155

Mansfield, D.A., 1981, Met.O.13 Tech. Note to be

Metz, W., 1979, Unpublished (but see Egger (1979))

Rex, D.F., 1950, Tellus, 2, 275-301

Taljaard, J.J., 1972, A.M.S. Met.Monograph, Vol. 13, No 35

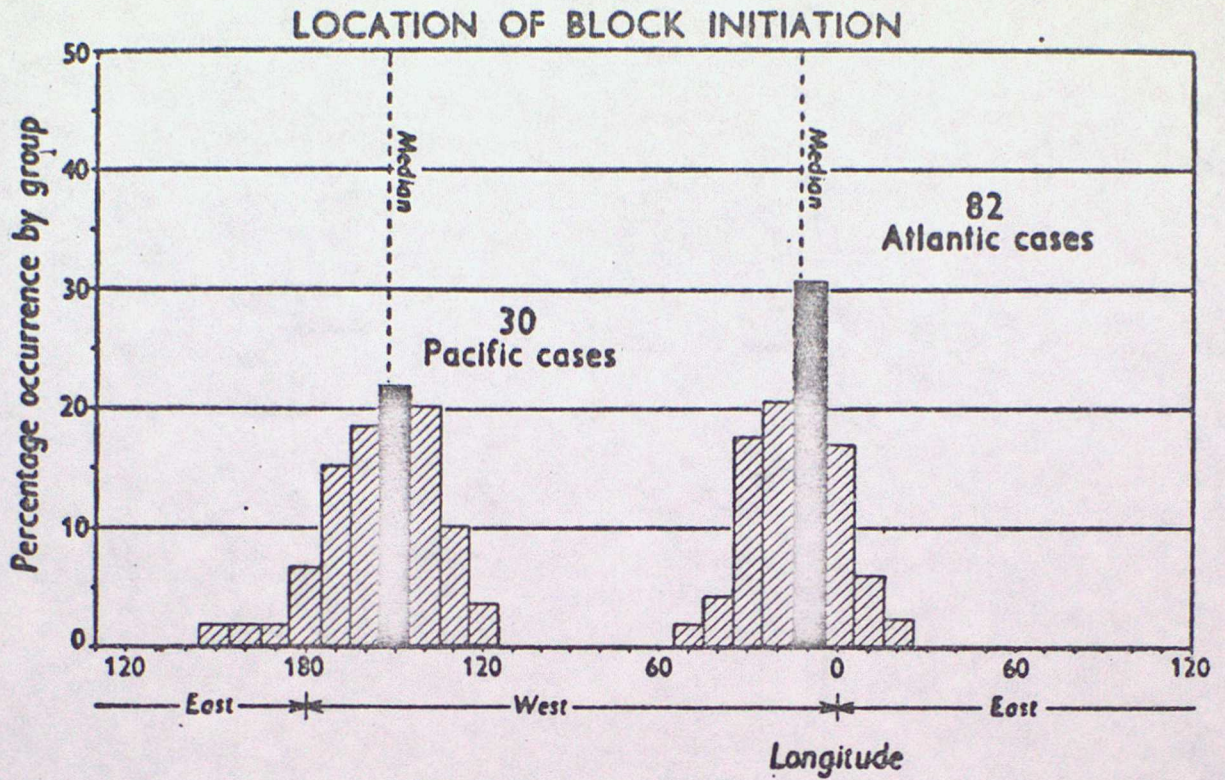


Figure 1

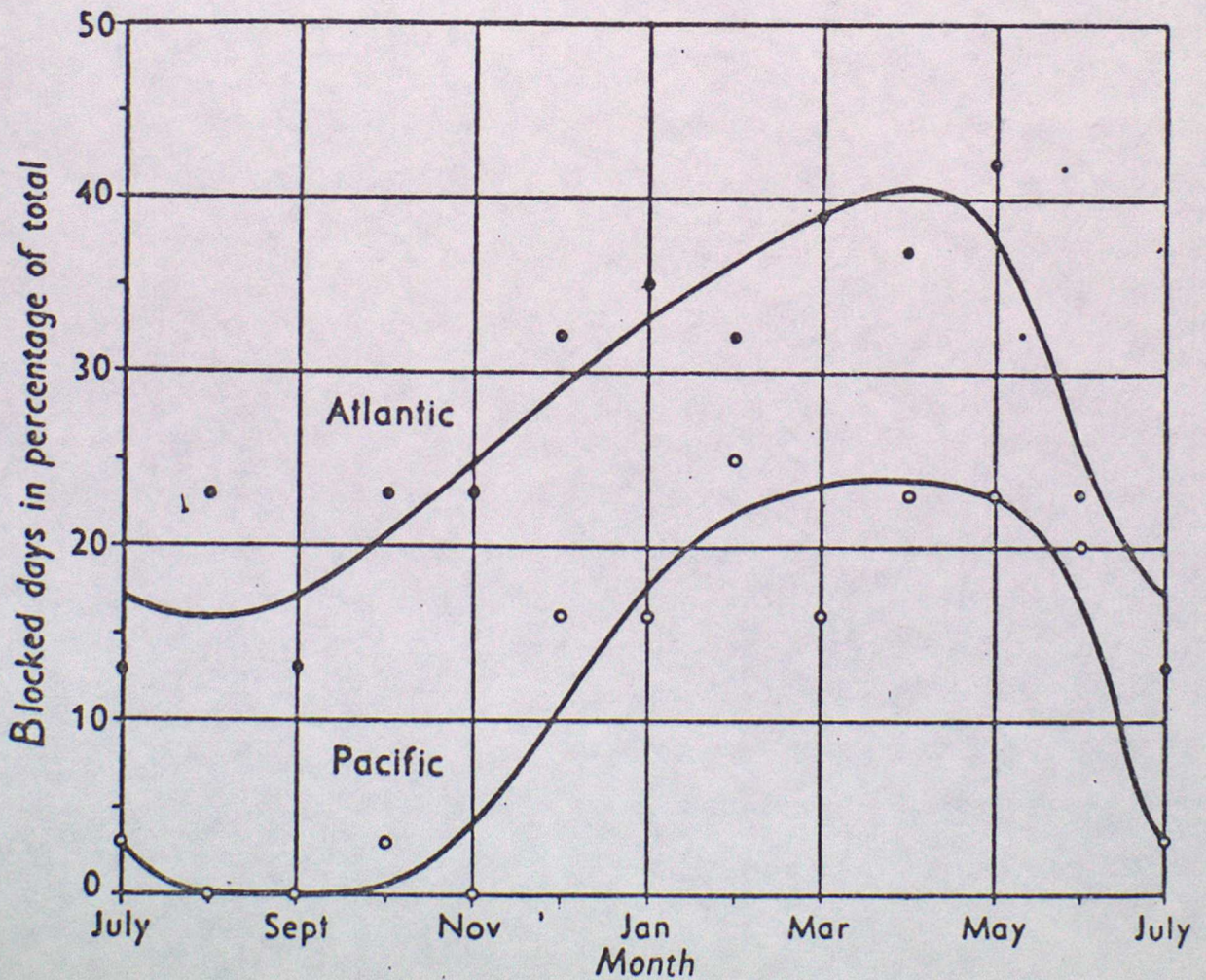


Figure 2

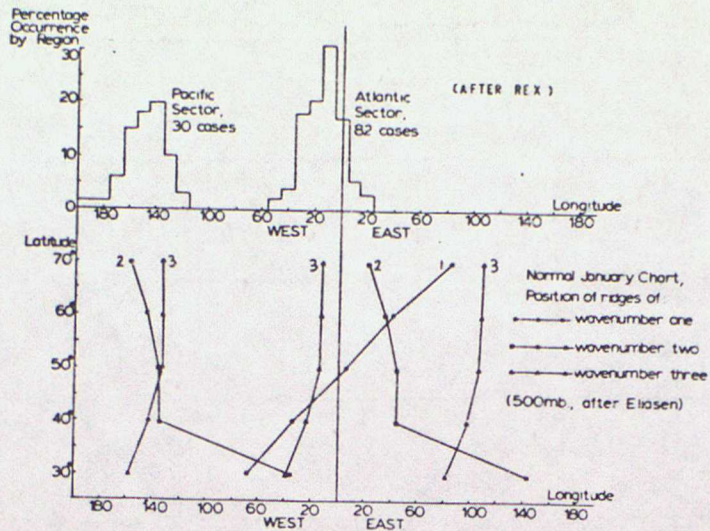
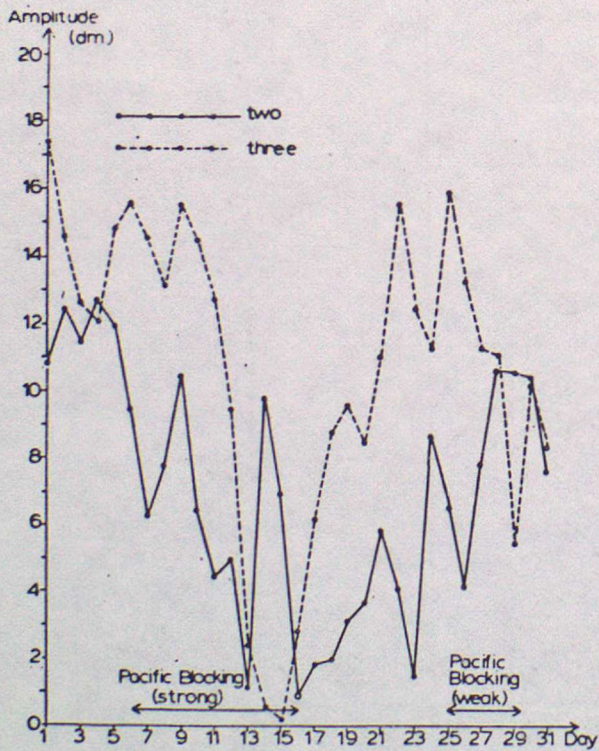
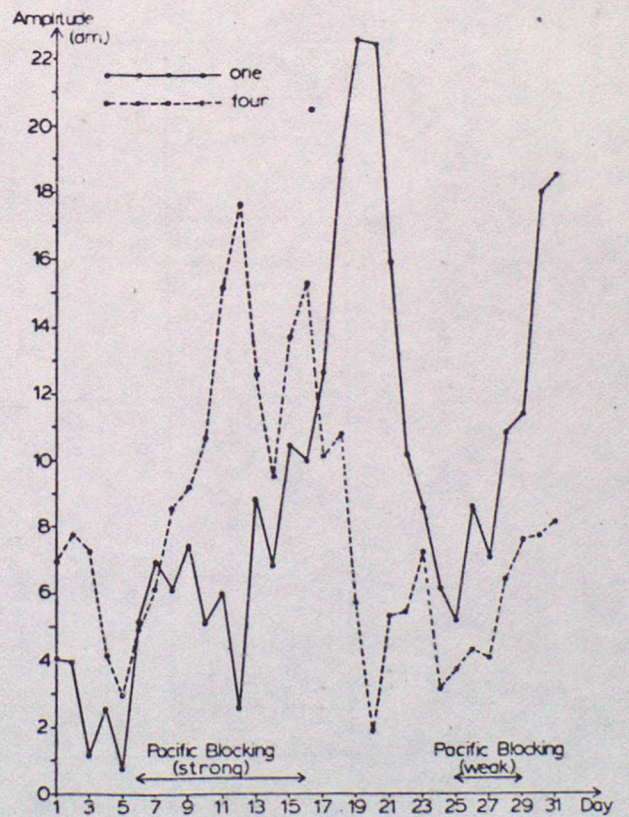


Figure 3 Comparison between the longitude of the initial splitting of the jet (Rex 1950) and the normal phases of the planetary waves at 500 mb (Eliassen 1958).

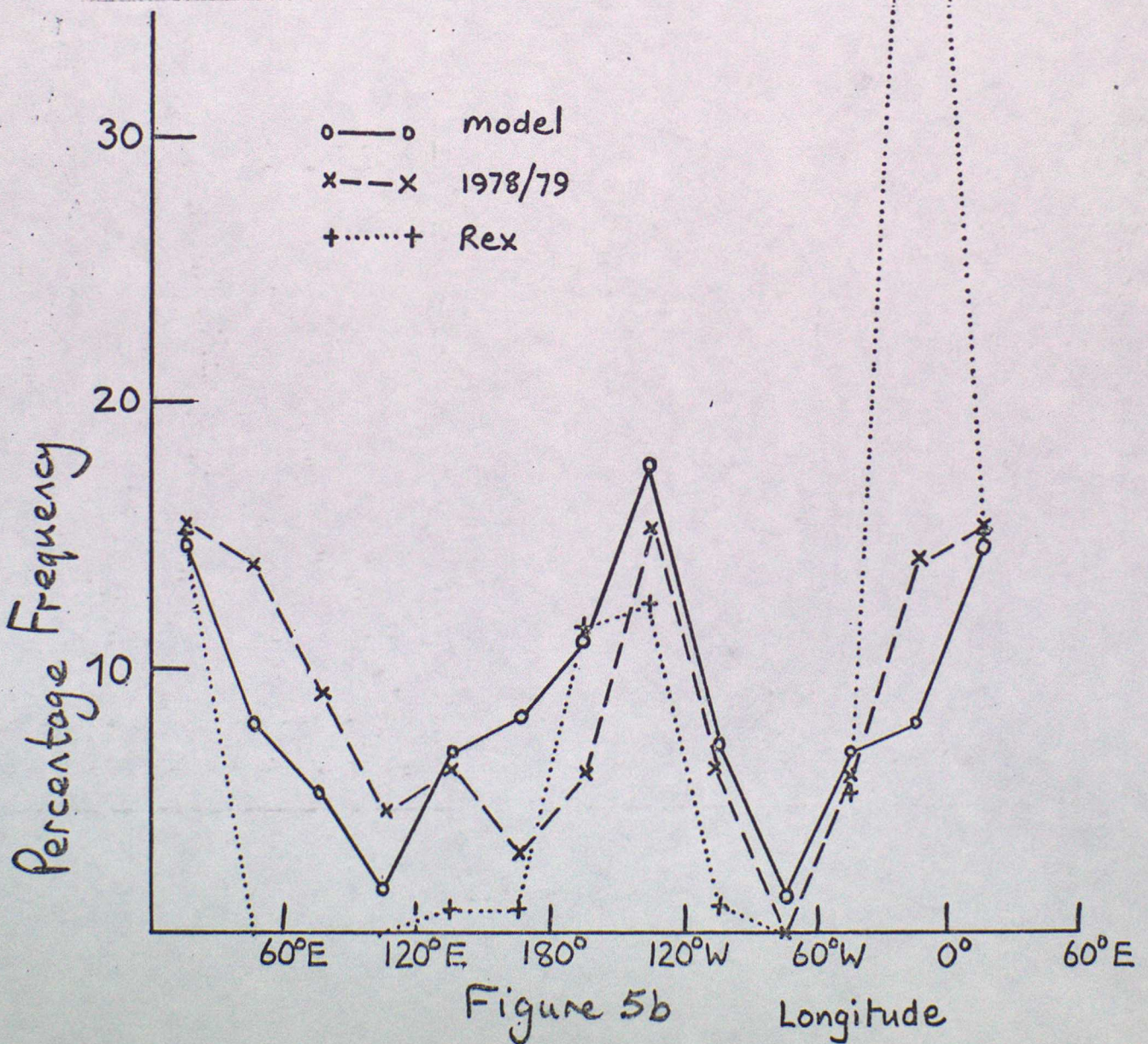
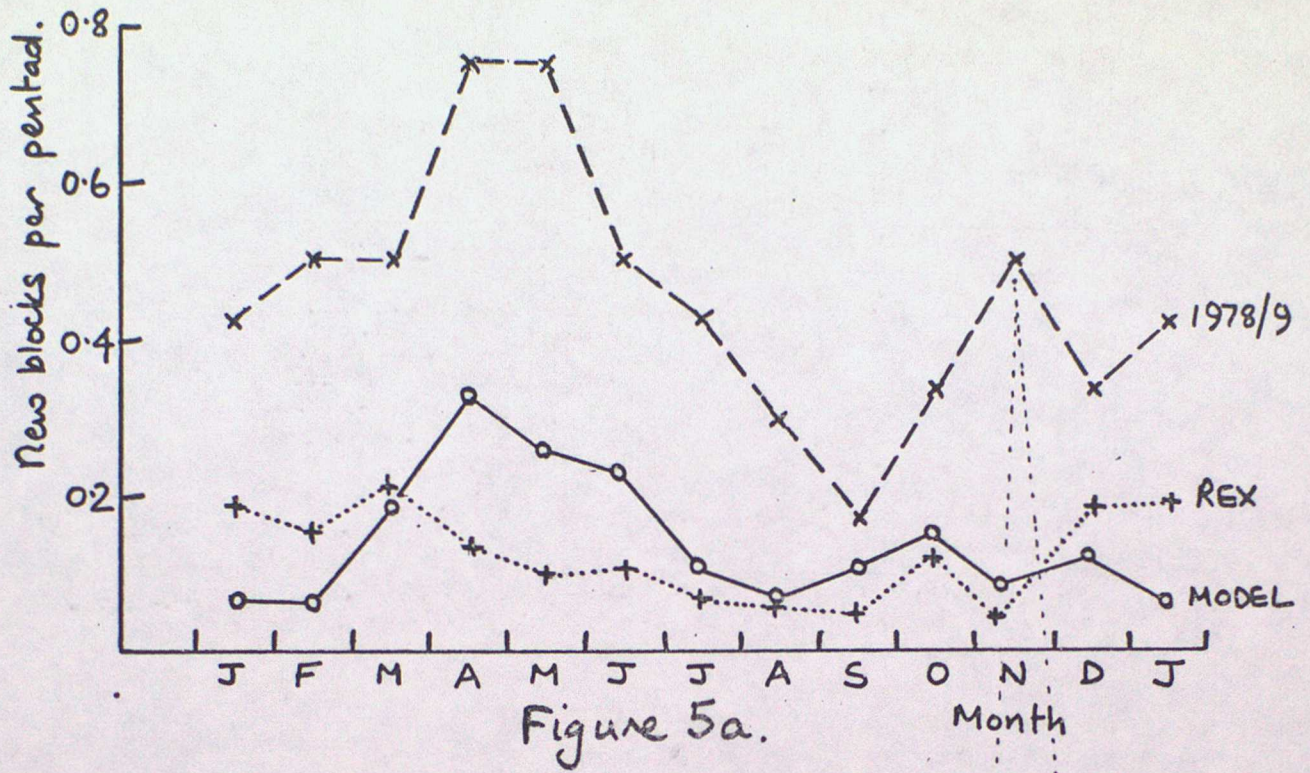


Amplitude of wavenumbers two and three, 60°N 500 mb, Jan. 1968.



Amplitude of wavenumbers one and four, 60°N 500 mb, Jan. 1968.

Figure 4



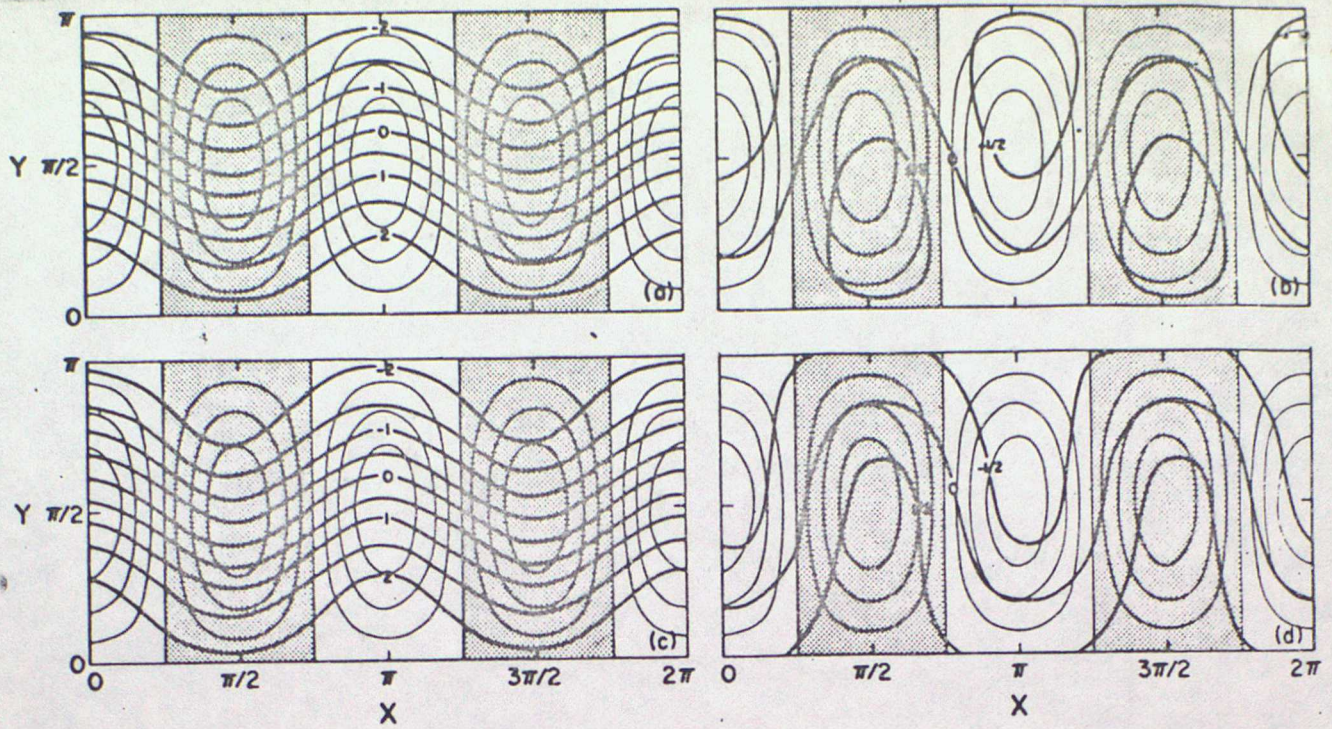


Fig. 6 Streamfunction fields of the stable first mode equilibria of a topographically forced flow. (a) and (b) for the spectral model; (c) and (d) for the grid point model. From Charney and DeVore, J. Atmos. Sci., (1979).

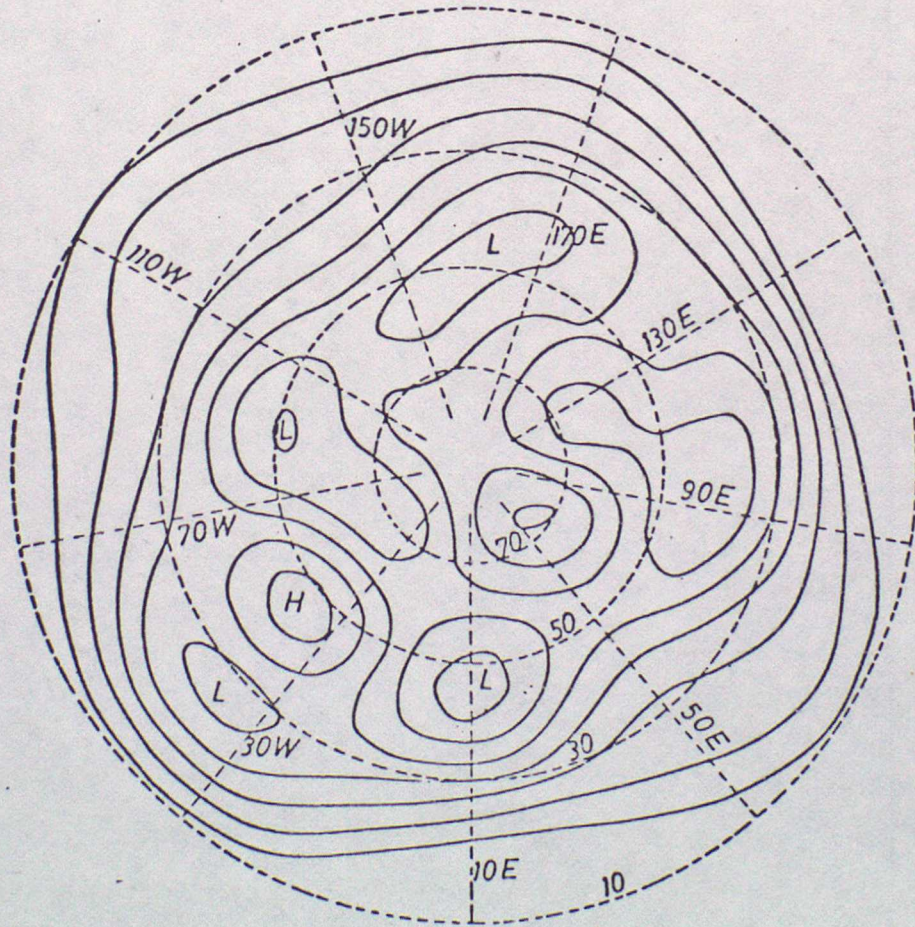


Fig. 8. Geopotential at day 51 of an integration on a sphere with orography of the Northern Hemisphere. After Metz (1979)

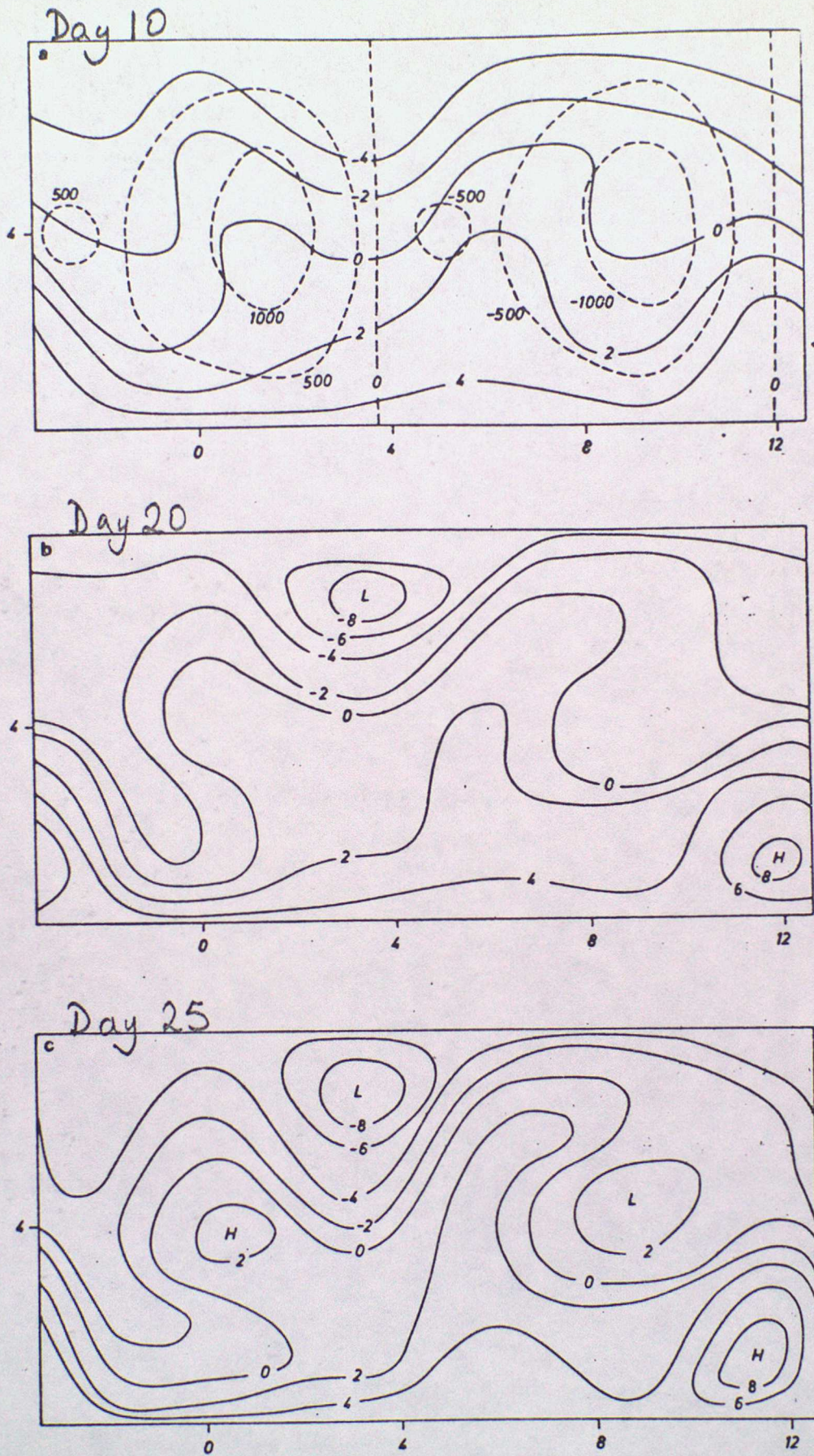


Fig. 7 Blocking in a channel caused by Newtonian forcing. Streamfunction ψ ($10^7 \text{m}^2 \text{s}^{-1}$) at day 10 (a), 20 (b) and 25 (c). Isopleths of the orography (m) are dashed. From Egger, J. Atmos. Sci., (1978).



THE EAST AFRICAN JET

1. Introduction

The existence of very strong winds near the Somali coast in summer have been known for some time. However it was Findlater (1969) who first showed that these winds were part of an extensive circulation that originates in the southern hemisphere and crosses the equator as a narrow low level jet. During the northern winter the current is just a feeble feature in the southern hemisphere, but later it expands and strengthens, and reaches its maximum development in July. It is then a major current circulating around the western periphery of the monsoon region. In fact Findlater has estimated that in July it could be responsible for about half the total low level cross-equatorial flow.

In the monsoon season the jet is typically about 500 km wide and 2 to 3 km deep as it crosses the equator. The jet has a mean speed of about 12 ms^{-1} but surges in excess of 50 ms^{-1} have been found.

It is thought that the existence of the jet is connected with the barrier effect of the East African Highlands. However, as far as is known, there is no equivalent cross-equatorial flow over South America or Indonesia despite the high topographic barriers in both these regions.

2. Observational studies

2.1 Mean flow pattern

The mean sea level pressure field is dominated by the southern hemisphere subtropical high (the Mascarene High) and the northern hemisphere Monsoon Trough - see Fig 1. In the southern Indian Ocean upstream of Africa the isobars show a high degree of zonal asymmetry. However near East Africa there is a ridge in the southern hemisphere with a trough to its north.

Fig 2 shows the mean monthly airflow at 1 km as described by Findlater (1977). The origins of the main flow lie in the SE Trades to the north of the Mascarene High; the Trades have typical speeds of 5 to 10 ms^{-1} . As the East African coast is approached the jet turns northwards and crosses the equator as a strong S'ly flow with a maximum speed of about 15 ms^{-1} at an altitude of 1.5 to 2.0 km. The flow is laterally bounded by the East African Highlands. Further north the jet leaves the coast at about 10°N and heads eastwards towards India (the SW'ly Monsoon).

Fig 3 shows the cross-section of the jet during July (from Findlater (1969)). This illustrates why the barrier effect of the East African Highlands is thought to be the cause of the jet. The jet maximum is about 200 km to the east of the edge of the high ground (the mountains are typically 2 km high).

Usually there is a marked inversion at about 3 km in summer and this can be thought of as acting as a flexible lid on the flow.

2.2 The transients

There appears to be at least 3 ways in which the behaviour of the EAJ varies from its average conditions

- (i) the jet can be fed by air originating to the east of Madagascar or by air flowing up the Mozambique channel - there are day to day variations in both the position and strength of the jet
- (ii) the current can be multi-cored

(iii) there is a diurnal variation in the jet with the minimum wind occurring when the surface heating is a maximum (about 1000 Z) and the maximum winds occurring in the early morning (about 0500 Z)

Analysis of the vertical velocity in the jet shows that in the core there tends to be ascent with descent on either side. Therefore there is often cloud and rain along the jet axis.

3. Models of the EAJ

3.1 A one-layer model

Most theoretical studies of the EAJ have used a one layer model with reduced gravity. In this model the bottom layer is forced by some means whereas the upper layer (above the inversion) is unforced and inactive - that is the pressure gradients and velocities are zero. The upper layer is dynamically inactive, but it does have the effect of reducing the effect of gravity in the lower layer by a factor $\Delta\rho/\rho_0$ where $\Delta\rho$ is the difference in density between the two layers and ρ_0 is the density in the lowest layer. The equations now become

$$\begin{aligned} \frac{\partial u}{\partial t} + u \frac{\partial u}{\partial x} + v \frac{\partial u}{\partial y} - fv &= -g' \frac{\partial h}{\partial x} + \nu \nabla^2 u - \frac{Ru}{D} + X \\ \frac{\partial v}{\partial t} + u \frac{\partial v}{\partial x} + v \frac{\partial v}{\partial y} + fu &= -g' \frac{\partial h}{\partial y} + \nu \nabla^2 v - \frac{Rv}{D} + Y \\ \frac{\partial h}{\partial t} + \frac{\partial (Du)}{\partial x} + \frac{\partial (Dv)}{\partial y} &= Q \end{aligned}$$

where h is the height of the interface (the free surface) and D is the depth of the fluid (i.e. $D = h - h_0$ where h_0 is the height of the topography); X , Y and Q are forcing terms and R is the Rayleigh friction coefficient. Usually an equatorial β -plane is used so $f = \beta y$

When using this simple model to investigate the behaviour of the EAJ it is important to remember that a number of possibly important processes are being ignored. For example no account is taken of the vertical shear above and below the jet, and also interactions between the upper and lower layers are ignored. (in fact sometimes the jet core occurs above the inversion). Despite these problems, and others, this model has been useful for investigating the dynamics of the EAJ.

3.2 Steady inviscid flow

Consider a jet that is unforced in the region of interest - the forcing is exterior to the region of interest. In this case X , Y and Q are zero, and because the flow is inviscid we have ν and R also zero. Now if the mountain barrier is represented by a vertical wall we have $h_0 = 0$ with $D = h$ inside the domain. The resulting equations can then be manipulated to give the potential vorticity equation which states that the potential vorticity $(\beta + f)/h$ is conserved by a parcel of air. In addition the Bernoulli function is also conserved.

For a typical current

$$v \gg u \quad \text{and} \quad \frac{\partial v}{\partial x} \gg \frac{\partial u}{\partial y}$$

and if it is assumed that the northward flow is geostrophic (this allows h to be related to the transport stream function ψ), then the conservation equations become

$$\frac{1}{h} \left(\frac{\partial v}{\partial x} + f \right) = F(\psi) \quad \frac{v^2}{2} + g'h = G(\psi)$$

Given the inflow conditions on the eastern boundary, $F(\psi)$ and $G(\psi)$ can be found and this allows h and ψ to be derived as functions of x and y .

Fig 4 shows an example of such a computation. As the flow approaches the boundary from the east it is deflected northwards into a boundary current flow whose width decreases as it moved north. Eventually the current turns away from the barrier and broadens. Complete separation of the jet from the boundary occurs when h goes to zero. This does not correspond to reality, but it is found that if friction is taken into account separation from the boundary can take place for non-zero values of h . Another problem is that in these solutions the maximum wind tends to occur at the boundary. This can be illustrated by rewriting the conservation of potential vorticity equation to give

$$\frac{\partial v}{\partial x} = h F(\psi) - \beta y$$

Usually $F(\psi) < 0$ and so in the northern hemisphere $\frac{\partial v}{\partial x} < 0$ which gives the highest speeds at the boundary. In the southern hemisphere there is the possibility of the jet maximum being away from the boundary.

Many of the deficiencies in this model are due to the neglect of friction.

3.3 Lateral friction

Anderson (1976) suggested that side friction was very important when trying to simulate the jet. He illustrated this by using a linear model

$$\begin{aligned} -fv &= -g' \frac{\partial h}{\partial x} + \nu \nabla^2 u \\ fu &= -g' \frac{\partial h}{\partial y} + \nu \nabla^2 v \\ H \left(\frac{\partial u}{\partial x} + \frac{\partial v}{\partial y} \right) &= Q \end{aligned}$$

where H is some average mean depth of the fluid. The Q term corresponded to a source-sink complex with the source in the SH corresponding to subsidence in the NH representing ascent in the monsoon trough. The boundary conditions far from the boundary are found by solving the equations with no barrier and with $Q = Q(y)$.

To illustrate the kind of results obtained it is convenient to follow Hart (1977) and set $Q = 0$; the vorticity equation then becomes

$$\beta v = \gamma \frac{\partial^3 v}{\partial x^3}$$

If the inflow has the same form as that used in the previous section then the solution is

$$v = B \exp\left(-\frac{\delta x}{2}\right) \sin(0.866 \delta x)$$

where $\delta = \sqrt{\frac{\beta}{\gamma}}$ and B is a function of β, γ and the inflow.

The outer half width of the solution appears reasonable if $\delta \approx 6 \times 10^4 \text{ m}^{-1}$. However the solution does have an unrealistic southward flow to the east of the jet.

3.4 Bottom friction and variable topography

Hart (1977) argued that the large vertical shears near the ground indicates the importance of bottom friction. He derived solutions to both the linear and non-linear cases where there was no forcing ($X = Y = Q = 0$) or horizontal friction. The topography was idealised but retained the essential characteristics of the actual topography. The solutions are shown in Fig 5. For the linear case there is an inner shear layer over the sloping topography, but for realistic values of R the jet is too narrow and has too high a speed. The effect of the non-linearities is to reduce the maximum speed and to broaden the jet.

Hart et. al. (1978) compared these results with observations obtained during MONEX 77. The results shown in Fig 6 indicate that by juggling the parameters of the model very good agreement can be obtained.

Bannon (1979a) used a model similar to the one used by Hart for his non-linear computations, but with a more realistic description of the topography (Madagascar was included) and the SE Trades. An example of his solutions are shown in Fig 7. Note the influence of Madagascar and the distortion of the pressure field near the boundary (compare with Fig 1).

4. The transients

The EAJ has considerable temporal variability with time scales extending from days to years. Recently Bannon (1979b) has used a depth-averaged numerical model to investigate these transients.

Observations have revealed that there is a marked diurnal variation in the jet - at night the jet maximum increases by about 30% and shifts 50 to 100 km. Bannon thought that this could be due to the reduction in surface drag at night and he examined this possibility by running the model with a time dependent drag coefficient over the land and a constant value over the sea. Fig 8 shows the results of the simulations along with results from MONEX 77. The numerical results are in reasonable agreement, except that the model changes only occurred overland whereas the observations show that off-shore there is a night-time increase.

There is also evidence that synoptic fluctuations to the south caused by the passage of mid-latitude disturbances over the Cape of Africa may explain some of the temporal variation in the jet strength. To simulate this effect Bannon solved the equations with an eastward moving wave travelling along the southern boundary - a wave number 6 with a period of 6 days was chosen. The forcing was specified in terms of the meridional velocity in the boundary. Some of the results are shown in Fig 9. Note that there is considerable variation in the jet maximum with a phase lag of 120° with the forcing. Also, unlike the diurnal variation, the variations in the boundary flow can produce large changes in the characteristics of the jet.

Bannon also investigated the suggestion that the 14 day period in the meridional pressure gradient over the Indian Ocean could affect the jet. He allowed Q to vary with a 14 day period. As with the southern boundary changes, the induced fluctuations caused the speed and width of the jet to vary, but not its position.

So far there appears to be no explanation of multi-cored jets.

5. References

Much of this lecture has been based on 3 review papers.

Anderson, D.L.T., 1980, GARP Publ. Series No 23, 317-355

Hart, J.E., 1977, Pure and Applied Geoph., 115, 1263-1282

Findlater, J., 1977, Pure and Applied Geoph., 115, 1251-1262.

Other references are

Anderson, D.L.T., 1976, M.W.R., 104, 907-921

Bannon, P.R., 1979a, J.Ats.Sc., 36, 2139-2152

Bannon, P.R., 1979b, J.Ats.Sc., 36, 2153-2168

Findlater, J., 1969, Q.J.R.M.S., 95, 362-380

Hart, J.E. et. al., 1978, M.W.R., 106, 1714-1724

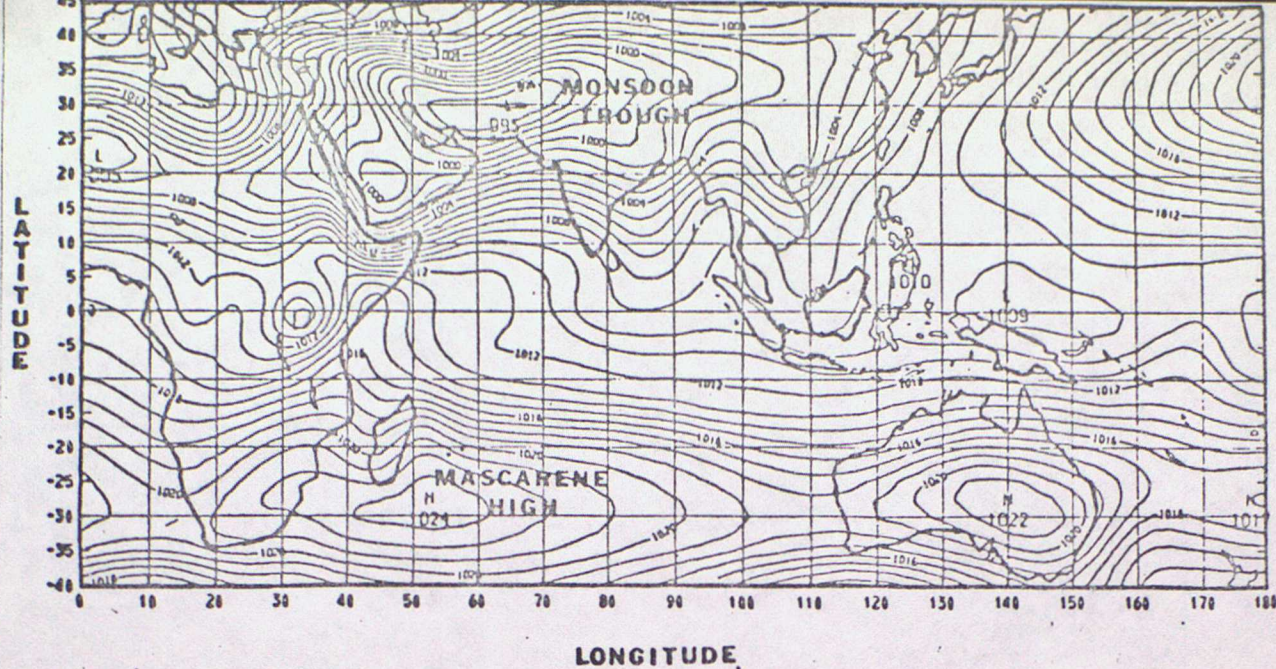


FIG. 1 Mean sea level pressure for July (after van de Boogaard, 1977). Contour interval 1 mb.

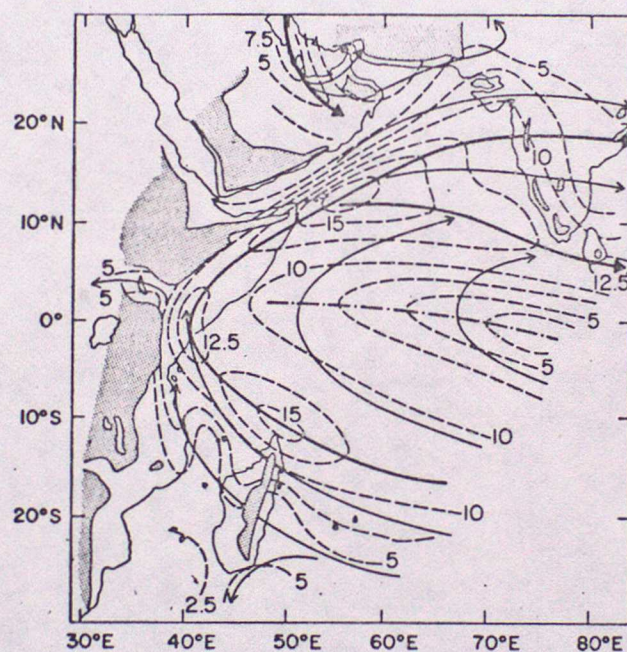


FIG. 2. Mean flow pattern at 1 km for July. Solid lines denote streamlines. Heavy solid line is the major streamline and axis of maximum flow. Dashed lines are isotachs at 2.5 m s^{-1} intervals. Dot-dashed line is the axis of minimum wind speed. Shaded areas correspond to orography $\geq 1 \text{ km}$. (Redrawn from Findlater, 1977.)

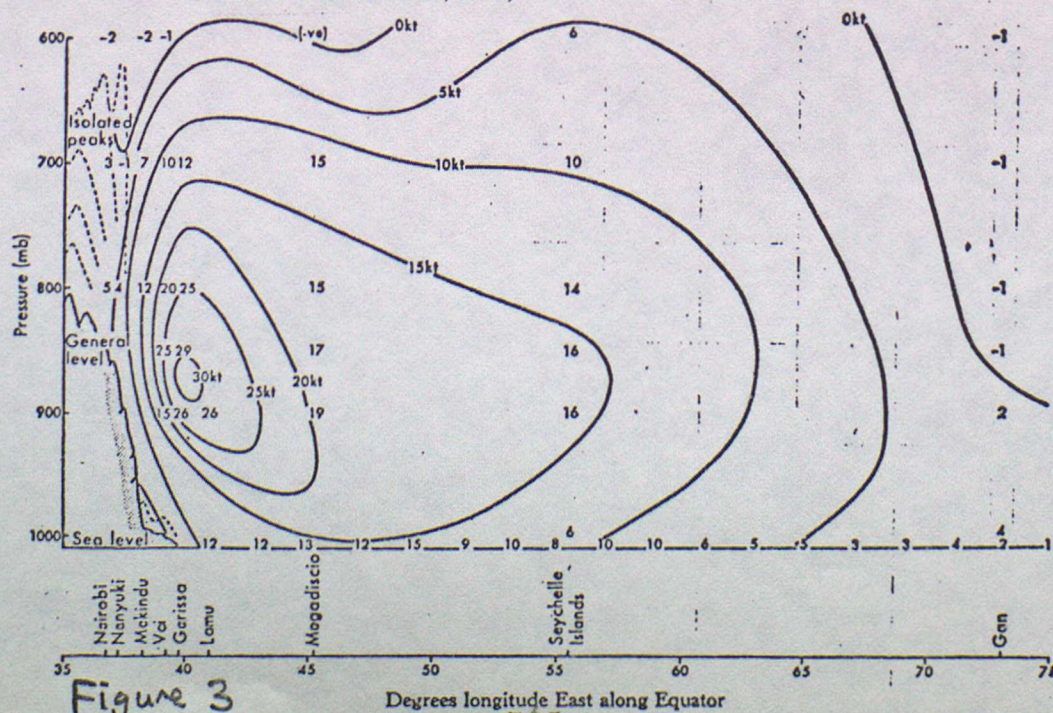
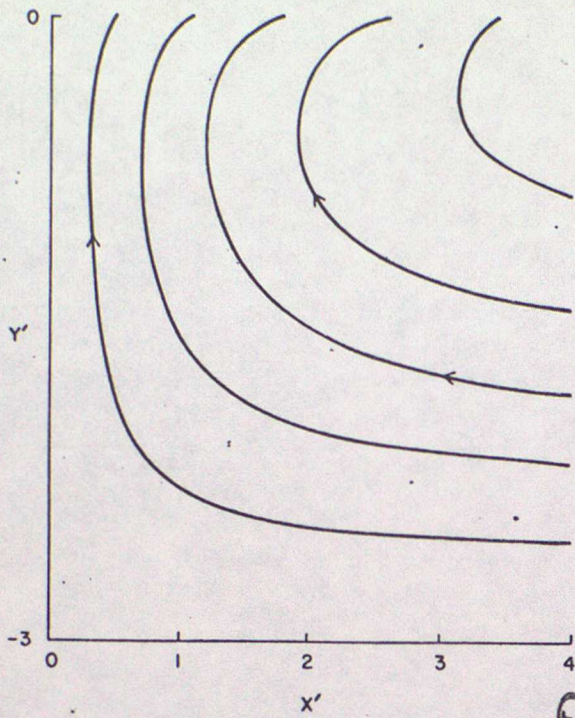


Figure 3

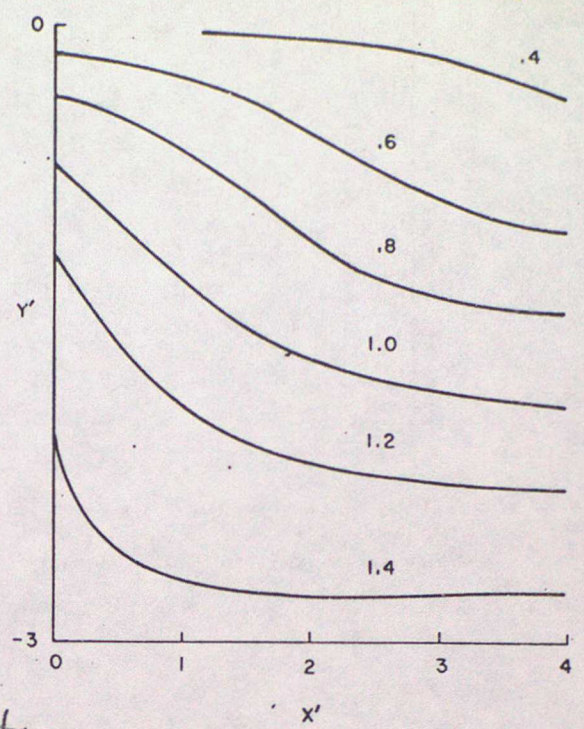
Degrees longitude East along Equator

non-dimensional transport streamlines



(c)

normalised free surface height



(d)

Figure 4

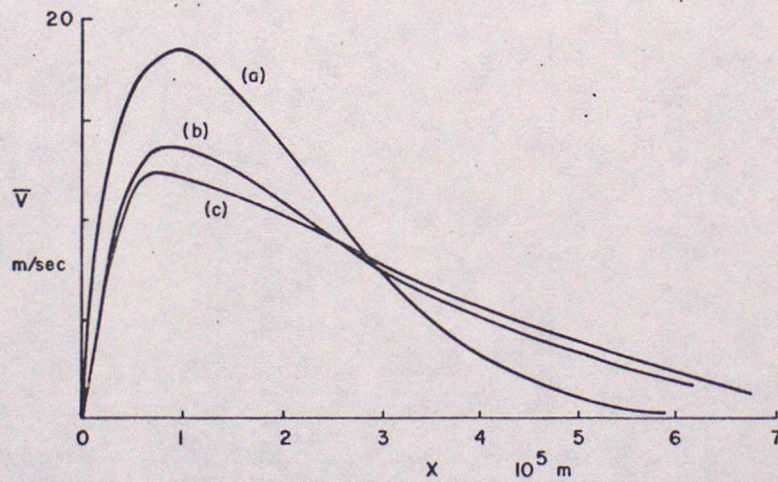


Figure 5

Velocity profile $\bar{v}(x)$ for linear (a) and nonlinear bottom friction models over variable terrain. In all cases, $\alpha = 1.25 \times 10^{-6} \text{ m}^{-1}$, $y_0 = y_s = -2 \times 10^6 \text{ m}$, and $U_0 = -5 \text{ m/sec}$. Curves (a) and (b) have $\tau = 4$ days, while for (c), $\tau_{sd} = 10$ days.

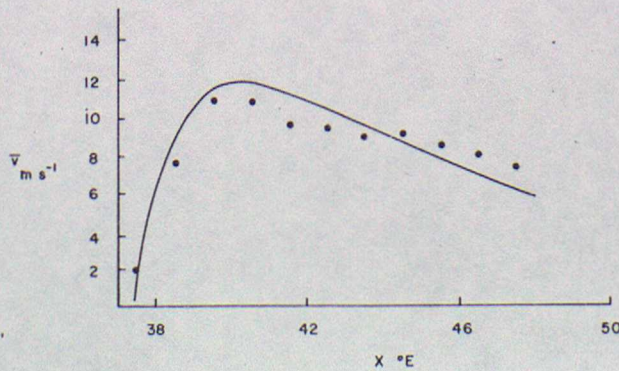
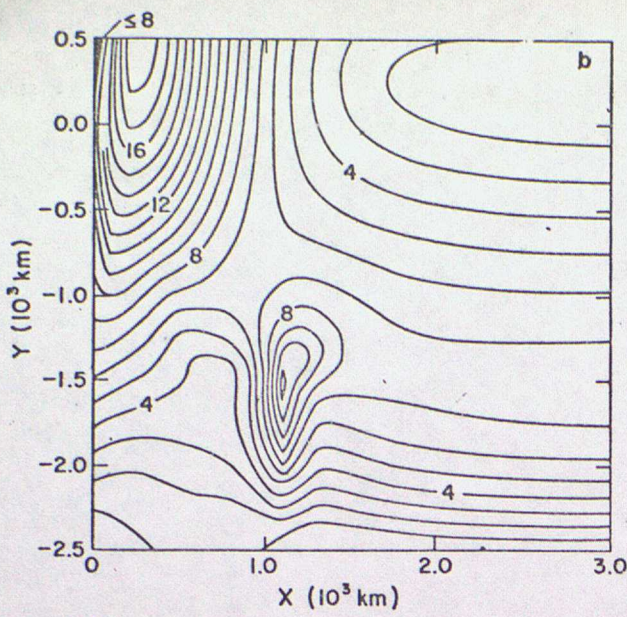
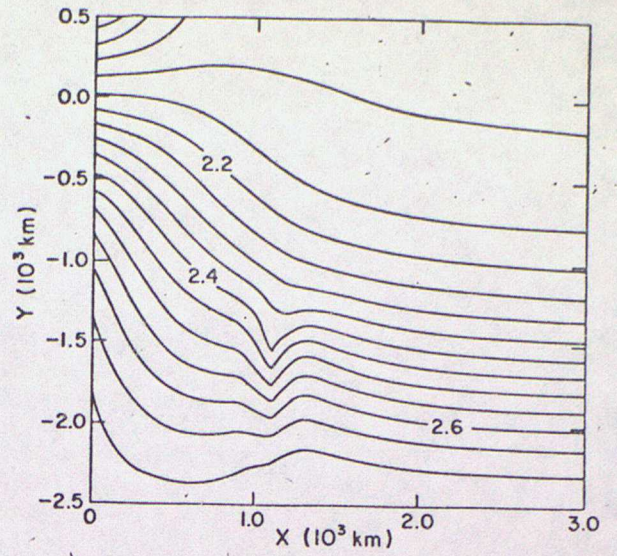


Fig. 6 Vertically averaged mean southerly wind component along track A for all flights (dots). The solid line is from a theoretical computation

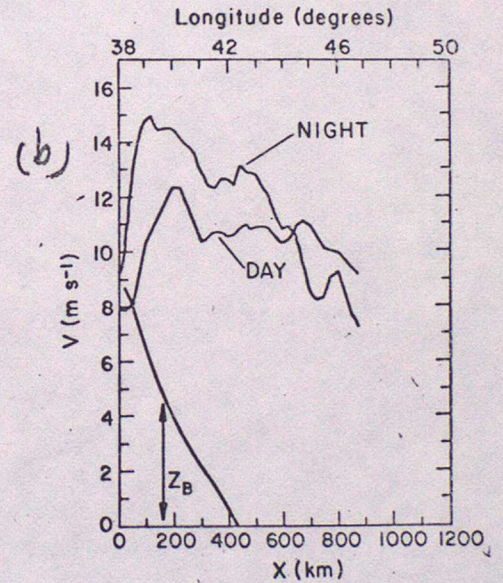
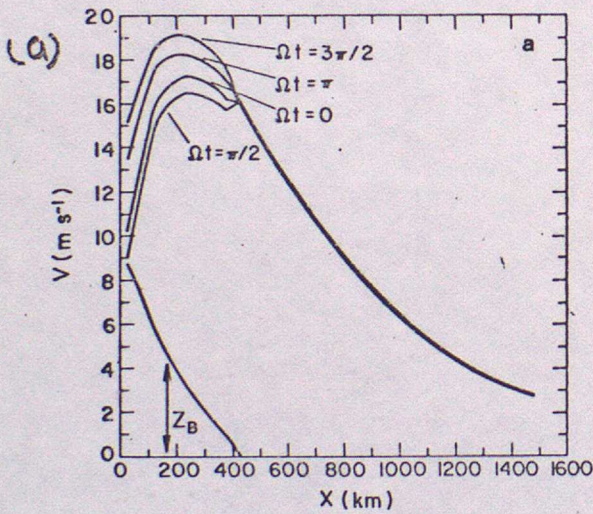


(a). Contour plot of wind speed for Experiment A. Contour interval is 1 m s^{-1} . For legibility, some contour lines have been eliminated in the northwest corner.



(b). Contour plot of the free surface height (km) for experiment A. Contour interval is 50 m.

Figure 7



Depth-averaged meridional wind at $\sim 2^\circ\text{S}$ as a function of longitude during MONSOON 77. Here "night" refers to 1900-0700 GMT and "day" to 0700-1900 GMT. The model orography is also shown. The true coastline is at 41.5°E .

Figure 8

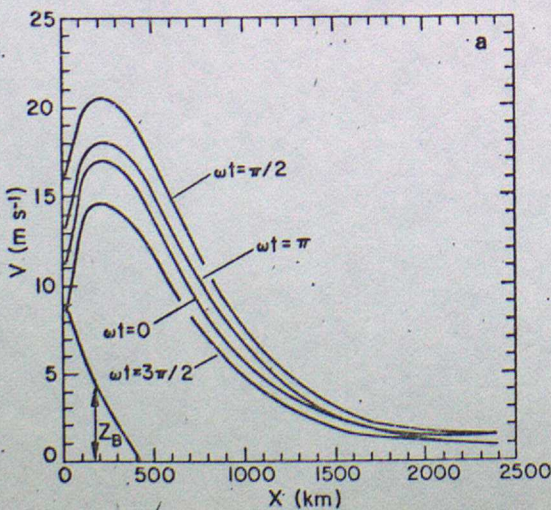


Figure 9



MONSOONS

1. Introduction

The word monsoon is derived from the arabic word for a season. Originally it referred to conditions in the Arabian Sea where for about 6 months of the year the flow is from the northeast and for the remainder of the year from the southwest. Nowadays the word refers to any seasonal wind.

The most well known monsoon is that which effects India and S.W. Asia, but there are other monsoons over Africa, N. Australia, parts of N. America and Chile. Also the term has been used to denote the onset of the summer rain period in N.W. Europe. Here we will only consider the monsoon that affects India and S.W. Asia. However it is important to remember that this monsoon is not just a regional phenomena - it is part of a system that extends from the southern oceans of the southern hemisphere to the northern reaches of Eurasia; and from West Africa to the Pacific.

2. The monsoon sequence

The transition from winter to summer monsoon conditions starts in March in the surface layer and by June the transition is complete. In March there are surface northeasterlies over the Arabia Sea and the Bay of Bengal whilst at 200mb there is strong westerly flow. During April a shallow heat low develops over southern India and moves northwards with the progress of summer. By May heat lows dominate North Africa and Asia with the main centre of low pressure over West Punjab. This causes an influx of moist southwesterly winds into Burma and Bangladesh and causes intense thunderstorms.

In June the subtropical fit that lies to the south of the Himalyas weakens and by the first half of July the westerlies disappear; the high level Tibetan anticyclone then grows with easterlies on its southern flank. Throughout June a trough develops over the Gauges Valley and links up with the heat low in the northwest. As this happens the moist monsoon winds extend eastward across northern India. The main features of the summer monsoon are

- (i) the monsoon trough whose position fluctuates; when it moves northwards the rainfalls in the foothills and produces a break in the rain on the Gauges Plain.
- (ii) fluctuations in the southwesterly flow.
- (iii) monsoon depressions that form in the Bay of Bengal and move westward along the axis of the trough.
- (iv) mid-tropospheric cyclones which develop in the N.E. Arabian Sea.

During autumn the westerlies intensify and move south as the Siberian anti-cyclone intensifies; winter then arrives suddenly in the Himalayas. Thereafter the thermal trough weakens as the insolation declines and this causes the southwesterly flow (and the paths of the monsoon depressions) to retreat southwards. In November a weak anticyclone predominates over the northern regions with a dry cool easterly flow to its south. During the winter monsoon the circulation in the north intensifies whilst to the south the remnants of the summer monsoon disappears. As the sun moves into the southern hemisphere the northeast monsoon extends across the equator.

3. The cause of the monsoon

The traditional explanation of the circulation distributions of both the winter and summer monsoon is based upon the interaction of the seasonally varying insolation and the distribution of the continents and oceans. Halley (1686) originated the concept of the monsoons as a planetary scale land-sea breeze circulation and in essence this view still prevails.

The first person to tackle the problem of the monsoon in a quantitative way appears to be Jeffreys (1926). He considered a circular land area surrounded by our infinite ocean - the air over the land being subjected to an annual cycle of heating and cooling. Here an extension of this type of analysis due to Asnani and Mishra (1975) will be presented. They examined the response of the atmosphere to a heating function

$$Q(x, y, p, t) = Q_0 f(p) e^{i(mxc + ly)} \sin\left(\frac{2\pi t}{T} - \alpha\right) = Q_0 f(p) F(x, y, t)$$

where $f(p)$ describes the vertical distribution of heating. Their model consisted of the quasi-geostrophic vorticity and thermodynamic equations with advection neglected. The basic equations are then

$$\frac{\partial}{\partial t} \nabla^2 \phi - f_0^2 \frac{\partial \omega}{\partial p} = 0 \qquad \frac{\partial}{\partial t} \frac{\partial \phi}{\partial p} - \frac{R s \omega}{p} + \frac{Q}{p c_p} = 0$$

where s is the static stability. From these, equations for ω and $\frac{\partial \phi}{\partial t}$ can be derived and by using

$$s = -\frac{c}{p} \qquad k = \frac{f_0}{2\sqrt{Rc}} \qquad \Omega = \frac{\omega}{p} = \frac{d}{dt} \ln p$$

the equations become

$$\left(p^2 \frac{\partial^2}{\partial p^2} + 2p \frac{\partial}{\partial p} + \frac{\nabla^2}{4k^2} \right) \frac{\partial \phi}{\partial t} = -\frac{R}{c_p} \frac{\partial}{\partial p} (pQ)$$

$$\left(p^2 \frac{\partial^2}{\partial p^2} + 2p \frac{\partial}{\partial p} + \frac{\nabla^2}{4k^2} \right) \Omega = -\frac{R}{c_p} \frac{1}{f_0^2} \nabla^2 Q$$

At the lower boundary Ekman pumping's assumed

$$w_f = \mu \nabla^2 \phi$$

using this, and the thermodynamic equation, suitable boundary conditions for Ω and $\frac{\partial \phi}{\partial t}$ can be derived.

Consider the solution when $f(p)$ describes a sensible heating profile (the function decreases upwards) and when there is no friction. The solution has the form

$$\frac{\partial \phi}{\partial t} = \frac{R}{c_p} Q_0 E(L, p) F(x, y, t)$$

where L is the effective horizontal wavelength

$$L = \frac{2\pi}{\sqrt{m^2 + L^2}}$$

Solutions for $E(L, p)$ are shown in Fig 1. In the summer (when $Q > 0$) E is negative in the lower levels and positive aloft - hence heating causes a fall of pressure in the lower levels with a rise in pressure above. This is to be expected, but what is not quite so obvious is that the magnitude of the pressure oscillations increases with the scale of the heating - in terms of the monsoon it means that the atmospheric response to the heating depends upon the dimensions of the land mass.

Fig 2 shows the effect of using various friction coefficients μ . In summer the friction causes the intensity aloft to exceed that below and also changes the phase so that aloft the heat wave is in phase with the heating, but below it lags the heating by up to 90° (without friction there is a 180° lag). This behaviour is consistent with what actually happens in monsoons.

The analysis was extended further by taking the annual mean pattern at $77.5^\circ E$ as a basic state and considering perturbations about this state. The perturbations are sinusoidal in x and t and so the equation give their structure in terms of y and p . It is assumed that the perturbations are caused by diabatic heating with no x -variation and only one wavelength between the poles. Fig 3 shows the resulting patterns of zonal wind at 3 monthly intervals. Clearly this simple model gives surprisingly good results with low level westerlies developing in the summer with easterlies above.

4. Numerical simulation of the summer monsoon

Gilchrist (1977) has compared simulations of the summer monsoon from 3 different models, but here we will concentrate upon the results reported by Washington and Daggupaty (1975) using the NCAR 6 layer model with a $2\frac{1}{2}^\circ$ lat/long grid.

Fig 4 shows the observed and model (average of days 91-120) 850mb streamlines and isotachs. The isotach pattern shows that the model can simulate the strong flow off the coast of Africa (the East African Jet), but in the Bay of Bengal the strong flow is too far south and too anticyclonic. Also the model does not reproduce the strong southerly flow onto the south facing slope of the Himalayas and this mirrors the failure of the model to simulate the shape of the monsoon trough. It has been suggested that this failure is linked to the inability of the model to create realistic monsoon depressions.

Fig 5 shows the flow at 200mb. The model reproduces the anticyclonic centre with the broad band of easterlies to the south of them; however the strength of the flow is considerably underestimated.

The results from other models are similar to those described above, so in general GCM's can reproduce the gross features of the summer monsoon well, but there are deficiencies in the details.

5. The role of the mountains

There have been arguments about the role of the mountains in the monsoon

- (i) whether the upper anticyclone is maintained by sensible heat from the Tibetan Plateau or by the release of latent heat associated with the orographic uplift of moist air on the mountain slopes.

(ii) whether the mountains have any influence on the abrupt northward shift of the subtropical jet which takes place before the onset of the summer monsoon.

There have been many attempts at studying these problems using numerical models. One of the first was an investigation by Murakami et al (1970) using a 2D 8 level model who studied the influence of the mountains on the lat-long distribution of zonal wind at a given longitude. The model allowed no zonal variations or cross-equatorial flow. Initially the atmosphere was dry and calm, and then the model was integrated forward in time, using July radiation, until a steady state was reached. When the mountains were not included there were only weak upper easterlies, but with mountains the zonal wind field was reasonably simulated. They found that it was the release of latent heat by convection on the south side of the mountains that was the rain source of heat for maintaining the upper anticyclone.

Another approach to the problem is to run a GCM with and without mountains. This was done by Hahn and Manabe (1975) using the GFDL 11-level model with a gridlength of about 270 km. Some of their results can be illustrated by reference to Fig 6. At the surface the exclusion of the mountains caused the main continental low to be displaced northwards whilst aloft the anticyclone lies to the south of Tibet rather than over the mountains. Examination of the temperatures revealed that when the mountains were included the maximum 500 mb temperatures were over Tibet whereas when they were excluded there was no maximum and the temperatures were about 10°C lower. They found that the primary cause of the high temperatures over the mountains was latent heat release induced by orographic uplift on the southern slopes. The behaviour of the subtropical jet was also investigated and it was found that without mountains the subtropical jet moved slowly northwards whereas when there were mountains there was an abrupt northward jump of about 20° of latitude in just a few days.

6. Monsoon depressions

Most monsoon depressions form over the warm waters of Bengal and travel westward at about 3ms^{-1} along the monsoon trough. During the four months of the summer monsoon up to about 10 depressions may form, but there is a good deal of variability. The depressions last between 2 and 5 days, but seldom beyond 7 days. The horizontal scale of the disturbances between 2000km and 3000km, and the vertical scale is about 10km. Monsoon depressions have a vertical structure similar to that of immature hurricanes (although the winds are not as high) with a cold core in the lower troposphere and a warm core above. The depressions produce continuous heavy rain along their left hand flank; this covers a region about 400km in width and about 500km ahead and behind the system. In some areas these depressions account for about 10% of the rainfall, but this is at the expense of other areas where the rainfall is correspondingly diminished - the depressions redistribute the rainfall.

Skukla (1977) investigated what kind of instability mechanism could explain the growth of monsoon depressions. We have already seen that in July the mean zonal wind has pronounced shear in both the horizontal and vertical, and this suggested to Skukla that the depressions are a result of joint barotropic - baroclinic instability. Now it can be shown that a necessary condition for this type of instability is that the gradient of potential vorticity on an isentropic surface should vanish; in July this condition is satisfied.

In order to find the growth rate and structure of the most unstable perturbations the equations are first linearised about the basic mean flow i.e. (y, p) . Then a wavelength is chosen (which gives the length of the channel) and the flow perturbed. The equations are then integrated forward in time until the perturbation was an exponential growth. When this happens the growth rate and phase speed can be computed; this process carried out for a series of different wavelengths. The results showed that the wavelength of maximum growth was about 3000km with an e-folding time of about 3 days. These values are quite realistic, but unfortunately the waves had the wrong structure - the maximum amplitude was at 150mb with the amplitude falling off rapidly towards the surface whereas in reality the maximum amplitude is at the surface and the disturbances are rarely detected at 200mb.

The failure of barotropic-baroclinic instability to explain the structure of the disturbances prompted Shukla (1978) to consider CISK-barotropic-baroclinic instability. Traditionally CISK has been introduced into models by making the total moist convective heating depend upon the total convergence of water vapour; however the problem remains of how to distribute the heating in the vertical. Sometimes arbitrary functions are used at a Kuo-type convection scheme, but in all cases it is found that the choice and behaviour of the fastest growing mode is very sensitive to the vertical distribution of heating. To overcome this problem Shukla used a very sophisticated convection scheme based on the theory of Arakawa and Schubert (1974). In this it is assumed that there is quasi-equilibrium between the destabilising effects of the large scale forcing and the stabilising effects of the cumulus ensemble. This assumption allows the parameterisation scheme to be closed. Shukla used a 3-level model to find the most unstable mode in the same way as in his previous study.

Some of Shukla's results are shown in Fig 7. In both sets of results the fastest growing waves are those with the shortest wavelength. However there are problems in interpreting results when the instability is driven by moist convection because the ability of a perturbation of a given wavelength to grow depends upon the availability of moisture on that scale. For example the growth rate of small scale wave may be large, but if the period such a wave is small the total moisture evaporated over one period may not be sufficient to sustain the precipitation; therefore the maximum growth of the wave may not take place. There have been several attempts at overcoming this problem and they have all had the effect of reducing the growth of the high frequency waves. Shukla suggested that the waves that dominate are those for which the ratio of their period to the e-folding time is a maximum (ie c_i / c_r is maximised). Fig 7 shows that when Ekman pumping was included the wavelength of maximum growth was about 3000km, but unfortunately it had a westerly phase speed. Without Ekman pumping the phase speeds are easterly, but still it is the shortest waves that grow the fastest. Clearly problems remain, but despite this Shukla examined the structure of the perturbations with wavelength of 2000-3000km and found that they had a reasonable structure (with a maximum at the surface) and that they formed at the latitude of the Bay of Bengal. However, unlike real disturbances, the perturbations had a warm core throughout the troposphere.

Obviously the instability mechanism for monsoon depressions is not entirely understood.

7. The future

There is still a great deal that is not known about the Asian monsoons - especially with regard to their variability (on scales of days to years) and their interaction with the oceans, stratosphere, southern hemisphere and mid-latitudes. To investigate these problems a series of Monsoon Experiments (MONEX) have taken place as part of GARP. The objectives of MONEX are set out in Table 1 and the results are awaited with interest.

8. References

- Arakaw, A and Schubert, W H., 1974 J.Atms Sc., 31, 674-701.
- Asnani, G C and Mishra, S K., 1975, MWR, 103, 115-130.
- Gilchrist, A., 1977, Pure and Appl. Geophysics, 115, 1431-1449.
- Halley, E., 1686, Phil. Trans. Roy. Soc., 16, 153-168.
- Hahn, D G and Manabe, S., 1975, J.Atms Sc., 32, 1515-1541.
- Murakami, T., et al, 1970, Proc. Conf. Summer Monsoon S E Asia 39-51.
- Shukla, J., 1977, Pure and Appl. Geophysics, 115, 1449-1463.
- Shukla, J., 1978, J.Atms.Sci, 35, 495-508.
- Washington, W M and Daggupaty, S M., 1975, MWR., 103, 105-114.

MONEX — primary scientific objectives
(Summer monsoon *)
(Winter monsoon **)

Description	Scientific problems to be solved (examples)	Monsoon data set
<p><i>Large-scale aspects of the monsoon</i></p> <ul style="list-style-type: none"> — Onset of the monsoon * — Active and break monsoons * — Effects of heat sources and orography *, ** 	<ul style="list-style-type: none"> — Physical processes involved in the "onset" of the monsoon — Unified, detailed descriptions of monsoon fluctuations associated with the phase change between "active" and "break" monsoons — Sensitivity study of monsoon circulation to heat sources 	<p>Diagnostic study and/or prediction experiment with Global models</p>
<p><i>Regional aspects of the monsoon</i></p> <ul style="list-style-type: none"> — Arabian Sea and western Indian Ocean studies * — Monsoon disturbances * — Cold monsoon surges ** — Heavy rainfall and dry spells (Indonesia—Malaysia) ** — Effects of heat sources and orography *, ** 	<ul style="list-style-type: none"> — Low level cross-equatorial jet: its structural details — Inversion: its detailed structure and mechanism of the maintenance — Formation of the depression — Relation between the regional disturbance development and the entire winter monsoon system — Physics of heavy rain making — Maintenance mechanism of dry spells — Influence of topography on the formation of equatorial disturbances 	<p>Limited area models</p>
<p><i>Interactions *, **</i></p> <ul style="list-style-type: none"> — Inter-hemispheric interaction — Interaction of regional monsoon circulation with: <ol style="list-style-type: none"> (a) the central and western Pacific circulation (b) the mid-latitude waves (c) the circulation in the stratosphere 	<ul style="list-style-type: none"> — Diagnostic studies on momentum, vorticity, moisture and energy balance of mean monsoonal circulation — Examination of possible existence of the atmospheric teleconnection between the monsoon region and the Pacific region (lateral coupling) — Examination of the dynamical and thermal coupling of the tropospheric and stratospheric circulations (vertical coupling) 	<p>Global models</p>

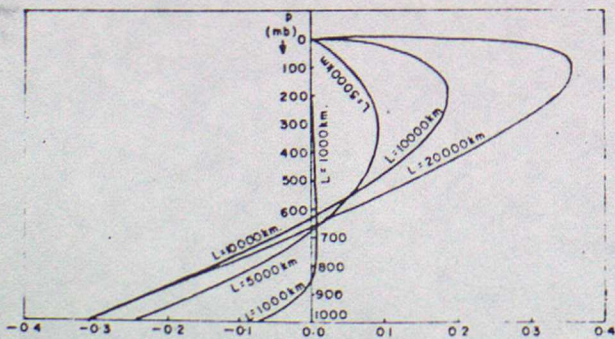


Fig. 1 Variation of E with respect to p for $Q_0/c_p = 10^{-6} \text{ K s}^{-1}$; $r = 1.0$; $L = 1000, 5000, 10,000, \text{ and } 20,000 \text{ km}$.

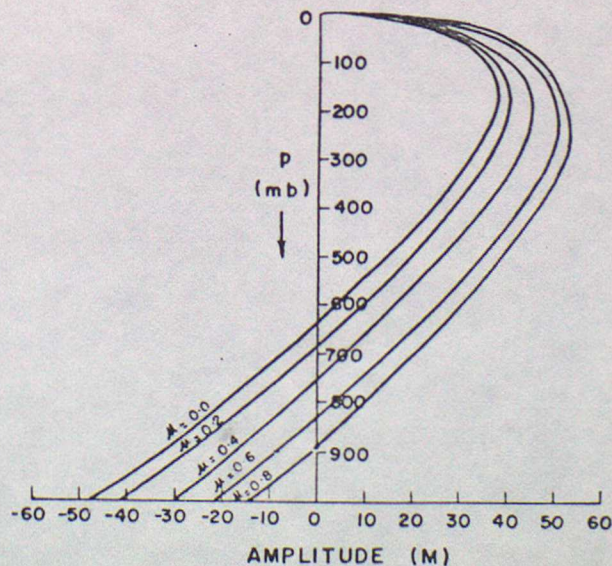


Fig. 2 Amplitude of Z (m) for annual oscillation with different values of μ ; $L = 13,500 \text{ km}$, $\alpha = 0$, $Q_0/c_p = 10^{-6} \text{ K s}^{-1}$.

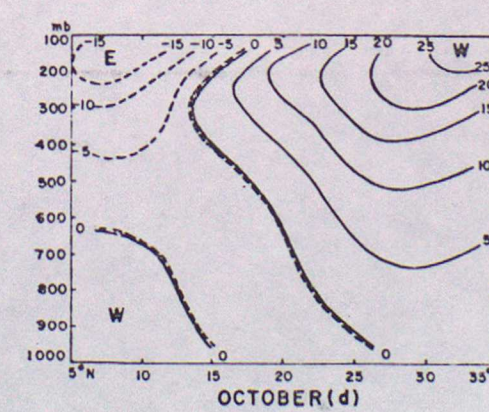
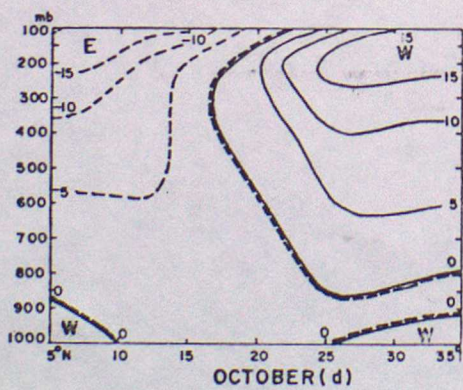
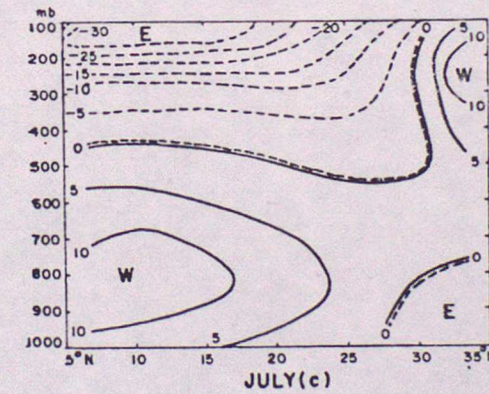
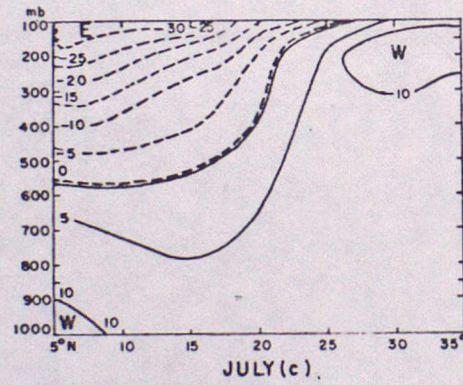
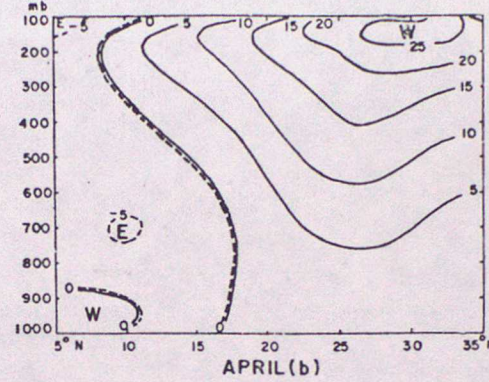
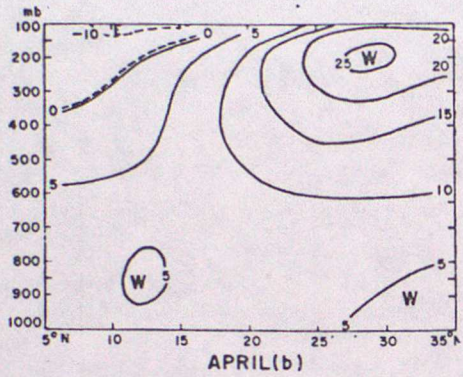
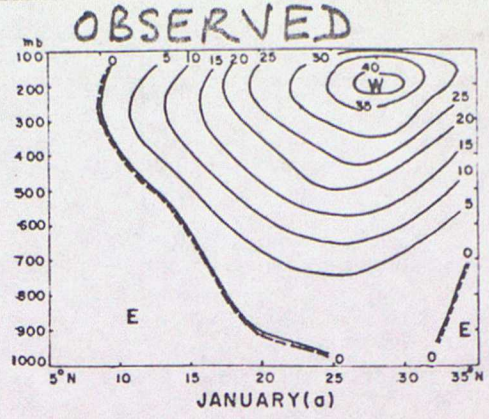
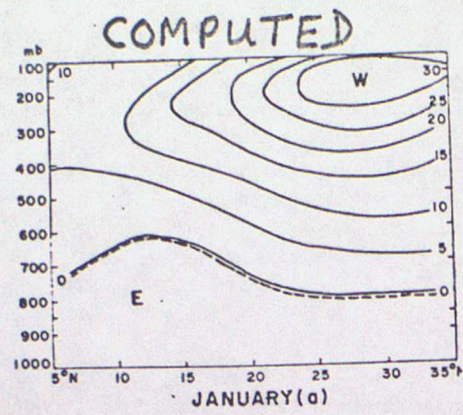
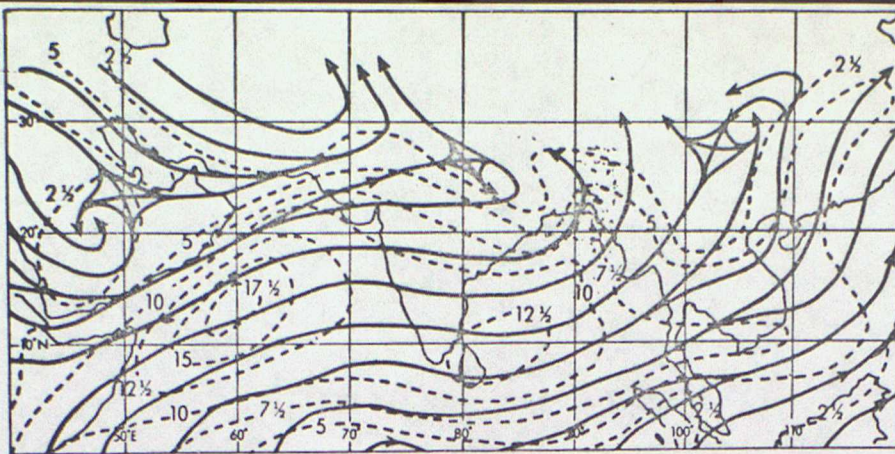
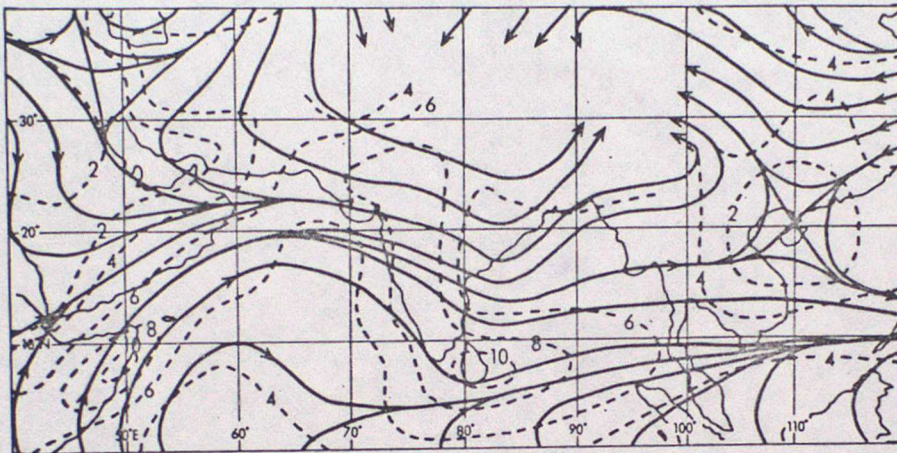


Figure 3



Observed

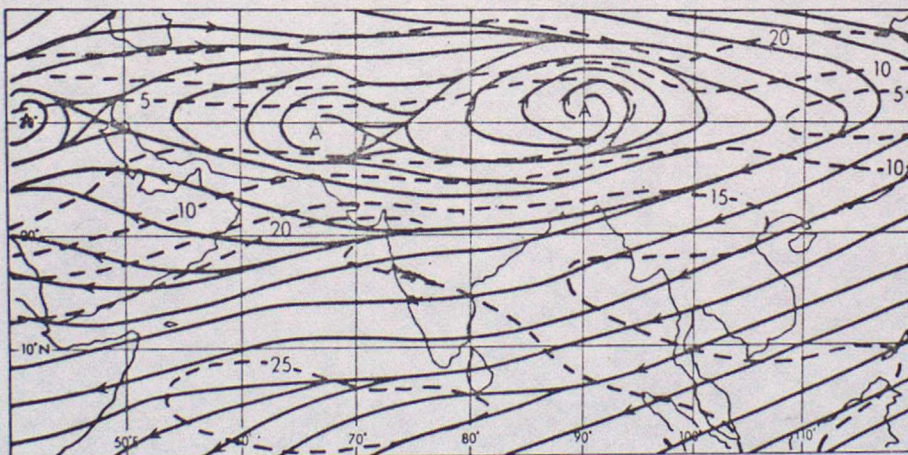
(a)



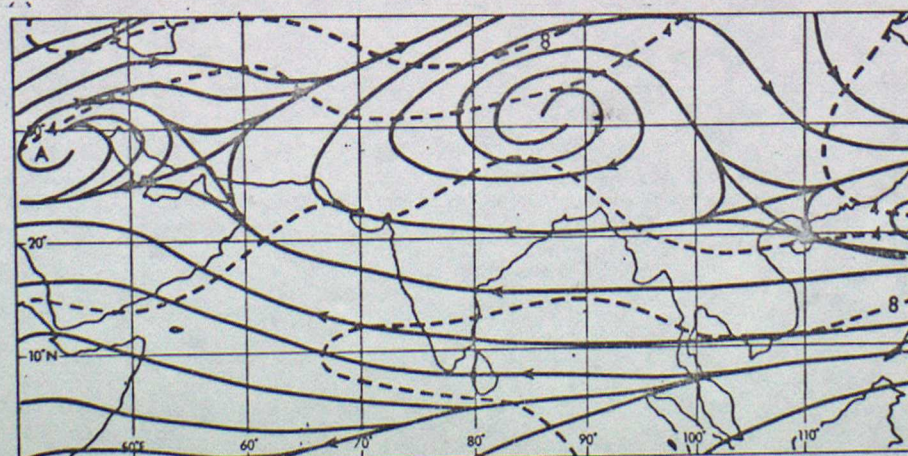
NCAR model

(c)

Fig. 4 - low level wind distribution (streamlines & isotachs)



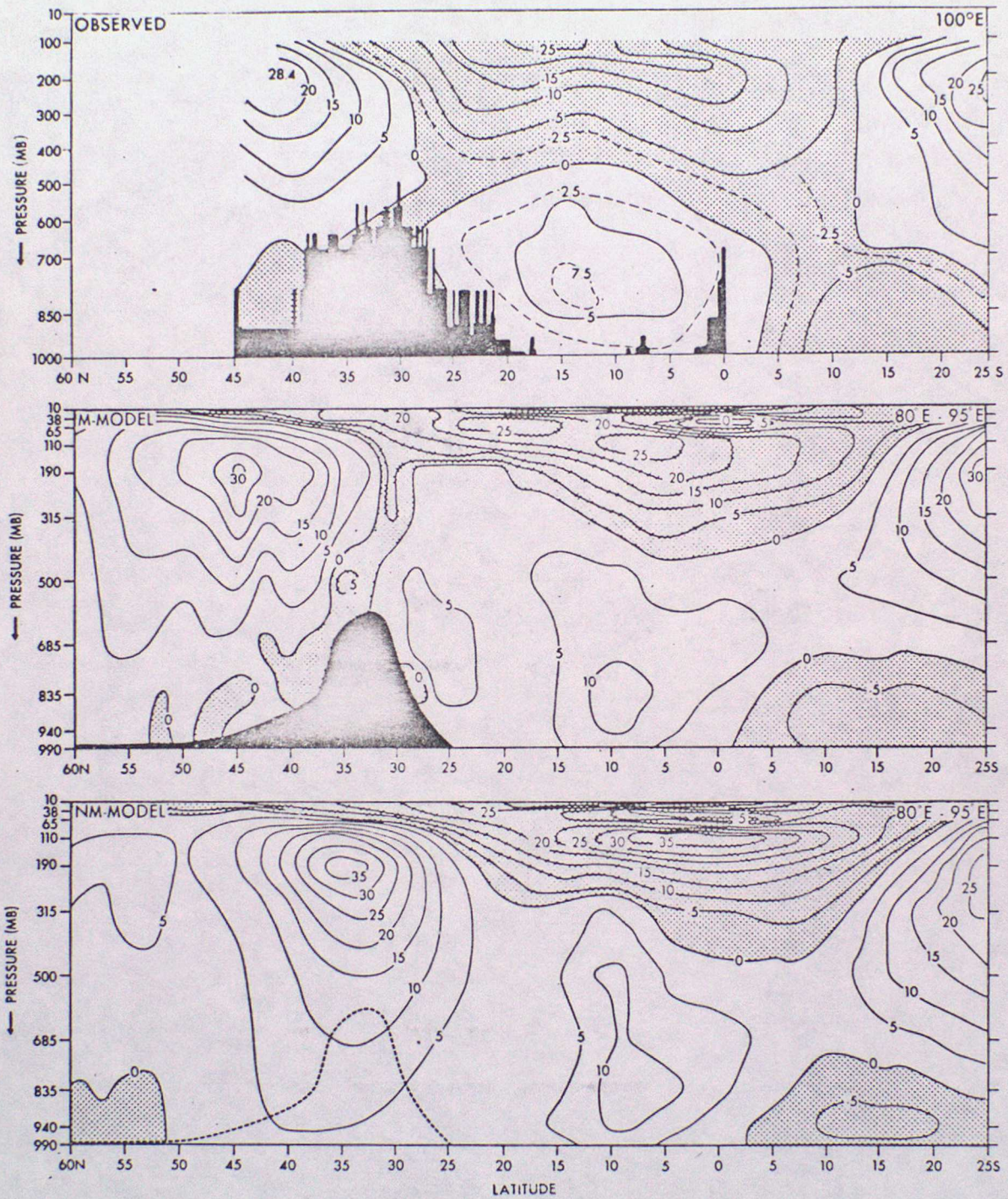
Observed



NCAR model

(c)

Fig. 5 - high tropospheric wind distribution



Top, observed latitude-pressure distribution of July mean zonal wind (m s^{-1}) along 100°E from Ramage (1971). Middle, computed latitude-pressure distribution of July mean zonally averaged ($80\text{--}95^\circ\text{E}$) zonal wind (m s^{-1}) for the M-model. Bottom, same as middle for the NM-model.

Figure 6

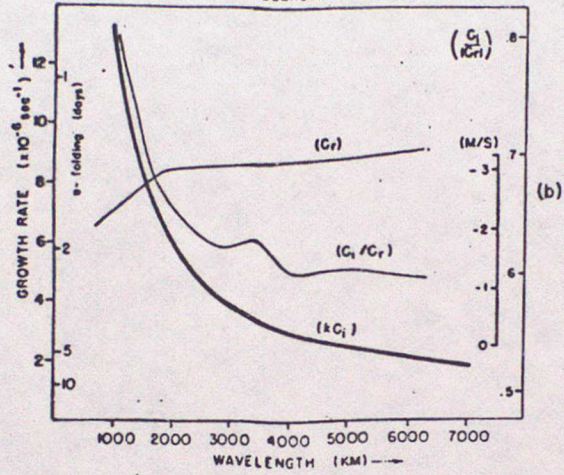
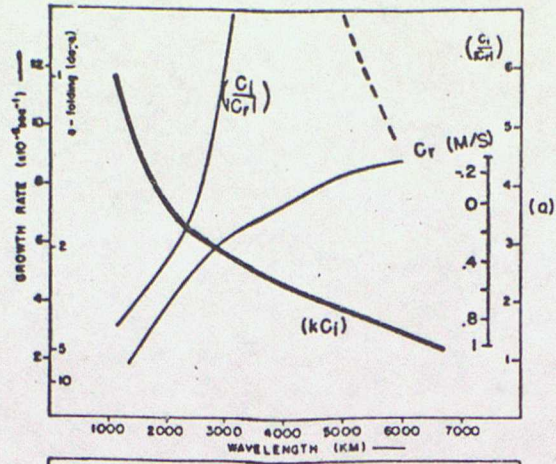


Fig. 7 Growth rate (kC_i), phase speed (C_r) and ratio (C_i/C_r) for the observed monsoon zonal wind $\bar{U}(y,z)$: (a) with Ekman pumping, (b) without Ekman pumping.

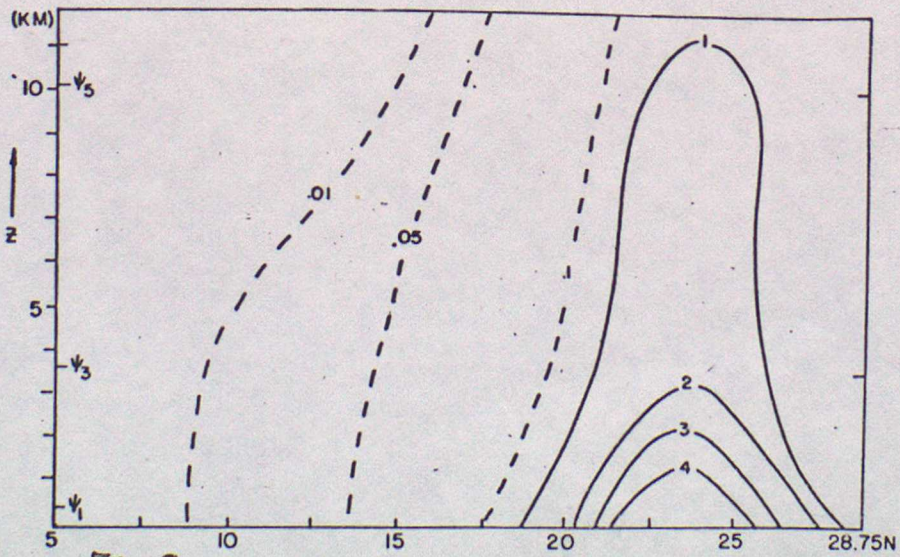


Fig 8 Latitude-height cross section of the amplitude of (ψ) for the perturbation of wavelength 2500 km.